Studies on the Modes of Action Underlying Renal Carcinogenic Mycotoxins in Rodents

（腎発がん性を有するマイコトキシンのげっ歯類における発がん機序に関する研究）

2014

The United Graduate School of Veterinary Sciences, Gifu University

(Gifu University)

KURODA, Ken

Studies on the Modes of Action Underlying Renal Carcinogenic Mycotoxins in Rodents

（腎発がん性を有するマイコトキシンのげっ歯類における発がん機序に関する研究）

KURODA, Ken

Contents

Abbreviations

6-TG: 6-thioguanine

8-OHdG: 8-hydroxydeoxyguanosine

ABC: avidin-biotin complex

ANOVA: analysis of variance

AP sites: apurinic/apyrimidinic sites

APNH: aminophenylnorharman

Ataxia telangiectasia mutated (ATM)

Aurka: aurora kinase A

BEN: Balkan endemic nephropathy

BER: base excision repair (BER)

Bak1: BCL2-antagonist/killer 1

Bard1: BRCA1 associated RING domain 1

Bax: BCL2-associated X protein

Bbc3: BCL2 binding component 3

bp: base pair

Brip1: *BRCA1-interacting protein 1*

CO: cortex

CP: cyclophosphamide

CTN: citrinin

Ccna2: *cyclin A2*

Ccnb1: cyclin B1

Ccnd1: *cyclin D1*

Ccne1: cyclin E1

Cdk1: *cyclin-dependent kinase 1*

Cdkn1a: *cyclin-dependent kinase inhibitor 1A*

Chek1: *checkpoint kinase 1*

DDR: DNA damage response

DMSO: dimethyl sulfoxide

DSBs: double-strand breaks

E2f1: E2F transcription factor 1

ECL: enhanced chemiluminescence

EDTA: ethylenediaminetetraacetic acid

ENU: ethylnitrosourea

ERK: extracellular regulated MAP kinase

Ercc1: *excision repair cross-complementation group 1*

Fen1: *flap structure-specific endonuclease 1*

GAPDH: *glyceraldehyde-3-phosphate dehydrogenase*

HBSS: Hank's balanced saline solution

HCl: hydrochloric acid

HE: hematoxylin and eosin

HEPES: 4-(2-hydroxyethyl)-1-piperazineethanesulfonic acid

HR: homologous recombination repair

Hgf: *hepatocyte growth factor*

Hrk: *harakiri, BCL2 interacting protein*

IPA: Ingenuity Pathway Analysis

IR: ionizing radiation

IARC: International Agency for Research on Cancer

KCl: potassium chloride

Lcn2: *lipocalin 2*

Lig4: *ligase IV*

MDA: malondialdehyde

MEK: mitogen-activated protein kinase kinase

MFs: mutant frequencies

MMC: mytomycin C

MMS: methyl methane sulfonate

MNPCEs: Micronucleated polychromatic erythrocytes

Mgmt.: *O-6-methylguanine-DNA methyltransferase*

NCEs: normochromatic erythrocyte

NER: nucleotide excision repair

NHEJ: nonhomologous end joining

NaOH: sodium hydroxide

OSOM: outer stripe of the outer medulla

OTA: ochratoxin A

PCEs: polychromatic erythrocytes

PCNA: proliferating cell nuclear antigen

PCR: polymerase chain reaction

PI3K: phosphoinositide 3-kinase

PKC: protein kinase C

PhIP: 2-Amino-1-methyl-6-phenylimidazo [4,5-b]pyridine

Pkmyt1: protein kinase, membrane associated tyrosine/threonine 1

Plk1: polo-like kinase 1

Polk: polymerase (DNA directed), kappa

RIPA: Radio-Immunoprecipitation Assay

ROM: the renal outer medulla

RT-PCR: reverse transcription PCR

Rad18: *RAD18 E3 ubiquitin protein ligase*

Rad51: *Rad51 recombinase*

Rad54l: RAD54 like

SDS-PAGE: Sodium dodecyl sulfate-polyacrylamide gel electrophoresis

Spi$^-$: sensitive to PII interference

TBARS: thiobarbituric acid reactive substances

TOPOII: topoisomerase II

Tris: tris (hydroxymethyl) aminomethane

UVB: ultraviolet B

Wee1: *Wee1 G2 checkpoint kinase*

Xpa: *xeroderma pigmentosum, complementation group A*

Xrcc1: *X-ray repair complementing defective repair in Chinese hamster cells 1*

Xrcc5: *X-ray repair complementing defective repair in Chinese hamster cells 5*

Xrcc6: *X-ray repair complementing defective repair in Chinese hamster cells 6*

γ-H2AX: phosphorylation of histone variant H2AX

General introduction

One of major causal factors of human carcinogenesis is nutrition and dietary carcinogens (1). Carcinogens in foods include chemical substances contained in nature or produced during cooking process, as well as contaminated substances such as pesticide residue, animal drugs and mycotoxins (2,3). As generally accepted, chemical carcinogenesis involved in multistep process of initiation, promotion and progression (4). Chemical substances which have initiation activity directly react with DNA, resulted in mutations in proto-oncogenes or tumor-suppressor genes related with cell cycle control, cell death and DNA repair, which means genotoxic effects (5). Some chemicals with genotoxic potential have been strictly regulated for protection of human health, such as the prohibition of usage in food additives or strict requirement to comply with regulation values in foods. Therefore, understanding the modes of action for chemical-induced carcinogenicity are essential for accurate assessments of the chemical hazards to human health.

Mycotoxins, secondary metabolites produced by several fungal species, are often found as contaminants in foodstuffs such as grains, coffee beans, nuts and animal feed (6). Ochratoxin A (OTA) and citrinin (CTN) are well known mycotoxins produced by *Aspergillus*, *Penicillium* or *Monascus* families, primarily *P. verrucosum*, *A. ochraceus* for OTA; *P. expansum*, *P.verrucosum*, *A. terreus* and *M. ruber* for CTN (7, 8). Contamination of these mycotoxins in food commodities such as cereals, coffee and cocoa beans, spices, dried vine fruits have been reported all over the world (8, 9). Toxicological properties of these two mycotoxins were summarized in Fig. 0-1. OTA, targeting the segment 3 (S3) in the renal proximal tubule cells, has been well known as nephrotoxic in domestic animals and rodents (10), and renal adenoma/carcinoma has been found at high incidences, which were approximate 70% in rats and 60% in mice (10, 11, 12). On the other hand, CTN has renal toxicity targeting the segment 1 (S1) in the renal proximal tubule cells, and in a long-term bioassay, 80-week exposure of rats to CTN also induced renal cell adenomas at a high frequency (13, 14). In the

human epidemiology, it has been reported that OTA and CTN might be causal factors of Balkan endemic nephropathy, a chronic kidney disease observed in Balkan countries, and also implicated in the induction of Urinary tract tumors in North Africa (15). Additionally, because of its clear evidence of carcinogenicity in both rats and mice, OTA has been classified as a 2B group compound by the International Agency for Research on Cancer (IARC) (16). Given that there have been a line of evidence that both of mycotoxins are detected in human serum and urine (9, 10), carcinogenic potential in rodents suggest possible cancer risk in human.

Modes of action underlying OTA and CTN-induced carcinogenesis have been debated long time, and remained to be concluded because several genotoxicity studies yielded both positive and negative results. There are several reports demonstrating presence or absence of OTA-specific DNA adducts in the kidney of rats treated with OTA (17, 18). Exposure to OTA had no effect on mutagenicity in most Ames tests (19); the exceptions were tests conducted on mouse kidney microsomes and rat

hepatocyte (20, 21). The results of other genotoxicity assays such as unscheduled DNA synthesis, *in vitro* sister chromatid exchange, and *in vitro* chromosomal aberration have not yielded consistent results by OTA treatment (19). Similarly, CTN has yielded negative in conventional Ames tests, but positive in the tests with medium derived from hepatocyte culture (22). There were both positive and negative results in *in vitro* comet assays (23, 24, 25) and positive scores in *in vitro* and *in vivo* chromosomal aberration tests, by CTN treatment (23, 26, 27, 28). These inconsistent outcomes make it especially difficult to judge whether OTA and CTN-induced renal carcinogenesis involves genotoxic mechanisms.

Reporter gene mutation assays using transgenic rodents are useful tools to investigate genotoxic mechanism of carcinogenic chemicals that shows equivocal outcomes in conventional mutagenicity tests (29). In this methods, we can investigate *in vivo* mutagenicity at the target organ with consideration of the absorption, distribution, metabolism, and excretion of the test chemicals (30, 31). Especially, *in vivo* reporter

gene mutation assay using *gpt* delta rodents can detect both of point mutations and deletion mutations by two different selection system (32). The lambda EG10 (Fig. 0-2) phage vector constructed for this system contains two positive selection methods: the *gpt* assay [6-thioguanine (6-TG) selection] using the *gpt* gene of *E. coli*, which mainly detects point mutations such as base substitutions and frameshifts, and the Spi$^-$ assay (Spi$^-$ selection) that utilizes the *red/gam* genes of lambda phage to detect deletions, including frameshifts (Fig. 0-3). An additional advantage of this assay is ability to identify the mutation spectra of each *gpt* or *red/gam* mutants by replication of mutant DNA, which recovered from *gpt* or Spi$^-$ mutant phages. Because chemical-induced gene mutations are results of chemical reactions between chemicals and DNA followed by DNA repair, mutation spectrum on the reporter genes provides mechanistic information of mutagenic agents (33).

Recently, it was reported that OTA increased mutant frequencies in Spi$^-$ assay, only in the outer medulla of the kidney, the carcinogenic target site of *gpt* delta rats (34).

Additionally, it was also reported that OTA increased Spi^- mutant frequencies in the kidney of *p53*-dificient *gpt* delta mice, but not in wild type mice, suggesting p53 has preventive effect on OTA-induced gene mutation (35). Although these results suggest possible participation of genotoxic mechanism in OTA-induced carcinogenesis in both rats and mice kidney, further study focused on detail information and induction mechanism of OTA-induced gene mutation should be performed. On the other hand, there have been little evidence of *in vivo* genotoxicity and carcinogenicity study of CTN. Thus, whether CTN has genotoxiciy *in vivo* is one of critical factors for estimating modes of carcinogenic action of CTN.

In the present study, to investigate the modes of action underlying renal carcinogenesis induced by OTA and CTN, three experiments were performed. In chapter 1, mutation spectrum of OTA-induced reporter gene mutations in the kidney of *gpt* delta rats were investigated. Moreover, induction mechanism of OTA-induced gene mutation were examined by comet assay and expression analysis of DNA

damage/repair-related genes and proteins. In chapter 2, the effects of p53 on DNA damages and reporter gene mutations in the kidney of mice induced by OTA were examined using *p53*-deficient (*p53*$^{-/-}$) mice. Additionally, mutation spectrum of OTA-induced gene mutation in the kidney of *p53*-deficient *gpt* delta mice kidney were investigated. In chapter 3, *in vivo* genotoxicity of CTN using reporter gene mutation assay, comet assay and micronucleus assay was investigated, and cell cycle progression induced by CTN were clarified to estimate the modes of carcinogenic action of CTN.

	Ochratoxin A (OTA)	Citrinin (CTN)
	✓ Mycotoxins produced by genera *Penicillium* and *Aspergillus* ✓ Common contaminants of foods (cereals, beans)	
Chemical structure	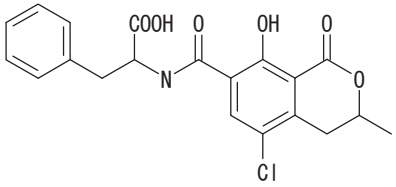	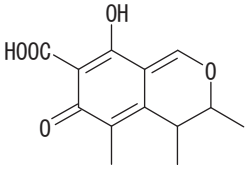
Target site of toxicity	Kidney (the proximal straight tubule, S3)	Kidney (the proximal convoluted tubule, S1)
Involvement in human disease	Balkan Endemic Nephropathy, Urinary Tract Tumor	
Carcinogenicity in rodents	Rats: Positive (kidney) Mice: Positive (kidney and liver)	Rats: Positive (kidney) Mice: Negative
IARC evaluation (Human risk)	Group 2B (Possibly carcinogenic to humans)	Group 3 (Not classified)
Genotoxicity	Remain to be determined Ames test: Positive or Negative Chromosome aberration test: Positive or Negative Comet assay: Positive Formation of DNA adduct: Positive or Negative	Remain to be determined Ames test: Positive or Negative Chromosome aberration test: Positive

Figure 0-1 Toxicological properties of OTA and CTN

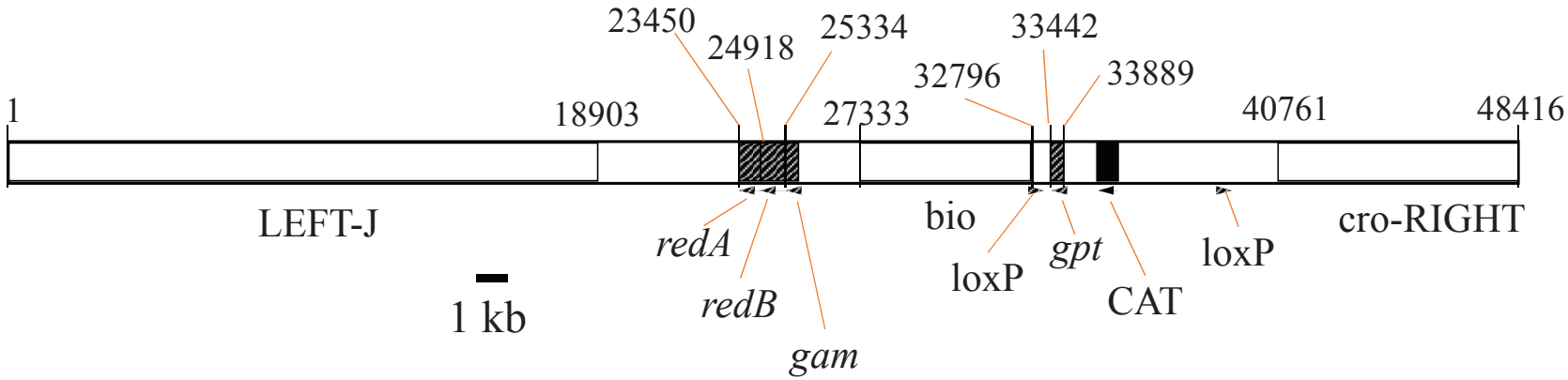

Plasmid name: lambda EG10 pre2.0
Plasmid size: 48416 bp
Construction date: 19990119

Figure 0-2 Construction of Lambda EG10 introduced into *gpt* delta rodents.
Lambda EG10 contains *red/gam* and *gpt* genes, which used for different positive selection system. Sequences of Lambda EG10 are available at *http://www.nihs.go.jp/dgm/dgm3/gptdeltainfo.html*. This figure was kindly provided by Dr. Kenichi Masumura, Division of Genetics and Mutagenesis, National Institute of Health Sciences.

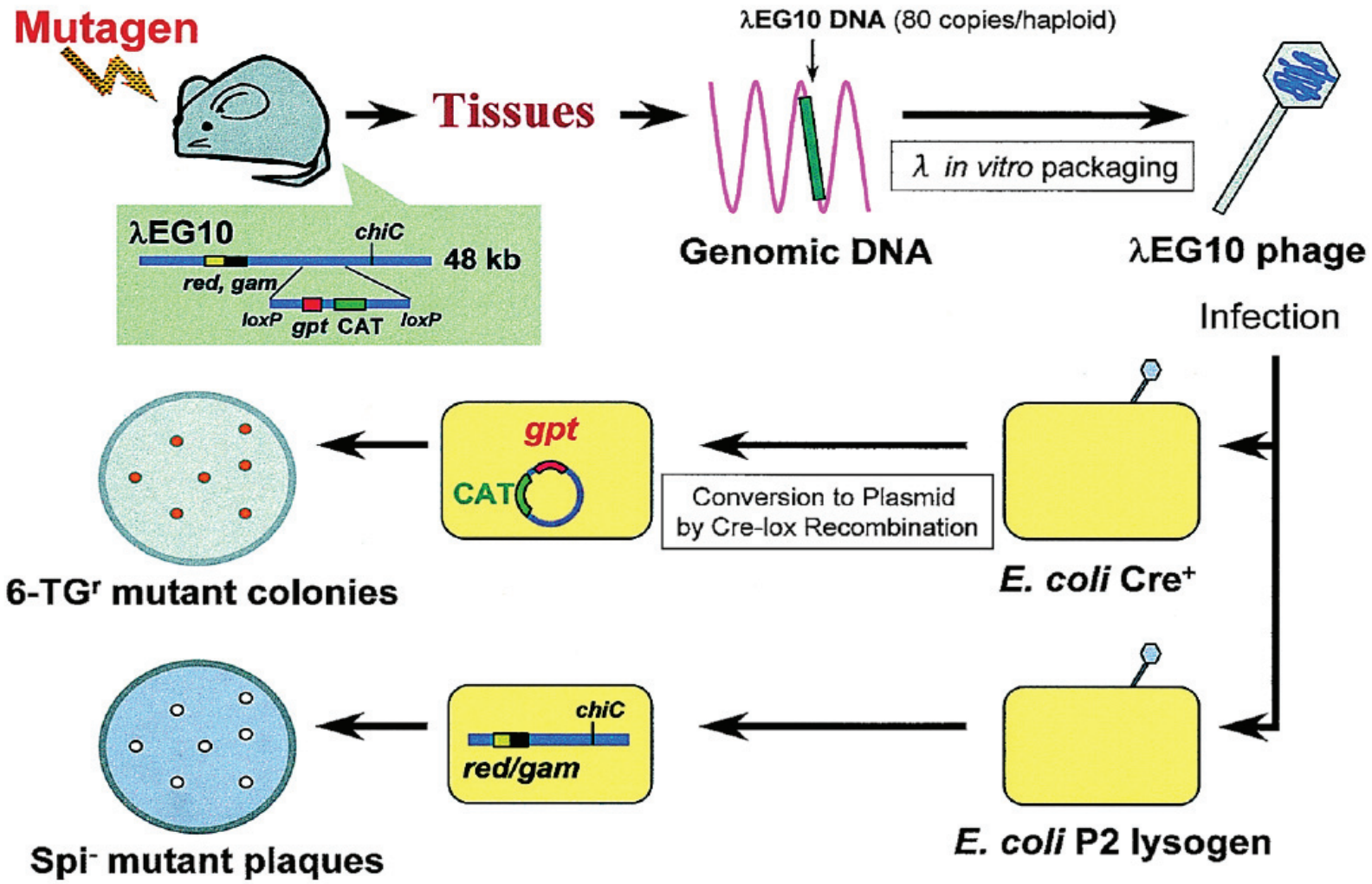

Figure 0-3 Protocols of *gpt* delta transgenic rodents mutagenicity assay.

Genomic DNA is extracted from transgenic rodent tissue, and lambda EG10 DNA is rescued as phage particles by *in vitro* packaging reactions. Two *E. coli* strains, YG6020 expressing Cre recombinase for 6-thioguanine (6-TG) selection and P2 lysogen for Spi$^-$ selection, are infected with the rescued λEG10 phages. Using *gpt* and Spi$^-$ selections, the frequencies of point or deletion mutations can be examined in the target organs (Nohmi et al., 2000).

Chapter 1

Ochratoxin A induces DNA double-strand breaks and large deletion mutations in the carcinogenic target site of *gpt* delta rats

Abstract

Ochratoxin A (OTA) is a carcinogen targeting proximal tubules at the renal outer medulla (ROM) in rodents. I previously reported that OTA increased mutant frequencies (MFs) of the *red*/*gam* gene (Spi^-), primarily deletion mutations. In the present study, Spi^- assays and mutation spectrum analyses in the Spi^- mutants were performed using additional samples collected in the previous study. Spi^- assay results were similar to those in the previous study, revealing large (over 1 kb) deletion mutations in the *red/gam* gene. To clarify the molecular progression from DNA damage to gene mutations, *in vivo* comet assays and analysis of DNA damage/repair-related mRNA and/or protein expression was performed using the ROM of *gpt* delta rats treated with OTA at 70, 210, or 630 μg/kg/day by gavage for 4 weeks. Western blotting and immunohistochemical staining demonstrated that OTA increased γ-H2AX expression specifically at the carcinogenic target site. In view of the results of comet assays, I suspected that OTA was capable of inducing double-strand breaks (DSBs) at the target

sites. mRNA and/or protein expression levels of homologous recombination repair-related genes (*Rad51*, *Rad18*, and *Brip1*), but not nonhomologous end joining-related genes, were increased in response to OTA in a dose-dependent manner. Moreover, dramatic increases in the expression of genes involved in G_2/M arrest (*Chek1* and *Wee1*) and S/G_2 phase (*Ccna2* and *Cdk1*) were observed, suggesting that DSBs induced by OTA were repaired predominantly by homologous recombination repair, possibly due to OTA-specific cell cycle regulation, consequently producing large deletion mutations at the carcinogenic target site.

Introduction

Ochratoxin A (OTA), a nephrotoxic mycotoxin produced by several fungal species, is often found as a contaminant in agricultural products (9). Since humans are exposed to OTA via consumption of various foods, the fact that OTA induces renal cell tumors with a high incidence in rodents suggests a possible cancer risk in humans (12, 13, 16). However, the mechanism through which OTA exerts its carcinogenic action is still controversial, particularly because genotoxicity tests have yielded both positive and negative results (36). Recently, Hibi et al. showed that OTA increases mutant frequencies (MFs) of the *red*/*gam* gene (Spi^-) at the renal outer medulla (ROM), the carcinogenic target site of *gpt* delta rats (34), suggesting involvement of genotoxic mechanisms in OTA-induced renal carcinogenesis.

The phenotype of the Spi^- (sensitive to PII interference) mutation in *gpt* delta rodents represents inactivation of the functions of both the *red* and *gam* genes. Research has suggested that disruption of these genes in the Spi^- mutant is caused by 1-

to 10,000-base pair (bp) deletions spanning these 2 tandem genes (37). 2-Amino-1-methyl-6-phenylimidazo [4,5-*b*]pyridine (PhIP) and aminophenylnorharman (APNH) are known to form specific DNA adducts on guanine base to induce single bp deletions of G:C in the *gam* gene, possibly due to translesion synthesis of DNA adducts (38, 39). Ionizing radiation (IR), ultraviolet B (UVB), or mytomycin C (MMC), which are known to induce DNA double-strand breaks (DSBs), cause large deletions exceeding 1 kb at this locus including the *red/gam* genes, possibly through the DSB repair process (40, 41, 42). Thus, mutagens elicit deletions of specific sizes and sequences in the *red/gam* genes, and deletion mutation spectra analyses are informative in the determination of their induction mechanisms (37). In the case of OTA, although mRNA levels of several genes related to DSB repair were changed at the carcinogenic target site by OTA treatment (43), the detail mechanisms underlying OTA-induced mutagenesis remain unclear.

DSB repair is initiated by Ataxia telangiectasia mutated (ATM)-mediated

phosphorylation of histone variant H2AX (γ-H2AX), which subsequently recruits specific proteins corresponding to 2 major DSB repair systems, homologous recombination repair (HR) and nonhomologous end joining (NHEJ) (44, 45, 46). Errors in the repair processes of the HR or NHEJ systems cause various mutations, including large deletions (37, 47, 48). Accordingly, information on the fluctuations in gene and/or protein expression associated with DSB repair, in addition to changes in direct markers of DNA damage, could be helpful to understanding the mechanisms through which OTA induces mutagenesis.

In the present study, I performed Spi$^-$ assays and mutation spectrum analyses of Spi$^-$ mutants obtained from the ROM of *gpt* delta rats fed OTA at a carcinogenic dose for 4 weeks, as reported in the previous study (34). Additionally, to clarify pathways leading from DNA damage to mutagenesis following OTA exposure, I performed *in vivo* comet assays and measured the expression levels of genes and proteins related to DNA damage/repair using the ROM of *gpt* delta rats treated with 3 different doses of

OTA for 4 weeks.

Materials and Methods

Experimental animals and housing conditions

The protocol for this study was approved by the Animal Care and Utilization Committee of the National Institute of Health Sciences. Specific pathogen-free, 5-week-old male F344/NSlc-Tg (*gpt* delta) rats carrying about 5 tandem copies of the transgene lambda EG10 per haploid genome were obtained from Japan SLC (Shizuoka, Japan) and acclimated for 1 week prior to the commencement of testing. Animals were housed in a room with a barrier system and maintained under a constant temperature (23 ± 2°C) and relative humidity (55% ± 5%). The air was changed 12 times/h, and lighting was on a 12-h light-dark cycle. Animals had free access to tap water.

Test compound

OTA was extracted from a culture of *Aspergillus ochraceus* (BD-5). Fermentative

production of OTA was performed based on the culture and extraction methods of Kumata et al. (49), with minor modifications. Several 500-mL Erlenmeyer flasks containing 100 g of polished rice were autoclaved before the addition of 20 mL of sterilized water. The rice was inoculated with spores of *A. ochraceus* and incubated for 2 weeks at 25°C. After incubation, 200 mL of chloroform-acetic acid (99:1) was added to the moldy rice in each flask. The extracts collected from the flasks were concentrated and precipitated with 4 L of hexane on a stirrer. The precipitate was dissolved in 500 mL of chloroform and subjected to chromatography using a silica gel column and mobile phases of benzene-acetic acid (100:0 to 88:12) with a linear gradient. The benzene-acetic acid (95:5 and 92.5:7.5) eluates were evaporated to dryness. Benzene was added to the extract, and the solution was heated followed by gentle cooling for crystallization of OTA. The purification of crystals was confirmed by high-performance liquid chromatography according to the method of Sugita-Konishi et al. (20). The purity of OTA was estimated to be greater than 95% from the area

percentage of the chromatogram (data not shown).

Animal treatment

Experiment 1: 4-week feeding study of OTA in gpt delta rats

Groups of 10 male *gpt* delta rats were administered OTA at a concentration of 5 ppm in the basal diet or were fed a basal diet without supplement (control) for 4 weeks. The dietary dose level of 5 ppm was selected as a carcinogenic dose reported in a 2-year carcinogenicity study in rats (51). Based on a preliminary study of OTA stability, the diet was prepared once every week and was stored in the dark at 4°C prior to use. At necropsy, the kidneys were extirpated, weighed, and cut along the long axis. For *in vivo* reporter gene mutation assays, the renal outer medulla (ROM) was macroscopically separated with curving scissors using the arcuate arteries at the boundary of the cortex and medulla as landmarks, as described in a previous report (34). The ROMs were stored at -80°C for *in vivo* mutation assays. Animal treatment of Experiment 1 was

performed in the previous study (34).

Experiment 2: 4-week oral gavage study of OTA in gpt delta rats

Groups of 5 male *gpt* delta rats were administered OTA by gavage, which is a standard method for *in vivo* comet assay, at a doses of 70, 210, or 630 μg/10 mL/kg/day for 4 weeks (7 days per week). Animals in the control group were administrated vehicle (0.1 M sodium bicarbonate water) only. OTA solution in 0.1 M sodium bicarbonate water was prepared once every week and was stored in the dark at 4°C prior to use. The doses of 70 and 210 μg/kg/day are carcinogenic doses reported in a 2-year carcinogenicity study in rats (13), and 210 μg/kg/day is equivalent to a dietary dose of 5 ppm. Animals were sacrificed 3 hours after the last dosing. The kidneys were extirpated, weighed, and cut along the long axis. Half of unilateral kidney was fixed in 10% neutral buffered formalin and routinely processed by embedding in paraffin and sectioning in blocks for immunohistochemical staining. The ROMs were collected as

described in the previous study (34) and used for *in vivo* comet assays, western blotting, and quantitative real-time PCR.

In vivo reporter gene mutation assay (Spi⁻ assay)

The ROMs from groups of 10 animals in Experiment 1 were used. Spi⁻ selection was performed using the method of Nohmi et al. (32). Briefly, genomic DNA was extracted from the ROMs of animals in each group using a Recover Ease DNA isolation kit (Agilent Technologies, Santa Clara, CA, USA), and lambda EG10 DNA (48 kb) was rescued as phages by *in vitro* packaging using Transpack packaging extract (Agilent Technologies). For Spi⁻ selection, packaged phages were incubated with *E. coli* XL-1 Blue MRA for survival titration and *E. coli* XL-1 Blue MRA P2 for mutant selection. Infected cells were mixed with molten lambda-trypticase agar plates. The next day, plaques (Spi⁻ candidates) were punched out with sterilized glass pipettes, and the agar plugs were suspended in SM buffer. The Spi⁻ phenotype was confirmed by spotting

the suspensions on 3 types of plates where XL-1 Blue MRA, XL-1 Blue MRA P2, or WL95 P2 strains were spread in soft agar. Spi$^-$ mutants, which made clear plaques on every plate, were counted.

Mutation spectrum analysis of Spi$^-$ mutants

Mutation spectrum analysis of Spi$^-$ mutants was performed as described in Masumura et al. (52). Briefly, the lysates of the Spi$^-$ mutants were obtained by infection of *E. coli* LE392 with the recovered Spi$^-$ mutants, and the lambda DNA was extracted from the lysates with the Gentra Puregene DNA kit (QIAGEN N.V., Venlo, Netherlands). The extracted DNA was used as a template for PCR analysis to determine the deleted regions. DNA fragments containing the deletions were amplified by PCR using primers 001–002 (5 kb in length), 005–012 (14 kb in length), or 005–006 (21 kb in length), followed by sequencing analysis of the PCR products. Sequence changes within and outside of the *gam/redBA* genes were identified by DNA

sequencing analysis at Takara Bio Inc. (Shiga, Japan). The appropriate primers for DNA sequencing were selected based on the results of PCR analysis. The entire sequence of lambda EG10 is available at http://www.nihs.go.jp/dgm/dgm3/gptdeltainfo.html

For the deletion size analysis, I categorized the deletion sizes into a single base pair (1 bp), 2 bp to 1 kb, and over 1 kb. Single base pair deletions were subdivided into "simple" and "in run"; the former occurred at nonrepetitive sequences, and the latter occurred at repetitive sequences (52).

The PCR primers used in this study were as follows:

primer 001: 5′-CTCTCCTTTGATGCGAATGCCAGC-3′

primer 002: 5′-GGAGTAATTATGCGGAACAGAATCATGC-3′

primer 005: 5′-CGTGGTCTGAGTGTGTTACAGAGG-3′

primer 006: 5′-GTTATGCGTTGTTCCATACAACCTCC-3′

primer 012: 5′-CGGTCGAGGGACCTAATAACTTCG-3′

In vivo comet assay

The ROMs from groups of 5 animals in Experiment 2 were cut into small pieces (1-2 mm sized) in HBSS (without Ca^{2+}/Mg^{2+}) medium with 1 mM EDTA and 25 mM HEPES containing 10% DMSO to obtain cell suspensions. Cell suspension were mixed with 0.5% low-melting point agarose (Takara Bio Inc.) in PBS and deposited on MAS-coated slide glass (Matsunami Glass Ind. Ltd., Osaka, Japan). The slides were placed in a lysis solution (2.5 mM NaCl, 0.1 M EDTA, 10 mM Tris, 10% DMSO, and 1% TritonX-100, pH 10) overnight in a refrigerator. DNA was allowed to denature in electrophoresis buffer (0.3 M NaOH, 1 mM EDTA, pH 13) for 20 min. The slides were placed into a horizontal electrophoresis tank and exposed to 0.7 V/cm (300 mA) for 15 min. The slides were then washed twice in neutralization buffer (0.4 M Tris, pH 7.5) and dehydrated in ethanol for 5 min. After staining with SYBR Gold (Life Technologies, Carlsbad, CA, USA), at least 100 randomly selected cells per slide were

visualized under a fluorescent microscope and subjected to image analysis using Comet Assay IV software (Perceptive Instruments Ltd., Bury St. Edmunds, England). The percentage of DNA in the comet tail (% tail DNA), the tail length, and the tail moment were used to evaluate the extent of DNA damage in individual cells.

Sodium dodecyl sulfate-polyacrylamide gel electrophoresis (SDS-PAGE) and western blotting

The ROMs from groups of 4 animals in Experiment 2 were homogenized using a Teflon homogenizer with ice-cold RIPA lysis buffer (Wako Pure Chemical Co., Osaka, Japan) containing mammalian protease inhibitor cocktail and phosphatase inhibitor cocktail 2 and 3 (Sigma-Aldrich, St. Louis, MO, USA). Samples were centrifuged at 15,000 × *g* for 30 min, and the resulting supernatants were used. Protein concentrations were determined using the Advanced Protein Assay (Cytoskeleton, Denver, CO, USA). Samples were separated by SDS-PAGE and transferred to 0.45-μm

polyvinylidene fluoride membranes (Millipore, Billerica, MA, USA). For detection of target proteins, membranes were incubated with anti-γ-H2AX monoclonal antibodies, anti-Rad51 monoclonal antibodies (Cell Signaling Technology, Inc., Danvers, MA, USA), or anti-actin monoclonal antibodies (pan Ab-5; Thermo Fisher Scientific, Fremont, CA, USA) at 4°C overnight. Secondary antibody incubation was performed using horseradish peroxidase-conjugated secondary anti-rabbit or mouse antibodies (Cell Signaling Technology) at room temperature. Protein detection was facilitated by chemiluminescence using ECL Prime (GE Healthcare, Little Chalfont, United Kingdom), and protein levels were quantified using Image Lab software (Bio-Rad Laboratories, Hercules, CA, USA). Cell extracts for positive control (UV-treated 293 cells) were purchased from Cell Signaling Technology.

Immunohistochemical staining for γ-H2AX

Paraffin-embedded sections from groups of 5 animals in Experiment 2 were used.

Immunohistochemical staining was performed using monoclonal anti-γ-H2AX antibodies (1:50, Cell Signaling Technology) at 4°C overnight followed by incubation with a high polymer stain at room temperature for 30 min (HISTOFINE Simple Stain, Nichirei Bioscience Inc., Tokyo, Japan).

RNA isolation and quantitative real-time PCR for mRNA expression

The ROMs from groups of 5 animals in Experiment 2 were soaked overnight in RNAlater-ICE (Life Technologies) at -20°C, and total RNA was extracted using an RNeasy Mini kit (Qiagen N.V.) according to the manufacturer's instructions. cDNA copies reverse transcribed from total RNA were obtained using a High Capacity cDNA Reverse Transcription kit (Life Technologies). All PCR reactions were performed with primers for rat *Chek1*, *Wee1*, *Ccna2*, *Cdk1*, *Rad51*, *Rad18*, *Brip1*, *Lig4*, *Xrcc5*, *Xrcc6*, *Fen1*, *Xrcc1*, *Ercc1* and *XPA*, and TaqMan Rodent GAPDH Control Reagents were used as an endogenous reference. PCR was carried out in an Applied Biosystems 7900HT

FAST Real-Time PCR System using TaqMan Fast Universal PCR Master Mix and TaqMan Gene Expression Assays (Life Technologies). The expression levels of target genes were calculated by the relative standard curve method and were determined by normalization to *GAPDH* expression. Data were presented as fold-change values of treated samples relative to controls.

Statistical analysis

In Experiment 1, variance in the data for body and kidney weights, Spi$^-$ assays, and mutation spectrum analyses of Spi$^-$ mutants were checked for homogeneity with the F-test. Student's t-tests were applied for homogeneous data, and Welch's t-tests were applied for heterogeneous data. In Experiment 2, variances in the data for body and kidney weights, parameters in comet assays, mRNA levels, and protein density data were evaluated for homogeneity using Bartlett's tests. When the data were homogenous, one-way analysis of variance (ANOVA) was applied. In heterogeneous

cases, the Kruskal-Wallis test was applied. When statistically significant differences were indicated, Dunnett's multiple tests were employed for comparisons between the control and treatment groups. A P value less than 0.05 was considered statistically significant.

Results

Experiment 1

General signs, body weight, and kidney weight

No deaths and no remarkable changes in general signs were observed in any group. In OTA-treated groups, significantly reduced kidney weights were observed (Table 1-1).

Spi⁻ assays and Spi⁻ mutation spectrum analyses of Spi⁻ mutants

Data for Spi⁻ selection assessing deletion mutations are summarized in Table 1-2. There was a statistically significant increase in Spi⁻ mutant frequencies (MFs) in the OTA 5 ppm group. The results of mutation spectrum analyses of Spi⁻ mutants were summarized in Table 1-3. All sizes of deletion mutations, insertions, and base substitutions tended to increase following OTA treatment. In particular, the specific mutation frequency of deletions over 1 kb increased about 5-fold in the OTA treatment group as compared with the control group. Detail characterization of deletions over 2

bp and complex-type deletions identified from OTA-treated and control rats are shown in Fig. 1-1. “Complex-type mutants” were defined as deletion mutants whose deletion sizes were not identified or whose junctions were unable to be identified by PCR and sequencing analysis because of complex rearrangements (52). Sizes of OTA-induced deletion were in the range of 1 to 5,999 bp. Sequences of the junctions of deletions induced by OTA varied and included direct junctions, with microhomology (1–3 bp) or with short insertions (2–3 bp).

Experiment 2

General signs, body weight, and kidney weight

There were no deaths or remarkable changes in general signs in all groups. As compared with the control group, significant decrease in body weights was observed at 630 μg/kg group. Decreases in kidney weights were observed following OTA treatment in a dose-dependent manner (Table 1-4).

In vivo comet assay

DNA damage parameters determined by *in vivo* comet assay using ROM of the *gpt* delta rats treated with OTA are summarized in Fig. 1-2. There were statistically significant increases in tail intensity, tail length, and tail moment in all OTA-treated groups.

Western blotting and immunohistochemical staining

Western blotting analysis using anti-γ-H2AX and anti-Rad51 monoclonal antibodies demonstrated increases in the protein expression levels of these targets in the ROMs of *gpt* delta rats treated with various doses OTA (Fig. 1-3A). In addition, there were significant increases in the relative density of protein bands representing γ-H2AX at OTA doses of 210 and 630 μg/kg, using actin as a loading control (Fig. 1-3B). Immunohistochemistry analysis revealed punctate signals representing γ-H2AX protein

in the nuclei of tubular epithelial cells located in outer stripe of the ROM (S3) of *gpt* delta rats treated with OTA (Fig. 1-4).

Quantitative real-time PCR

Expression levels of mRNAs encoding cell cycle-related proteins were examined. G_2/M arrest-related genes, i.e., *Chek1* and *Wee1*, and S/G_2 phase-related genes, i.e., *Ccna2* and *Cdk1*, were all increased by OTA treatment in a dose-dependent manner (Fig. 1-5). The expression of genes involved in homologous recombination repair (*Rad51*, *Rad18*, and *Brip1*) was significantly increased by OTA treatment in a dose-dependent manner (Fig. 1-6). On the other hand, the expression of mRNAs involved in nonhomologous end joining repair (*Xrcc5*, *Xrcc6*, and *Lig4*) were not altered by OTA treatment (Fig. 1-7). The expressions of mRNAs involved in base excision repair (*Fen1* and *Xrcc1*) and nucleotide excision repair (*Ercc1*, *Xpa*) were not increased by OTA treatment (Fig. 1-8).

Discussion

In the present study, 4-week feeding of OTA at a carcinogenic dose increased Spi$^-$ MFs in the ROMs of *gpt* delta rats, in line with the previous report (34). Mutation spectrum analysis of Spi$^-$ mutants (*red/gam* mutants) demonstrated that OTA caused deletion mutations of various sizes, ranging from 1 to 5,999 bp. In particular, the specific mutation frequencies of deletions over 1 kb in OTA-treated rats increased 5-fold compared with those in the control group. As reported in *in vitro* study (53), these data implied that OTA induced large deletion mutations at the carcinogenic target site.

Exposure of *gpt* delta mice to IR, UVB, and MMC induced large deletions of over 1 kb in the *red/gam* genes at relatively higher level (37). These environmental mutagens are known to induce DNA DSBs possibly due to their characteristic properties, i.e., direct and/or indirect disjuncture of chemical bonds by IR energy, inhibition of DNA replication fork interactions with UV-induced photoproducts, and MMC-induced

intrastrand cross-linking (41, 42, 54). Given that the occurrence of DSBs is thought to be a trigger for large deletion mutations (37, 55, 56), it is highly probable that OTA has the potential to accumulate DSBs.

As DSBs are the most dangerous type of DNA damage affecting maintenance of cellular function, the DNA damage response (DDR), leading to cell cycle arrest and DNA repair, is initiated by DSBs for cellular defense against the accumulation of gene mutations (57, 58). As one of primary and crucial events of the DDR, ATM-mediated phosphorylation of H2AX (γ-H2AX) occurs, which facilitates the recruitment and retention of a number of DSB repair factors to sites of DSBs (46,59). Therefore, the expression of γ-H2AX is thought to be a promising marker of DSBs (60, 61). In the present study, western blot analysis using protein extracts from ROMs of *gpt* delta rats revealed obvious increases in γ-H2AX expression by OTA treatment in a dose-dependent manner. In addition, immunohistochemical analysis clearly demonstrated the site-specific localization of γ-H2AX-positive cells in the tubular

epithelium of the outer stripe of the ROM. Comet assays using ROMs of *gpt* delta rats treated with OTA yielded positive results, suggesting DNA strand breaks, as previously reported (62, 63, 64, 65). The overall data strongly indicated that OTA induced DSBs in the ROMs of *gpt* delta rats.

As the detrimental effects of OTA on steric structures of DNA, the formation of OTA-specific DNA adducts were observed in human tissues by ^{32}P postlabeling methods, and were confirmed by mass spectrum analysis in animal tissues (17, 66, 67, 68). The appearance of apurinic/apyrimidinic (AP) sites in the rat kidney, as well as inhibition of topoisomerase II (TOPOII) activity in cultured cells, have also been reported (69, 70). It has been accepted that DSBs occur through various causes, such as inhibition of the replication fork due to the formation of bulky adducts, cleavage of AP sites during base excision repair, and suppression of TOPOII activity (71, 72, 73). In particular, AP site are known to be related with oxidative stress (17). However, in the previous study, 8-OHdG (8-hydroxydeoxyguanosine) levels in the kidney DNA of

rats treated with OTA were not changed (34). Treatment with antioxidant affected OTA-induced renal toxicity, but not the carcinogenicity (74). Thus, the precise mechanisms underlying OTA-induced DSBs remain unclear.

Gene mutations derived from DSBs arise during the repair process, and there are 2 major pathways mediating DNA repair, NHEJ and HR (47, 48, 75). These two pathways are mutually exclusive, and the major factor determining which pathway is used is the cell cycle stage (76). In NHEJ, Xrcc5 and Xrcc6 bind onto broken ends followed by direct ligation by Lig4, and this process occurs throughout the cell cycle (77). In contrast, HR is initiated by resection of broken ends through interaction with BRCA1, generating single-stranded DNA onto which the Rad51 recombinase assembles as a nucleoprotein filament. Since this structure invades homologous duplex DNA of sister chromatids, which are used as templates for repair DNA synthesis, HR is more effective in late S and G_2 phases of cell cycle (78, 79). OTA induces G_2/M arrest and increases cell proliferation through another functional mechanism, thereby increasing

the ratio of cells in S/G_2 phase (80, 81, 82). In fact, the present quantitative PCR analysis of mRNA expression also demonstrated that genes related to G_2/M arrest (*Chek1* and *Wee1*) and S/G_2 phase (*Ccna2* and *Cdk1*) were significantly increased by OTA treatment in a dose-dependent manner. In particular, CDK1 has been reported to accelerate the resection of broken ends in the HR process and simultaneously inhibits NHEJ (74, 75), implying that DSBs induced by OTA may be repaired predominantly by HR. Additional quantitative PCR analysis has shown that the mRNA expression levels of HR factors (*Rad51* and *Rad18*: recruiters of Rad51 (83), *Brip1*: interactor with BRCA1 (84)) increased in response to OTA in a dose-dependent manner, and confirmation of Rad51 overexpression at the protein level strongly support my hypothesis, despite specific mutation frequencies at the junction sites of Spi^- mutants, revealing no obvious characteristics of HR (85). In contrast, no OTA treatment-related changes were detected in NHEJ factors (*Xrcc5*, *Xrcc6*, and *Lig4*), which were reported to be altered during NHEJ in response to IR (86). In general, HR is believed to be an

error-free repair system. However, there have been several evidences that HR can induce large deletion mutations (47, 87). Although it is also known that excision of bulky adducts may be a potential source of large deletions (88), the present data showed that mRNA levels of genes related to base excision and nucleotide excision repair were not increased by OTA treatment. Thus, the overall data suggested that large deletions induced by OTA may occur during HR.

In conclusion, the present data clearly indicated that OTA induced DSBs at carcinogenic target sites in the DNA of *gpt* delta rats when applied at carcinogenic doses. OTA-induced DSBs appeared to be predominantly repaired by HR, consequently leading to large deletion mutations. Further studies are necessary to clarify the mechanisms underlying OTA-induced DSBs.

Group	Deletion size	Sequence of the junction of deletion
Control	**-1267 bp** (with microhomology 12)	cgcgagttttgaatg gttcgcggcggc gtgtttgtgcatcca
	Complex (recombination with complimentary sequence)	ctctcctttgatgcg atcgccagcatttcg
	Complex	Not identified
OTA 5 ppm	**-136 bp**	gccgacacgttcagc atcgtcatcaaacgc
	-2454 bp (with microhomology 3 bp)	tcgtctgtttctact ggt tgcgattcagcgaga
	-2294 bp +2 bp (with insertion 2 bp)	caacatcgtcatcaa <gg> cttaatatcttcaac
	-3900 bp	atgtctgccatcttt aaggagatagcaaat
	-4253 bp + 3 bp (with insertion 3 bp)	ggcgttgcaaatgat <tta> cgaccaaatgccgct
	-4474 bp	atctacataaacacc aggtgagagatctga
	-5528 bp (with microhomology 1 bp)	tgattgcgcctaccc g accacgcctttgggg
	-5999 bp (with microhomology 3 bp)	tcagtggcgtggagt gca tccatctggattctc
	Complex (recombination with unknown sequence)	cttttgtgaaaggga gcagtggcgggggc
	Complex	Not identified

Figure 1-1 Detail characterization of over 2 bp deletions recovered from the renal outer medulla (ROM) of *gpt* delta rats treated with OTA for 4 weeks.

A partial genetic map of the lambda EG10 transgene including the *gam* and *redBA* target region of Spi$^-$ selecton is shown in the right part. Horizontal gray bars represent the deleted regions of mutants. Junctions are indicated as spaces between left and right sequences. Short homologous sequences in the junctions of the mutants are underlined. Inserted sequences are shown in <parenthesis>. The exact junctions and deletion sizes of "complex" deletions could not be determined due to complex recombination.

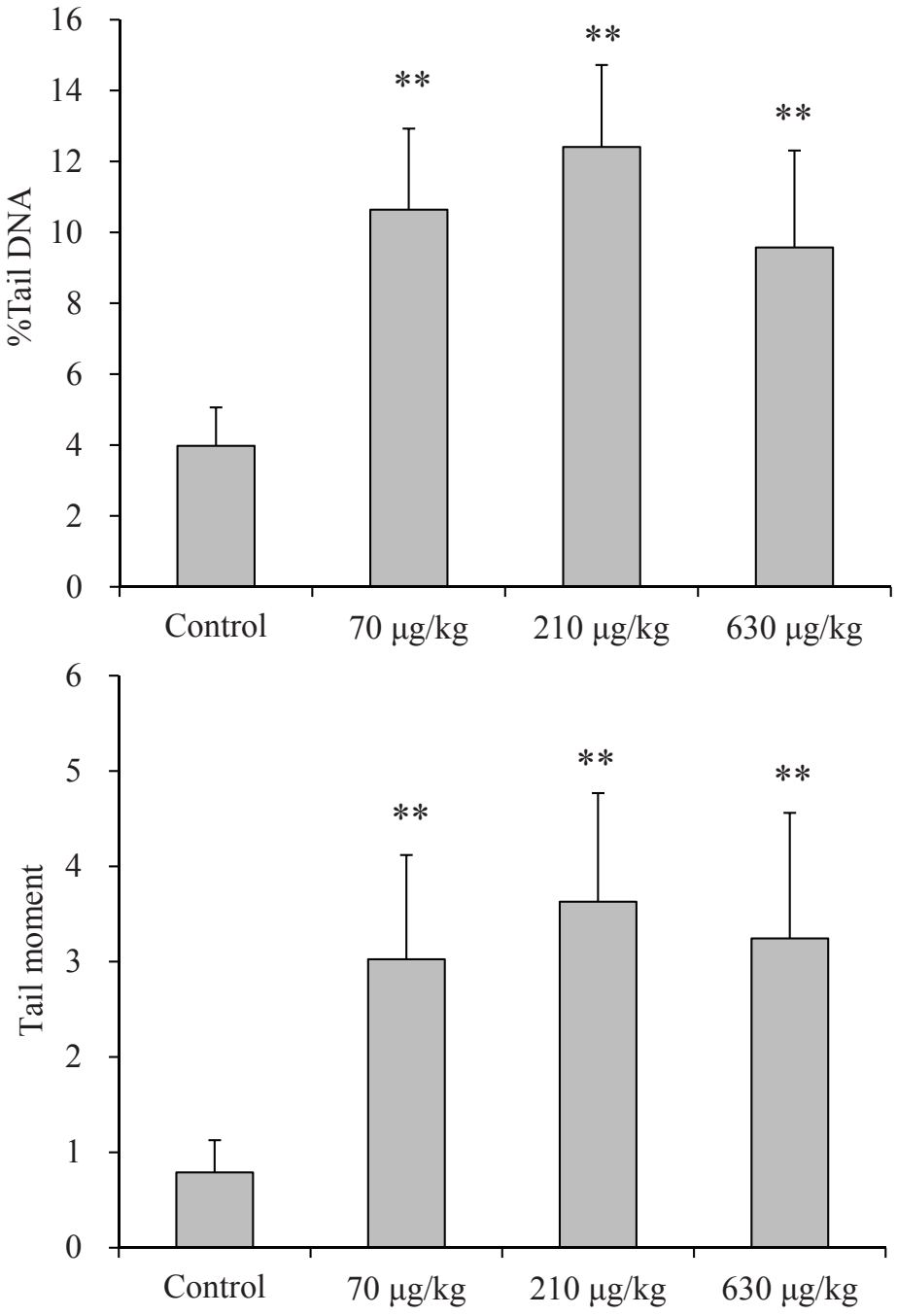

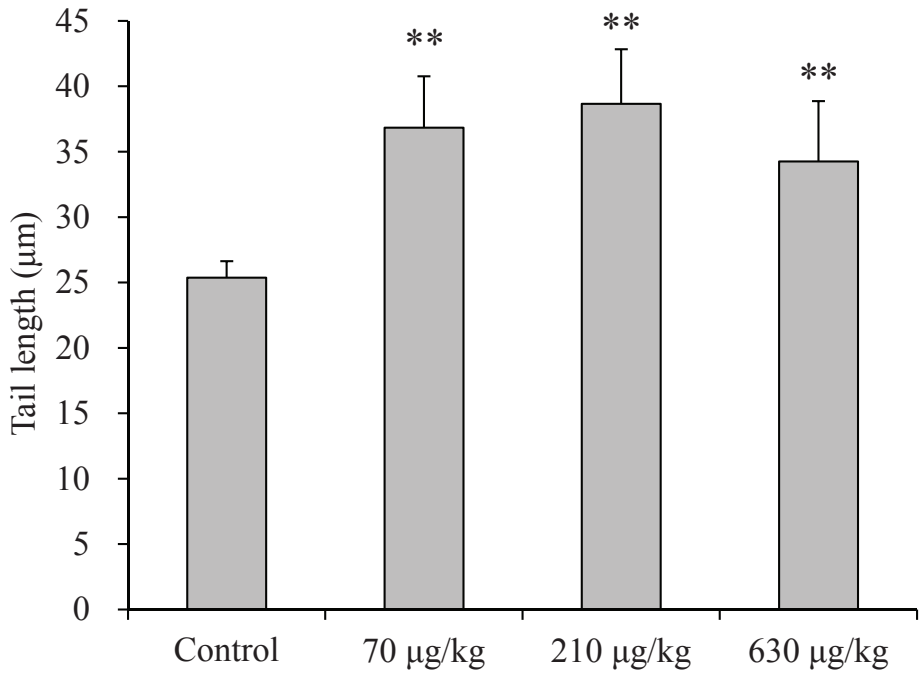

Figure 1-2 Parameters for *in vivo* comet assay in the ROM of *gpt* delta rats treated with OTA by oral gavage for 4 weeks.

Each value is the mean ± SDs of data for 5 rats.

**: Significantly different from the control group at $p < 0.01$.

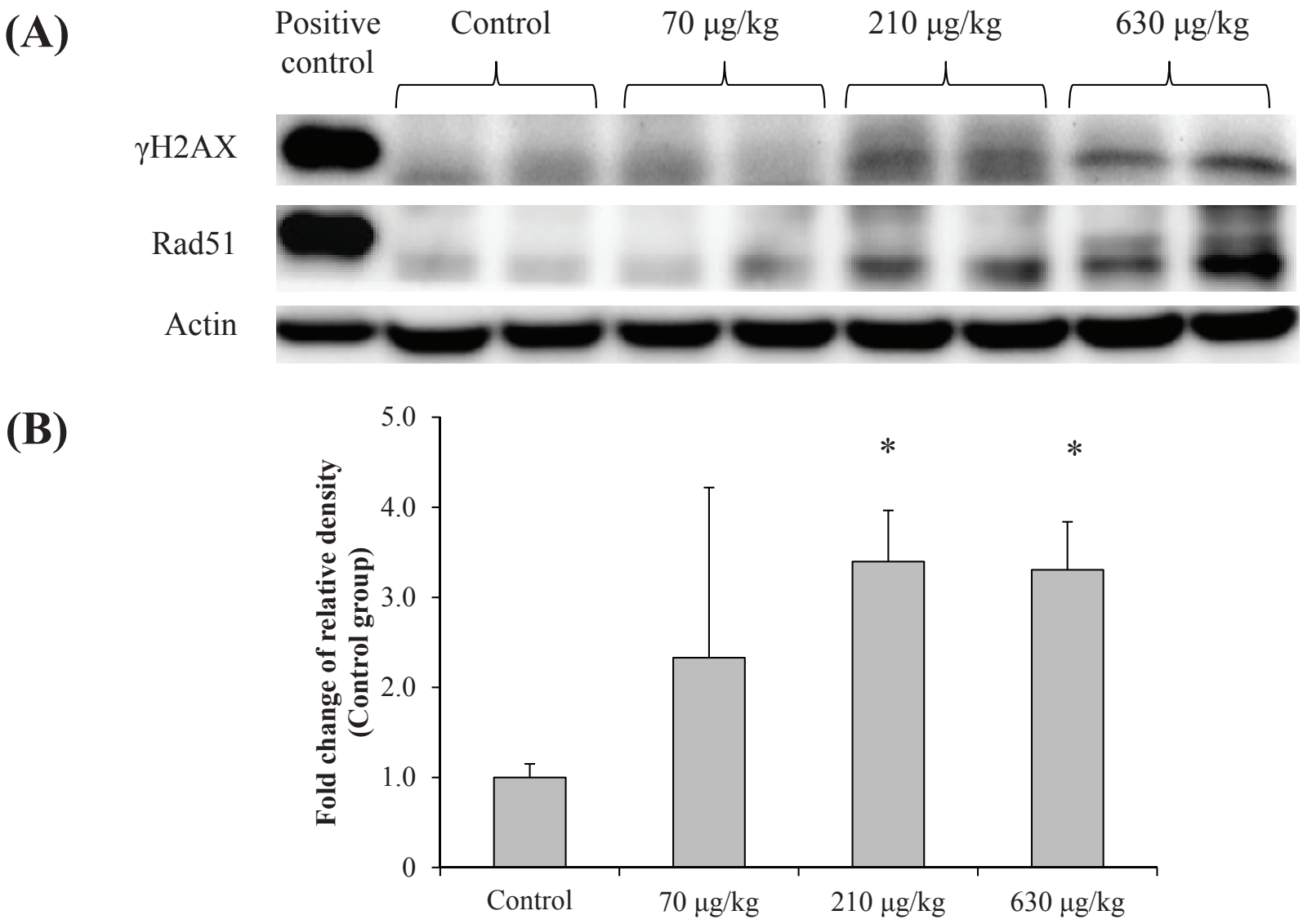

Figure 1-3 (A) Western blotting analysis of γ-H2AX and Rad51 from the ROM of *gpt* delta rats treated with OTA for 4 weeks.

Positive control: Extracts of UV-treated 293 cell.

(B) Densitometric analysis of γ-H2AX signals normalized to actin levels in the same tissue sample.

Each value is the mean ± SDs of data for 4 rats. *: Significantly different from the control group at $p < 0.05$.

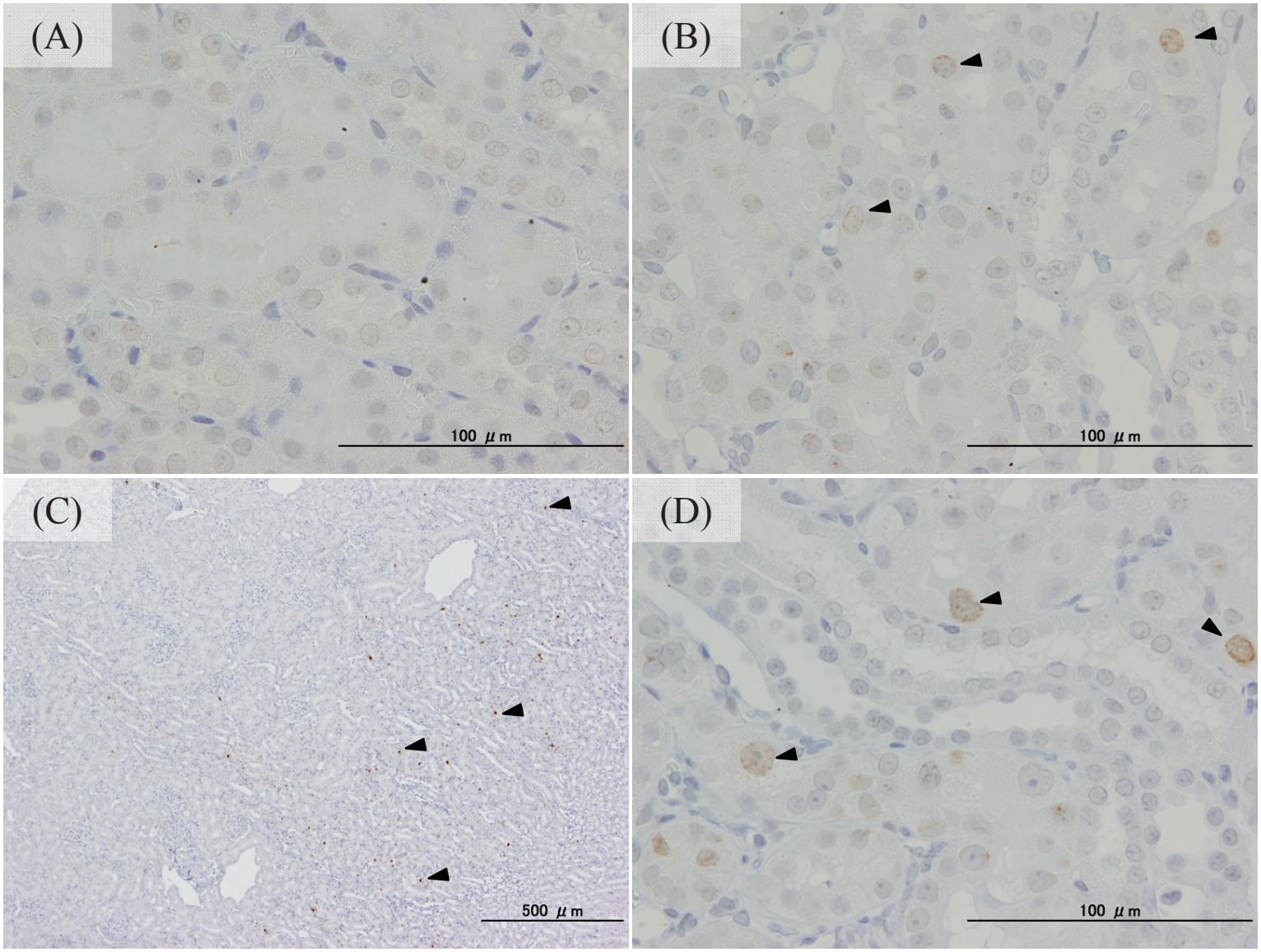

Figure 1-4 Immunohistochemical staining of γ-H2AX in the kidney of *gpt* delta rats treated with vehicle (A: control) and OTA 210 μg/kg (B) and 630 μg/kg (C, D) for 4 weeks.

Note no remarkable signal was observed in the control section. In the 210 and 630 μg/kg sections, punctate signals (arrow head) were observed in the nuclei of proximal tubule epithelium, which were specifically located at the outer stripe of the ROM.

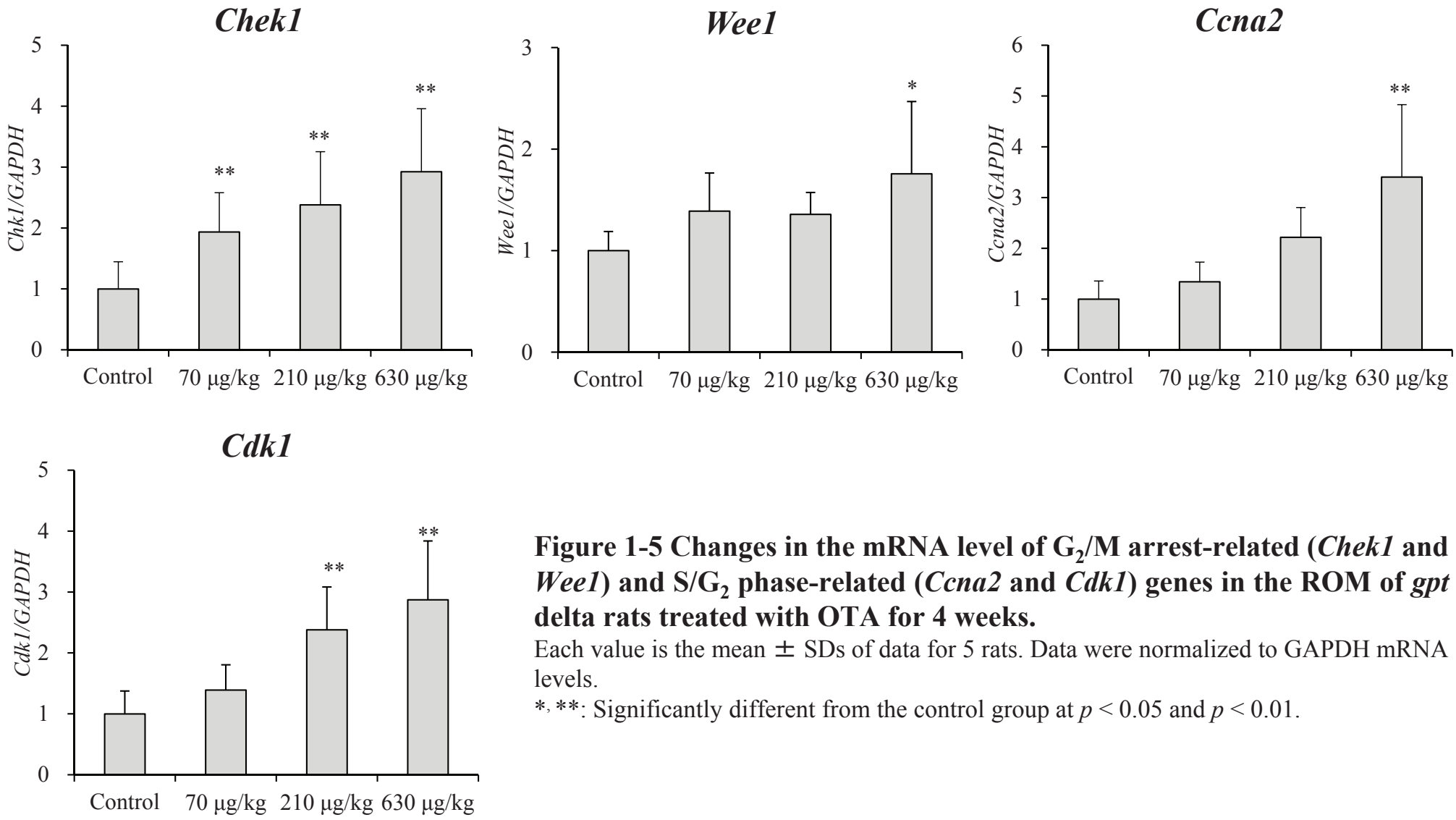

Figure 1-5 Changes in the mRNA level of G_2/M arrest-related (*Chek1* and *Wee1*) and S/G_2 phase-related (*Ccna2* and *Cdk1*) genes in the ROM of *gpt* delta rats treated with OTA for 4 weeks.

Each value is the mean ± SDs of data for 5 rats. Data were normalized to GAPDH mRNA levels.

*, **: Significantly different from the control group at $p < 0.05$ and $p < 0.01$.

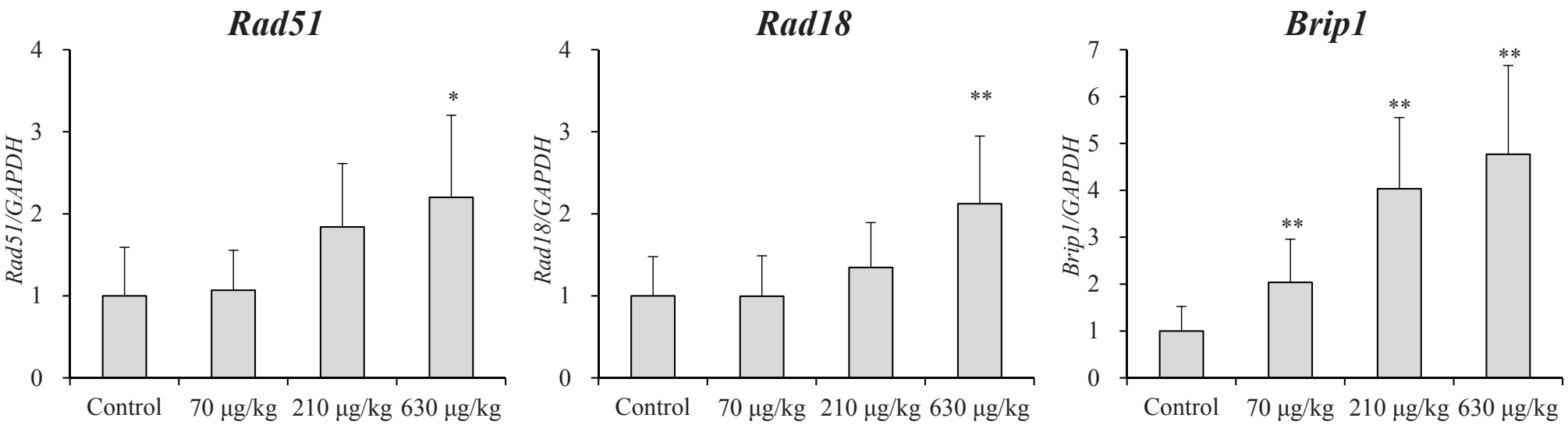

Figure 1-6 Changes in the mRNA level of homologous recombination repair-related genes (*Rad51*, *Rad18*, *Brip1*) in the ROM of *gpt* delta rats treated with OTA for 4 weeks.

Each value is the mean ± SDs of data for 5 rats. Data were normalized to GAPDH mRNA levels.

*, **: Significantly different from the control group at $p < 0.05$ and $p < 0.01$.

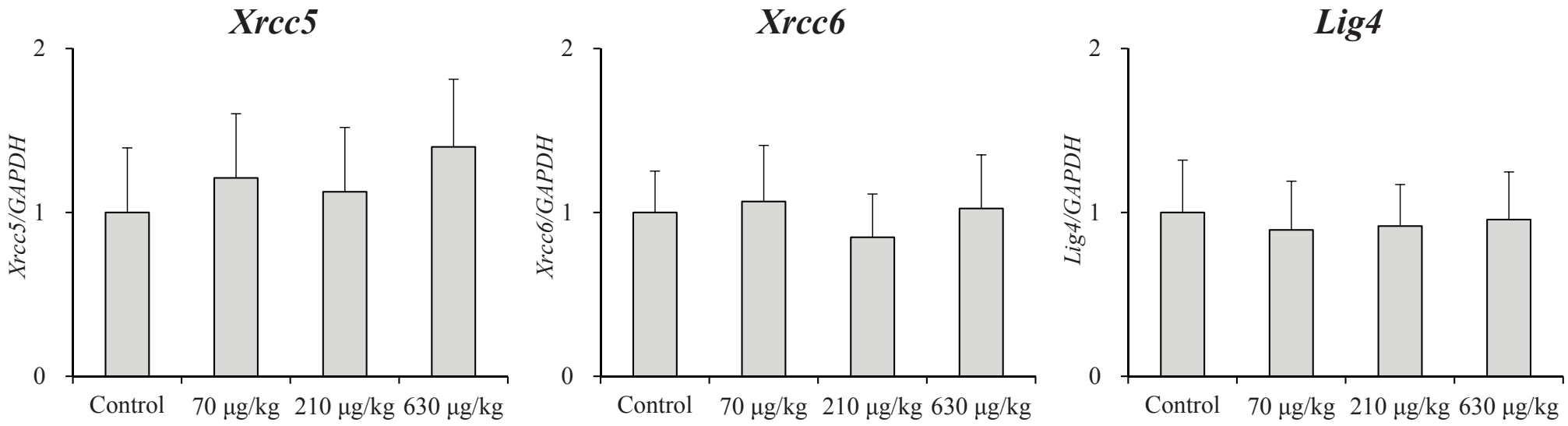

Figure 1-7 Changes in the mRNA level of nonhomologous end joining-related genes (*Xrcc5*, *Xrcc6* and *Lig4*) in the ROM of *gpt* delta rats treated with OTA for 4 weeks.

Each value is the mean ± SDs of data for 5 rats. Data were normalized to GAPDH mRNA levels.

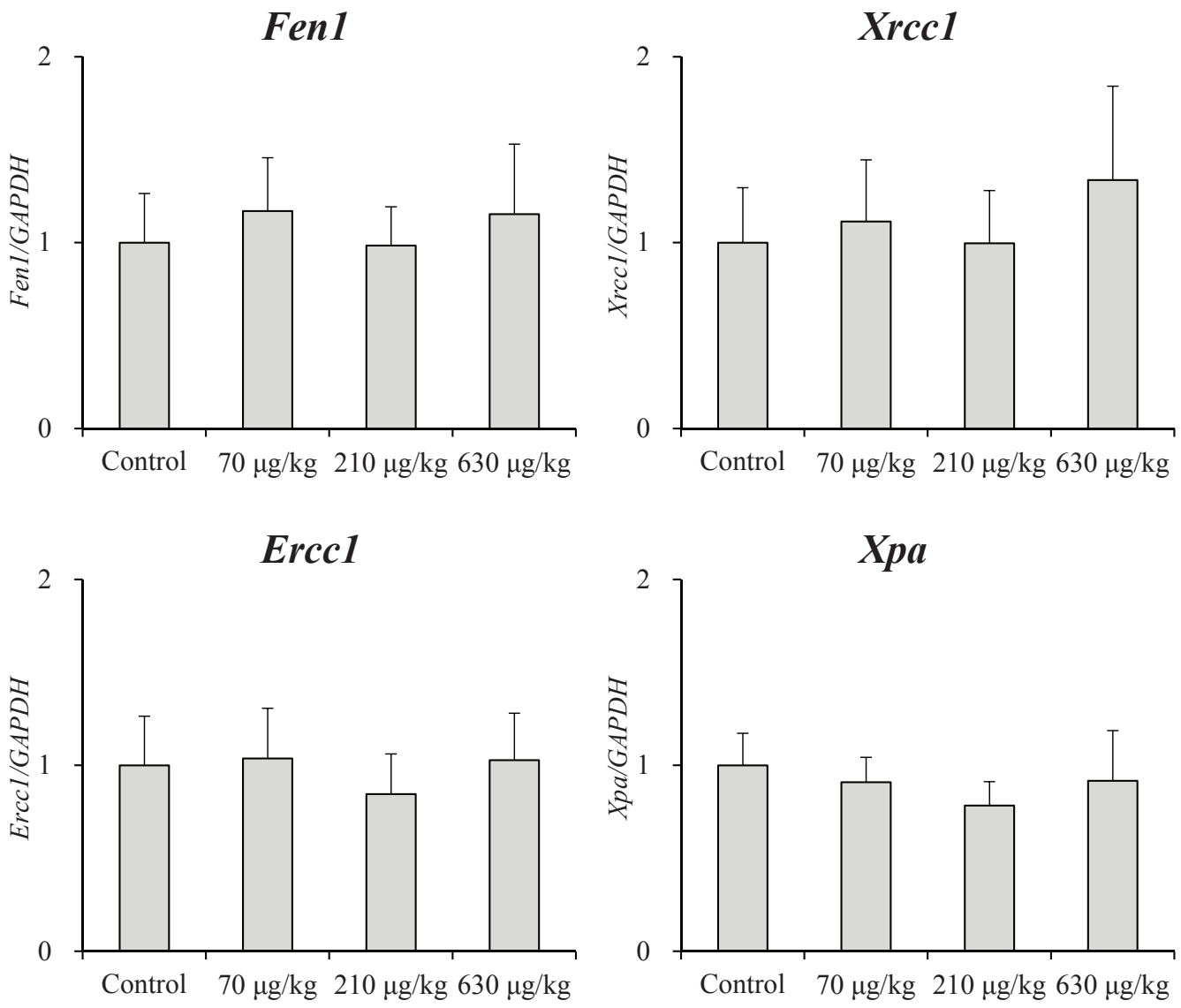

Figure 1-8 Changes in the mRNA level of base excision repair-related (*Fen1*, *Xrcc1*) and nucleotide excision repair-related (*Ercc1*, *Xpa*) genes in the ROM of *gpt* delta rats treated with OTA for 4 weeks.

Each value is the mean ± SDs of data for 5 rats. Data were normalized to GAPDH mRNA levels.

Table 1-1 Final average body and kidney weights of F344 *gpt* delta rats treated with OTA for 4 weeks.

Group	Final body weight (g)	Kidney weight	
		Absolute (g)	Relative (g%)
Control	239.0 ± 15.1[a]	1.71 ± 0.07	0.72 ± 0.03
OTA 5 ppm	236.4 ± 14.8	1.42 ± 0.09**	0.60 ± 0.04**

[a]: Mean ± SD

** Significantly different from the control group at $p < 0.01$.

Table 1-2 Spi$^-$ mutant frequencies (MFs) in the ROM of F344 *gpt* delta rats treated with OTA for 4 weeks.

Group	Animal No.	Plaques within XL-1 Blue MRA (× 10^5)	Plaques within WL95 (P2)	MFs (× 10^{-6})	Mean ± SD
Control	1	12.5	5	4.00	2.37 ± 1.92
	2	20.4	1	0.49	
	4	16.2	1	0.62	
	5	14.8	1	0.68	
	6	16.0	5	3.12	
	7	11.7	7	5.98	
	8	15.4	1	0.65	
	9	15.7	5	3.19	
	10	11.7	3	2.56	
OTA 5 ppm	11	17.3	9	5.21	4.56 ± 1.94*
	12	15.8	5	3.17	
	13	15.1	4	2.65	
	14	10.5	7	6.65	
	15	13.7	6	4.39	
	16	19.3	4	2.08	
	17	10.2	8	7.87	
	18	12.2	4	3.27	
	19	15.3	10	6.54	
	20	13.3	5	3.75	

* Significantly different from the control group at $p < 0.05$.

Table 1-3 Mutation spectra of Spi$^-$ mutatnts in the ROM of F344 *gpt* delta rats treated with OTA for 4 weeks.

Groups		Control			OTA 5 ppm		
		No.	%	Specific mutation frequencies ($\times 10^{-6}$)	No.	%	Specific mutation frequencies ($\times 10^{-6}$)
1bp deletion		25	86	2.06 ± 1.79[a]	46	73	3.34 ± 1.46
	Simple						
	G/C	4	14	0.31 ± 0.49	11	17	0.83 ± 0.85
	A/T	0	0	0	1	2	0.08 ± 0.24
	In run						
	G/C	10	34	0.88 ± 1.20	18	29	1.37 ± 0.77
	A/T	11	38	0.87 ± 0.66	16	25	1.07 ± 0.95
2 bp ～1 kb		0	0	0	1	2	0.07 ± 0.23
>1 kb		2	7	0.14 ± 0.29	8	13	0.67 ± 1.00
Complex		1	3	0.09 ± 0.28	3	5	0.19 ± 0.44
Insertion		0	0	0	1	2	0.06 ± 0.18
Base substitution		1	3	0.07 ± 0.21	4	6	0.29 ± 0.39

[a]: Mean ± SD

Table 1-4 Final body and kidney weights of F344 *gpt* delta rats treated with OTA by oral gavage for 4 weeks.

Group	Final body weight (g)	Kidney weight	
		Absolute (g)	Relative (g%)
Control	232.4 ± 16.5[a]	1.62 ± 0.11	0.70 ± 0.03
OTA 70 μg/kg	239.7 ± 15.1	1.54 ± 0.11	0.64 ± 0.02**
OTA 210 μg/kg	229.5 ± 11.8	1.36 ± 0.05**	0.59 ± 0.03**
OTA 630 μg/kg	214.6 ± 15.3*	1.22 ± 0.09**	0.57 ± 0.01**

[a]: Mean ± SD

*, **: Significantly different from the control group at $p < 0.05$ and $p < 0.01$.

Chapter 2

Role of p53 in the progression from ochratoxin A-induced DNA damage to gene mutations in the kidneys of mice

Abstract

Carcinogenic doses of ochratoxin A (OTA) cause increases of mutant frequencies (MFs) of the *red/gam* gene (Spi^-) in the kidneys of *p53*-deficient *gpt* delta mice, but not in *p53*-proficient mice. Here, I investigated the role of p53 in the progression from OTA-induced DNA damage to gene mutations. To this end, *p53*-proficient and -deficient mice were administered 5 mg/kg OTA for 3 days or 4 weeks by gavage. After 3 days of administration, comet assays were performed and there were no differences in the degrees of OTA induced DNA damage between *p53*-proficient and -deficient mice. However, the frequencies of γ-H2AX-positive tubular epithelial cells in *p53*-deficient mice were significantly higher than those in *p53*-proficient mice, implying that p53 inhibited the progression from DNA damage to DNA double strand breaks (DSBs). Evaluation of global gene expression and relevant mRNA/protein expression levels demonstrated that OTA increased the expression of *Cdkn1a*, which encodes the p21 protein, in *p53*-proficient mice, but not in *p53*-deficient mice. Moreover, in *p53*-deficient mice, mRNA levels of cell cycle progression and DSB repair (homologous recombination repair [HR])-related genes were significantly increased. Thus, G_1/S arrest due to activation of the p53/p21 pathway may contribute to the prevention of DSBs in *p53*-proficient mice. In addition, single base

deletions/insertions/substitutions were predominant, possibly due to HR. Overall, these results suggested that OTA induced DSBs at the carcinogenic target site in mice and that p53/p21-mediated cell cycle control prevented an increase in the formation of DSBs, leading to gene mutations.

Introduction

Ochratoxin A (OTA), a nephrotoxic mycotoxin, is regarded as a possible human carcinogen because it exhibits renal carcinogenicity, targeting proximal straight tubules in both of rats and mice (9, 13, 16). Although the mechanism of the carcinogenic action of OTA is not fully understood, studies have suggested the involvement of genotoxic mechanisms in OTA-induced carcinogenesis. Recent experiments demonstrated the presence of OTA-specific DNA adducts in the kidneys of rats (66). Moreover, exposure to OTA induces DNA double-strand breaks (DSBs) followed by mutations in *red/gam* genes (Spi^-) at the carcinogenic target site of *gpt* delta rats (34, 89). Interestingly, OTA increases mutant frequencies (MFs) of Spi^- in the kidneys of *p53*-deficient *gpt* delta mice, but not in wild-type mice (35). Moreover, OTA increases p53 protein levels in the kidneys of mice and upregulates p53 target genes in the kidneys of rats (35, 43, 81). Therefore, it is likely that p53 is activated by OTA treatment and consequently prevents OTA-induced gene mutations.

Recent studies have demonstrated that p53 plays a critical role in regulation of various DNA repair systems, including nucleotide excision, DSB repair, and translesion synthesis, and partially in base excision, through transactivation-dependent or -independent mechanisms (90, 91). Because my previous data showed that large

deletion mutation occurred in the kidneys of OTA-treated rats during DSB repair (89), disruption of the repair process due to lack of p53 might be responsible for the high susceptibility of *p53*-deficient mice to OTA-induced mutagenicity. On the other hand, after exposure to various types of genotoxic stresses, p53 transactivates a collection of target genes associated with inhibition of cell cycle progression and promotion of apoptosis, thereby preventing genomic instability (92). Therefore, p53 may function at various steps to prevent OTA-induced mutagenesis. Clarification of the roles of p53 activity in several steps from formation of DNA damage to gene mutations will be useful for improving our understanding of OTA-induced genotoxicity and carcinogenicity.

In the present study, I first performed *in vivo* comet assays and immunohistochemical analyses of γ-H2AX in the kidneys of *p53*-proficient and -deficient mice treated with OTA to clarify the site of p53 activity during progression from chemical exposure to the occurrence of DSBs. Secondly, global gene expression analysis using cDNA microarray, followed by semiquantitative analyses of the mRNA and/or protein expression levels of relevant targets were performed for *p53*-proficient and -deficient OTA-treated mice to investigate p53-dependent and -independent gene fluctuations during OTA-induced mutagenesis. Finally, I analyzed the mutation

spectrum of Spi$^-$ mutants obtained from the kidneys of *p53*-deficient *gpt* delta mice treated with OTA, and the molecular mechanisms involved in OTA-induced mutagenesis were clarified.

Materials and Methods

Experimental animals and housing conditions

The protocol for this study was approved by the Animal Care and Utilization Committee of the National Institute of Health Sciences. Homozygous *p53*-deficient ($p53^{-/-}$) and -proficient ($p53^{+/+}$) mice were acquired by intercrossing of heterozygous *p53*-deficient ($p53^{+/-}$) mice with a C57BL/6 background, as established by Tsukada et al. (93). Homozygous *gpt* delta transgenic mice of the C57BL/6J genetic background, which carries 80 tandem copies of the transgene lambda EG10 (32), were mated with heterozygous of *p53*-deficient ($p53^{+/-}$) mice also of the C57BL/6J background (93); *p53*-proficient ($p53^{+/+}$) and heterozygous *p53*-deficient ($p53^{+/-}$) *gpt* delta mice were obtained. Homozygous *p53*-deficient ($p53^{-/-}$) *gpt* delta mice were then acquired by intercrossing heterozygous *p53*-deficient ($p53^{+/-}$) *gpt* delta mice. Genotypes of the *p53* and *gpt* genes were examined by polymerase chain reaction (PCR), as described in previous studies (93, 94). Male *p53*-proficient and -deficient mice (10 weeks old) and male *p53*-proficient and -deficient *gpt* delta mice (10 weeks old) were used for experimentation. Animals were housed in polycarbonate cages (5 mice per cage) with wood chips in a room with a barrier system and were maintained under constant temperature (23 ± 2°C), relative humidity (55% ± 5%), and lighting (12-h light/dark

cycle) with regular air changes (12 times/h). All mice had free access to an Oriental CRF-1 basal diet (Oriental Yeast Co., Ltd., Tokyo, Japan) and tap water.

Test compound

OTA and methyl methane sulfonate (MMS) were purchased from Sigma (Sigma-Aldrich Co., St. Louis, MO, USA). OTA was dissolved in vehicle (0.1 M sodium bicarbonate water) and stored at -20°C before use. MMS was dissolved in distilled water and stored at 4°C in a refrigerator before use.

Animal experiment

Experiment 1

Groups of male *p53*-proficient and -deficient mice (n = 5 each) were administered 5 mg/5 mL/kg OTA by oral gavage once daily for 3 days. Animals in the control groups received vehicle only. Dose levels were selected based on the carcinogenic dose reported in a 2-year carcinogenicity study in mice (12) and the previous study (35). Three hours after the final administration, the kidneys were excipitated and used for *in vivo* comet assays. For the positive control group, mice were administered one dose of 50 mg/5 mL/kg MMS and sacrificed 24 h later.

Experiment 2

Groups of male *p53*-proficient and -deficient mice (n = 10 each) were administered 5 mg/5 mL/kg OTA by oral gavage once daily for 4 weeks (5 consecutive days per week). At necropsy, about 72-hours after the last dosing, kidneys were weighed, and a portion of the harvested kidneys was fixed in 10% neutral buffered formalin. Fixed tissues were embedded in paraffin, sectioned, and stained with hematoxylin and eosin (HE) or used for immunohistochemical staining. The remaining kidney tissues were stored at -80°C for analysis of gene, mRNA, and protein expression.

Experiment 3

Groups of male *p53*-proficient and -deficient *gpt* delta mice (n = 5 each) were administered 5 mg/5 mL/kg OTA by oral gavage once daily for 4 weeks (5 consecutive days per week). At necropsy, about 72-hours after last dosing, kidneys were stored at -80°C for reporter gene mutation assays (Spi^- assays). Unlike in the rat case in chapter 1, mice kidneys were too small to divide renal cortex and outer medulla, and whole kidneys were used for Spi^- assays.

In vivo comet assay

The kidney tissues from groups of 5 animals in Experiment 1 were used for *in vivo* comet assay. The procedure of comet assay is described in the Chapter 1.

Measurement of apoptosis and karyomegaly

Apoptotic and karyomegalic cells of the renal tubules in HE-stained sections were counted in 4–5 randomly selected areas in the outer medulla of each animal (magnification, 200×), and the percentages of these cells were calculated relative to at least 1000 renal tubule cells in the outer stripe of outer medulla (OSOM). Apoptotic cells were identified morphologically by nuclear pyknosis, the appearance of apoptotic bodies, and increased cytoplasmic eosinophilia. Karyomegalic cells were identified morphologically as cells having nuclei at least 2-3 times larger than the standard nucleus size of renal tubule cells in the outer medulla.

Immunohistochemical staining for γ-H2AX and cleaved caspase-3

Paraffin-embedded sections from groups of 4-5 animals in Experiment 2 were analyzed. Immunohistochemical staining for γ-H2AX was performed as described in Chapter 1. At least 1,000 tubular cells located at the renal cortex (CO) and OSOM were counted

for each kidney, and percentages of γ-H2AX-positive cells were calculated. Immunohistochemical staining for cleaved caspase-3 was performed using polyclonal anti-cleaved caspase-3 (1:100, Cell Signaling Technology) at 4°C overnight followed by incubation with biotin-labeled rabbit IgG and visualization by ABC method.

Enzyme-linked immunosorbent assay for detection of p53

The kidneys from groups of 5 animals in Experiment 2 were homogenized using a Teflon homogenizer with 2 volumes of ice-cold RIPA lysis buffer (Wako Pure Chemical Co., Osaka, Japan) containing mammalian protease inhibitor cocktail (Sigma-Aldrich). Samples were centrifuged at 10,000 × *g* for 20 min, and the resulting supernatants were used. Concentrations of p53 per μg tissue were determined using a pan p53 enzyme-linked immunosorbent assay (ELISA) kit (Roche Applied Science, Penzberg, Germany).

RNA isolation

The frozen stored kidneys from groups of 5 animals in Experiment 2 were soaked overnight at -20°C in RNAlater-ICE (Applied Biosystems/Ambion, Austin, TX, USA), and total RNA was then isolated using RNeasy Mini Kits (Qiagen GmbH, Hilden,

Germany). The concentration and quality of total RNA were analyzed using a UV-VIS spectrophotometer (Nanodrop ND-1000, NanoDrop Technologies, Wilmington, DE, USA) and an Agilent 2100 Bioanalyzer (Agilent Technologies, Santa Clara, CA, USA).

Global gene expression analysis by cDNA microarray

Total RNA from groups of 4 animals in Experiment 2 were labeled with cyanine-3 dye using a Quick Amp Labeling Kit (Agilent Technologies). RNA concentration, dye incorporation, and quality were analyzed using a UV-VIS spectrophotometer and an Agilent 2100 Bioanalyzer. Fluorescently labeled cRNA was hybridized to Agilent 4 × 44 K whole mouse genome microarray gene expression chips following the manufacturer's protocol (Agilent Technologies). Hybridized microarray chips were then scanned using an Agilent Microarray Scanner (Model G2565BA, Agilent Technologies). Feature Extraction software (Agilent Technologies) was employed for image analysis and data extraction processes. Normalization of gene expression data and filtering probe sets by expression levels, flags, and errors were performed using GeneSpring software (Agilent Technologies). Differences in gene expression between the control and OTA-treated groups in *p53*-proficient and -deficient mice were analyzed by analysis of variance (cutoff value: $p < 0.05$; multiple testing corrections:

Benjamini-Hochburg false discovery rate [FDR]). Genes deregulated by p53 were extracted by t tests (cutoff value: $p < 0.05$, fold change > 1.5) between OTA-treated *p53*-proficient and -deficient groups. Gene function analyses of extracted genes were performed using IPA (Ingenuity Pathway Analysis) (Tommy Digital Biology, Ltd., Tokyo, Japan).

Quantitative real-time PCR for mRNA expression

Changes in the expression levels of several genes extracted from the results of the cDNA microarray were confirmed by reverse transcription PCR (RT-PCR) analysis of mRNA levels. cDNA samples from groups of 5 animals were prepared by reverse transcription of total RNA using a High Capacity cDNA Reverse Transcription kit (Life Technologies). All PCR assays were performed with primers for rat *Cdkn1a*, *Pkmyt1*, *Ccnb1*, *Ccne1*, *E2f1*, *Plk1*, *Aurka*, *Cdk1*, *Rad51*, *Rad54l*, *Brip1*, *Bard1*, *Polk*, *Bax*, *Bak1*, *Bbc3*, or *Hrk*, and TaqMan Rodent GAPDH Control Reagents were used as an endogenous reference. PCR was carried out in an Applied Biosystems 7900HT FAST Real-Time PCR System using TaqMan Fast Universal PCR Master Mix and TaqMan Gene Expression Assays (Life Technologies). The expression levels of target genes were calculated by the relative standard curve method and were determined by

normalization to *GAPDH* expression. Data were presented as fold-change values of treated samples relative to those of the vehicle control groups in *p53*-proficient mice.

Sodium dodecyl sulfate-polyacrylamide gel electrophoresis (SDS-PAGE) and western blotting

The kidneys from groups of 3 animals in Experiment 2 were used for SDS-PAGE and western blotting. The procedure for sample preparation was described in Chapter 1. For detection of target proteins, membranes were incubated with anti-p21 monoclonal antibodies (F-5; Santa Cruz Biotechnology, Inc., Dallas, TX, USA) or anti-actin monoclonal antibodies (pan Ab-5; Thermo Fisher Scientific, Fremont, CA, USA) at 4°C overnight. Secondary antibody incubation was performed using horseradish peroxidase-conjugated secondary anti-rabbit or mouse antibodies (Cell Signaling Technology) at room temperature. Protein detection was facilitated by chemiluminescence using ECL Prime (GE Healthcare, Little Chalfont, UK). The positive control (lysates of p21-transfected 293 cells) was purchased from Santa Cruz Biotechnology.

In vivo reporter gene mutation assay (Spi⁻ assay)

The kidneys from groups of 5 animals in Experiment 3 were used. Spi$^-$ selection was performed described as Chapter 1.

Mutation spectrum analysis of Spi$^-$ mutants

Mutation spectrum analysis of Spi$^-$ mutants was performed as described in Chapter 1

Statistical analysis

The data for body and kidney weights, parameters in comet assays, mRNA expression levels, *in vivo* mutation assays, and mutation spectrum analyses were analyzed by Student's t-test or Welch's t-test depending on homogeneity. A P value less than 0.05 was considered statistically significant.

Results

In vivo comet assay

The parameters of *in vivo* comet assays using the kidneys of *p53*-proficient and -deficient mice treated with OTA for 3 days are summarized in Table 2-1. Although administration of OTA significantly increased DNA damage, no differences were observed between *p53*-proficient and -deficient mice treated with OTA. However, DNA damage was significantly increased in MMS-treated kidneys of *p53*-deficient mice compared with those of *p53*-proficient mice.

Body and kidney weights and percentages of cells exhibiting karyomegaly and apoptosis

Body and kidney weights of *p53*-proficient and -deficient mice treated with OTA for 4 weeks are summarized in Table 2-2. In both genotypes, significant decreases in final body and kidney weights were observed in the OTA-treated groups as compared with relevant vehicle control groups for each genotype. Histopathological analysis demonstrated that OTA increased the percentages of both apoptotic cells and karyomegalic cells in the OSOM in the kidneys of both genotypes (Figs. 2-1A, 2-1B). As previously reported (35), the percentages of apoptotic and karyomegalic cells in *p53*-deficient mice were significantly higher than those in *p53*-proficient mice (Table

2-2). Immunohistochemical analysis of cleave caspase-3 demonstrated that positive signals were detected in the nucleus of apoptotic cells identified by histopathological feature (Figs. 2-1C, 2-1D).

Immunohistochemical staining for γ-H2AX

Immunohistochemical staining for γ-H2AX in the kidneys of *p53*-proficient and -deficient mice treated with OTA is shown in Fig. 2-2. The percentages of γ-H2AX-positive cells in the cortex (CO) and the outer stripe of outer medulla (OSOM) are summarized in Fig. 2-3. Almost no positive signals were observed in vehicle control sections in both *p53*-proficient and -deficient mice. In OTA-treated *p53*-proficient mice, some tubular epithelial cells exhibited punctate signals representing γ-H2AX expression in nuclei. These tubular epithelial cells were preferentially located at the OSOM rather than the CO. On the other hand, γ-H2AX-positive tubular cells were clearly increased in the kidneys of *p53*-deficient mice treated with OTA as compared with those of *p53*-proficient mice treated with OTA.

Global gene expression analysis by cDNA microarray

When comparing OTA-treated *p53*-proficient mice and OTA-treated *p53*-deficient mice, 1,073 genes were extracted under the cutoff condition of $p < 0.05$ and with at least 1.5-fold change in expression. Gene function and pathway analysis using IPA revealed changes in gene clusters associated with DNA damage/repair, cell proliferation/cell cycle, apoptosis, and p53 signaling. Major extracted genes from the above categories are listed in Tables 2-3 and 2-4 with values compared with relevant vehicle control group in each genotype. Genes affected by *p53* status include cell cycle arrest-related (such as *Cdkn1a* and *Pkmyt1*), cell cycle progression-related (such as *Ccne1* and *Plk1*), DNA DSB repair (such as *Rad51* and *Bard1*), translesion synthesis (such as *polk*), and pro-apoptotic genes (such as *Bax* and *Hrk*).

ELISA and western blotting

Since several nonspecific bands were detected by western blotting of p53, expression of p53 protein was determined by ELISA (Fig. 2-4A). It was reported that p53 concentration in several mouse tissues (brain, eye, testes) using the same ELISA kit were about 10 to 250 pg/g tissue (96), which is consistent with the previous data in the kidney of *p53*-proficient mice (about 80 pg/g tissue). As compared with the control group of *p53*-proficient mice, significant increases in p53 protein concentrations in the

kidney extracts in *p53*-proficinet mice treated with OTA were observed. Although signals were detected in *p53*-deficient mice to some extent, these were considered as nonspecific signals because these values were significantly lower than those in *p53*-proficient mice, and were not altered by OTA treatment.

Western blotting of p21 protein, which is encoded by *Cdkn1a*, demonstrated that OTA increased p21 expression in the kidneys of *p53*-proficient mice, but not in those of *p53*-deficient mice (Fig. 2-4B).

Quantitative real-time PCR for mRNA expression

Several genes were altered by OTA treatment in a p53-dependent manner, as shown by cDNA microarray. These results were confirmed by PCR analysis of mRNA expression levels (Fig. 2-5, 6, 7, 8, 9). Expression levels of *Cdkn1a*, a p53-dependent inducer of G_1/S arrest, were transiently increased by OTA treatment in the kidneys of *p53*-proficient mice. In *p53*-deficient mice, significant yet slight increase of *Cdkn1a* by OTA treatment was observed in the absence of elevation of p21 protein level. This change was possibly due to p53-independent pathway (97), but the rise without elevation of p21 protein level was not biologically significant. On the other hand, OTA significantly increased the expression of G_2/M arrest-related *Pkmyt1* in

p53-deficient mice, which was significantly higher than those in *p53*-proficient mice. Several genes related to cell cycle progression, including *Ccne1*, *Ccnb1*, *Cdk1*, *Plk1*, and *Aurka*, were increased by OTA treatment in *p53*-proficient mice, and those in *p53*-deficient mice were significantly higher than those in *p53*-proficient mice. The same trends were observed for the expression of HR -related genes (i.e., *Rad51*, *Rad54l*, *Bard1*, and *Brip1*). The expression of *polk* mRNA was increased by OTA only in *p53*-proficient mice. Expression of the p53-dependent pro-apoptotic factor *Bax* was increased by OTA only in *p53*-proficient mice. The expression levels of other pro-apoptotic factors (i.e., *Bak1*, *Bbc3*, and *Hrk*) were increased by OTA independent of p53 status; a particularly dramatic increase was observed for *Hrk* expression following OTA treatment in *p53*-deficient mice.

Spi⁻ assay and mutation spectrum analysis of Spi⁻ mutants

Data for Spi⁻ assays in the kidneys of *p53*-proficient and -deficient *gpt* delta mice treated with OTA are summarized in Table 2-5. As compared with the vehicle control group for each genotype, a significant increase in Spi⁻ MFs was observed only in OTA-treated *p53*-deficient mice. Mutation spectrum analysis using Spi⁻ mutant phages is summarized in Table 2-6. In *p53*-proficient mice, no changes in MFs were observed

between the vehicle control and OTA-treated group. In *p53*-deficient mice, the specific MFs of single-base deletions of G/C in repetitive sequences, single-base substitutions, and insertions were significantly increased by OTA treatment.

Discussion

Hibi et al. previously reported that 4-week treatment with 5 mg/kg OTA increased Spi$^-$ MFs in the kidneys of *p53*-deficient *gpt* delta mice, but not in those of *p53*-proficient mice. OTA induced significant increases of Spi$^-$ MFs in DNA extracted from the outer medulla of rat kidney, but not from the whole kidney (34). Considering that the site-specific localization of OTA in the kidneys of mice was similar to that of rats, it is likely that OTA is able to increase Spi$^-$ MFs in the outer medulla of mouse kidney. At any rate, it is no doubt that p53 prevents OTA-induced gene mutations (35). The present data showed that exposure of *p53*-proficient mice to OTA caused a significant increase in p53 protein expression in the kidney. Moreover, DSBs have been shown to play a key role in OTA-induced gene mutations in *gpt* delta rats (89). Because p53 has several functions in the progression from DNA damage and subsequent DSBs to gene mutations, I compared OTA-induced DNA damage and DSBs in *p53*-proficient and -deficient mice to clarify the sites of p53 activity and roles of p53 in these processes. In the present study, I used alkaline comet assay which can detect strand breaks and alkali-labile sites derived from DNA base modification such as alkylated bases and bulky base adducts. (98). Comet assays demonstrated that OTA increased DNA damage in the kidneys of mice; however, no differences were observed

in the degree of DNA damage between *p53*-deficient and -proficient mice. Immunohistochemical analysis of γ-H2AX, a representative marker of DSBs (61), showed that OTA induced DSBs at the OSOM in the kidneys of mice, as was previously observed in *gpt* delta rats (89). Interestingly, in *p53*-deficient mice, the percentages of γ-H2AX-positive cells were much higher than those in *p53*-proficient mice, implying that the absence of p53 enhanced the occurrence of OTA-induced DSBs. Although there have been several reports that OTA induces DSBs *in vitro* and *in vivo* (89, 99), the underlying mechanisms remain unknown. In general, DSBs are thought to be induced as a consequence of the replication fork encountering DNA damage, such as DNA adducts, apurinic/apyrimidinic (AP) sites, and single-strand breaks (48). As a matter of fact, OTA is known to induce specific DNA adducts and/or AP sites *in vivo* (66, 69, 72), implying that these DNA damages may incur DSBs when replication fork encounters. Given that the severity of OTA-induced DNA damage was almost the same between *p53*-deficient and -proficient mice in the present study, my overall data suggest that p53 does not affect OTA-induced DNA damage, but prevents progression from DNA damage to DSBs. Additionally, the present comet assay demonstrated that MMS-induced DNA damage was increased even in the absence of p53, as previously reported (100). This observation could be explained by the participation of p53 in

repairing DNA alkylation by methyltransferase, nucleotide excision repair (NER) or base excision repair (BER) (101, 102), which suggests that DNA damages induced by OTA do not mainly repaired by such kind of DNA repair system, although there was an increase of gene expression level of *mgmt* in OTA-treated mice.

Global gene expression analysis in the kidneys of *p53*-deficient and -proficient mice treated with OTA demonstrated that OTA-treatment in mice of both genotypes induced intergenotypic differences in several genes, including those involved in cell cycle control, DNA repair, and apoptosis. *Cdkn1a* mRNA expression and the expression of p21, which is encoded by *Cdkn1a*, were significantly increased by OTA treatment only in *p53*-proficient mice. The primary function of p53-dependent cell cycle control is G_1/S arrest triggered by p21, which is directly transactivated by p53 and inhibits cyclin-dependent kinases essential for cell cycle progression (103). Taken together, these data suggested that OTA-induced genotoxic stress causes activation of the p53/p21 pathway, followed by G_1/S arrest. This hypothesis is strongly supported by the observation that lack of p53 resulted in significantly higher increases in mRNA levels of cell cycle progression-related genes (i.e., *Ccne1*, *Ccnb1*, *Cdk1*, *Plk1*, and *Aurka*) than those in the presence of p53. Likewise, dramatic increases in the mRNA expression of genes related to HR (i.e., *Rad51*, *Rad54*, *Brip1*, and *Bard1*), one of the

major DSB repair systems (104), were observed in *p53*-deficient mice. Because the DNA replication process is essential for the occurrence of DSBs (105, 106), the observation that *p53*-deficient mice harbored many DSBs following OTA exposure might be due to disorders of cell cycle control. Additionally, the mRNA expression of *Polk*, a p53-dependent Y-family polymerase that functions to correct errors by translesional synthesis upon formation of bulky DNA adducts (91), was slightly increased by OTA treatment, only in *p53*-proficient mice. However, since it is well known that Polk does not correct errors, but transverses damaged bases in an error-free manner, it remains unclear whether these slight changes of *polk* contribute to formation of DSBs in OTA-treated mice.

As previously reported (35), histopathological examinations demonstrated that the percentages of apoptotic cells in the OSOMs of *p53*-deficient mice administered OTA were significantly higher than those in *p53*-proficient mice, which was supported by immunohistochemical analysis for cleaved caspase-3. Histopathological examinations demonstrated that the percentages of apoptotic cells in the OSOMs of *p53*-deficient mice administered OTA were significantly higher than those in *p53*-proficient mice, in line with the previous report (35). Indeed, global gene expression and subsequent mRNA expression analysis in the present study demonstrated that OTA increased

mRNA levels of *Bax*, *Bak1*, and *Bbc3* in *p53*-proficient mice. All of these targets are members of the pro-apoptotic Bcl-2 family of proteins transcriptionally activated by p53 (107). In p53-deficient mice, however, I observed activation of another pathway that involved *Hrk*, a p53-independent apoptotic factor whose expression is triggered by DNA damage (108, 109). DSBs could ultimately become apoptosis-triggering lesions in the absence of appropriate repair (110). Because of the consistency of the sites where DSBs and apoptosis were detected, I propose that some cells harboring DSBs undergo apoptosis via p53-dependent and -independent pathways. The percentages of cells exhibiting karyomegaly were also increased by OTA treatment in *p53*-deficient mice as compared with *p53*-proficient mice, in line with the previous report (35). Thus, the present global gene expression analysis indicated that the imbalance between cell cycle progression and arrest was responsible for the observed lesions.

Hibi et al. previously performed *gpt* and Spi$^-$ assays in the kidney of *p53*-proficient and -deficient mice treated with OTA, in which Spi$^-$ MF, but not *gpt* MF, was increased (35). Therefore, I focused on the effects of p53 on the mutation spectrum of Spi$^-$ mutants in the present study. In order to achieve this aim, additional study using *p53*-preoficient and -deficient mice was performed under the same protocol as previously reported in Hibi et al. (35). From this analysis, unlike the results observed

in rats, in which large deletions were apparent (89), single-base pair (bp) deletions in repetitive sequences, insertions, and base substitutions were predominant in Spi$^-$ mutants from the kidneys of *p53*-deficient *gpt* delta mice exposed to OTA. The reasons for these differences in mutation spectra of Spi$^-$ mutants between rats and mice remain unknown. However, because various types of mutations, including large deletions and frameshift mutations, arise during the HR process (47, 111, 112), DSBs may be a starting point ultimately resulting in gene mutations common to both rats and mice. On the other hand, it has recently been demonstrated that OTA increased frequencies of gene mutations *in vitro* possibly due to oxidative DNA damages or hydroquinone metabolite-related DNA adducts (113, 114). Increases of alternative mutations, base substitutions, in *red/gam* genes observed in the present study may result from these mechanisms. However, no increase of *gpt* MFs in the kidney of *gpt* delta mice treated with OTA (34) indicates that a high proportion of repetitive sequences in *red/gam* gene may contribute to base substitutions by OTA, so that further investigation should be required.

In conclusion, OTA induced DSBs at the carcinogenic target site in the kidneys of mice, similar to the observations made in rats. p53 prevented formation of DSBs and following gene mutation, possibly due to p53/p21-mediated cell cycle control.

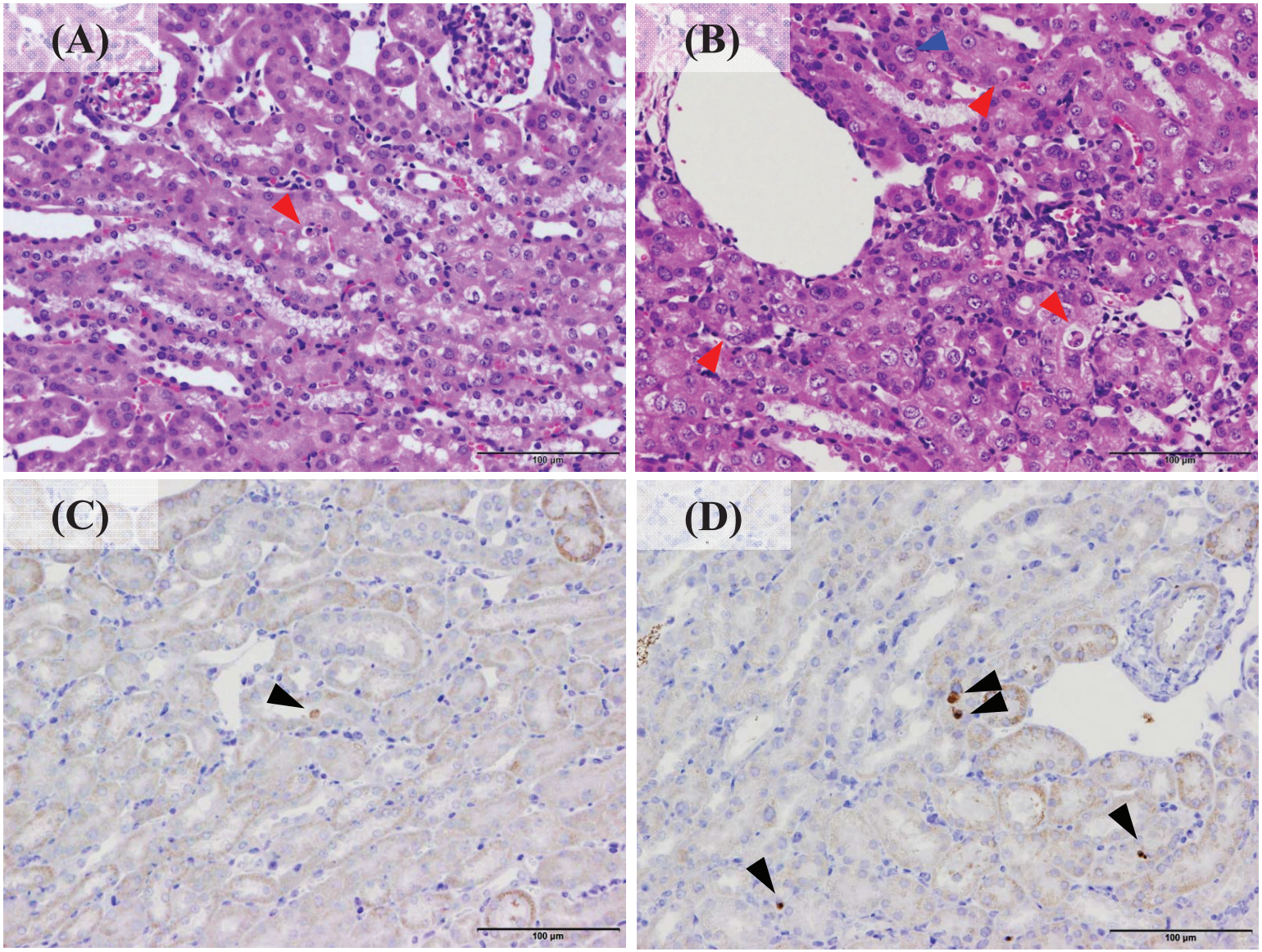

Figure 2-1 Representative photos of HE staining for quantitative analysis of apoptotic and karyomegalic cells at the outer stripe of outer medulla (OSOM) of the kidney in *p53*-proficient mice (A) or *p53*-deficient mice (B) treated with OTA at 5 mg/kg for 4 weeks. Immunohistochemical staining of cleaved caspase-3 at the OSOM of the kidney in *p53*-proficient mice (C) or *p53*-deficient mice (D) treated with OTA at 5 mg/kg for 4 weeks. Red and blue arrow heads show apoptotic and karyomegalic cells, respectively. Black arrow heads show cleaved caspase-3-positive cells.

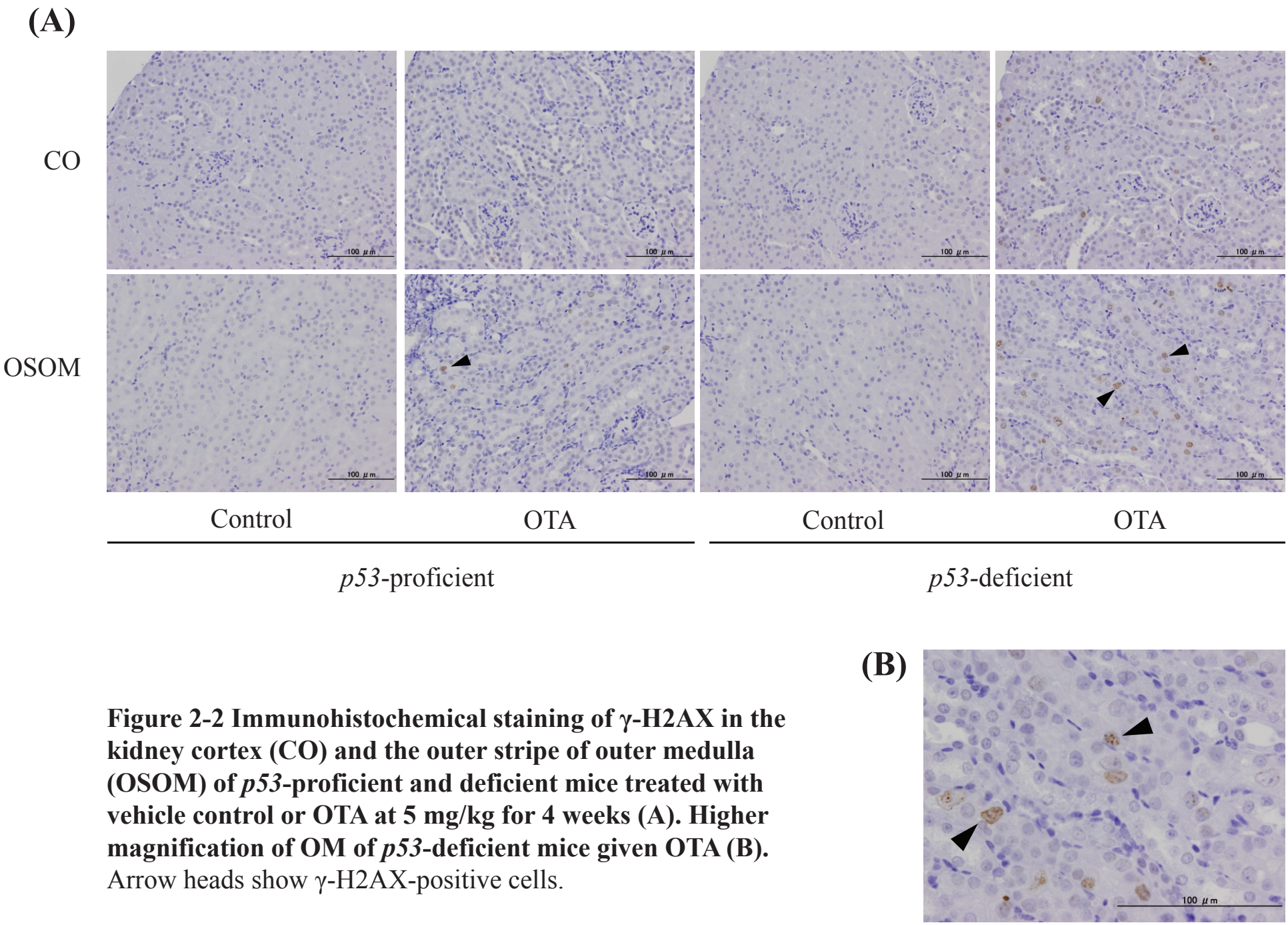

Figure 2-2 Immunohistochemical staining of γ-H2AX in the kidney cortex (CO) and the outer stripe of outer medulla (OSOM) of *p53*-proficient and deficient mice treated with vehicle control or OTA at 5 mg/kg for 4 weeks (A). Higher magnification of OM of *p53*-deficient mice given OTA (B).
Arrow heads show γ-H2AX-positive cells.

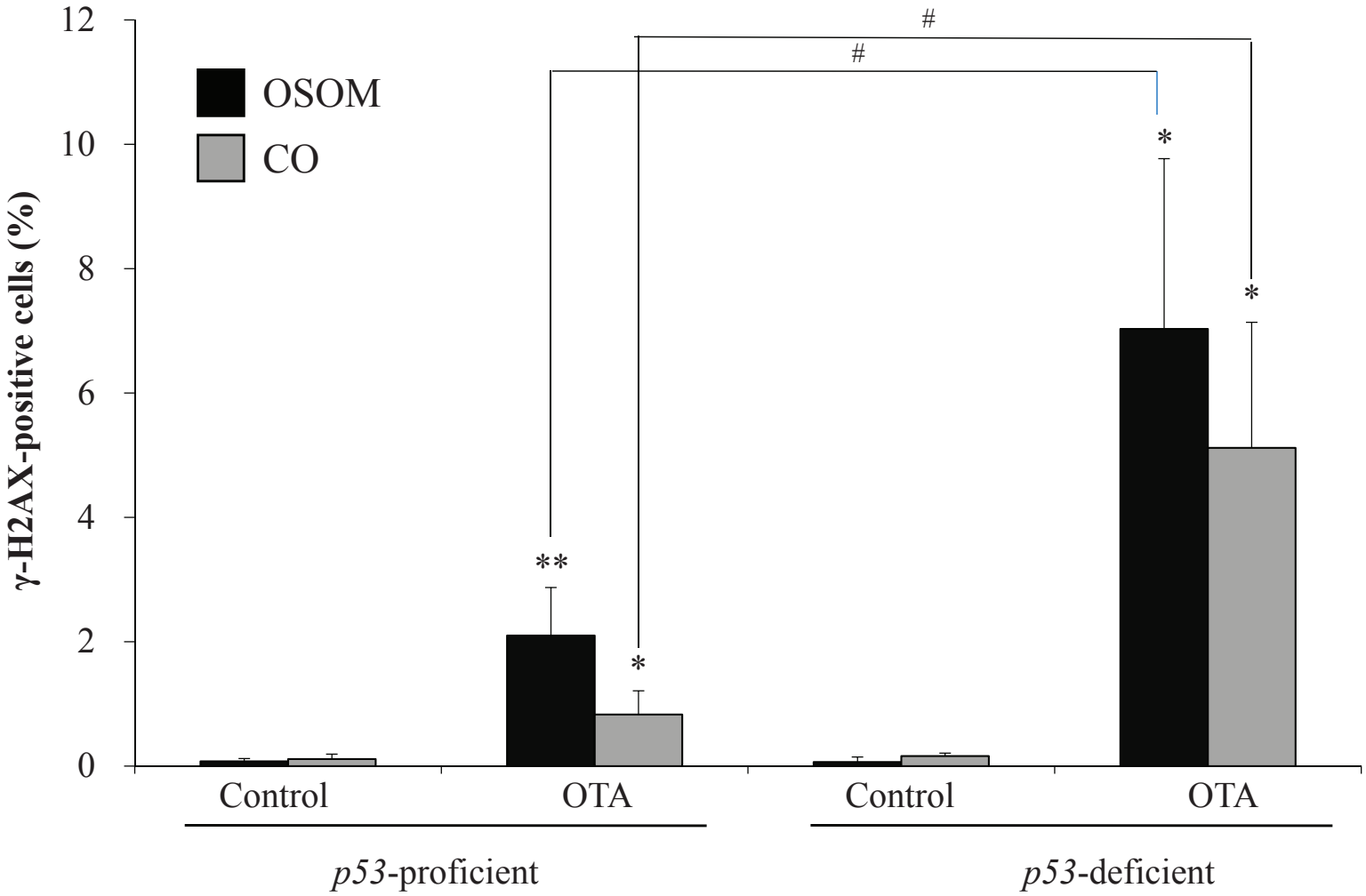

Figure 2-3 The percentages of γ-H2AX-positive cells in the renal cortex (CO) and the outer stripe of outer medulla (OSOM) of *p53*-proficient and *p53*-deficient mice treated with vehicle control or OTA at 5 mg/kg for 4 weeks.

Values are mean ± SD of data for 4-5 mice. *, **: Significantly different from the relevant control groups (the same genotype) at $p < 0.05$ and 0.01, respectively. #: Significantly different from the OTA-treated group of *p53*-proficient mice at $p < 0.05$.

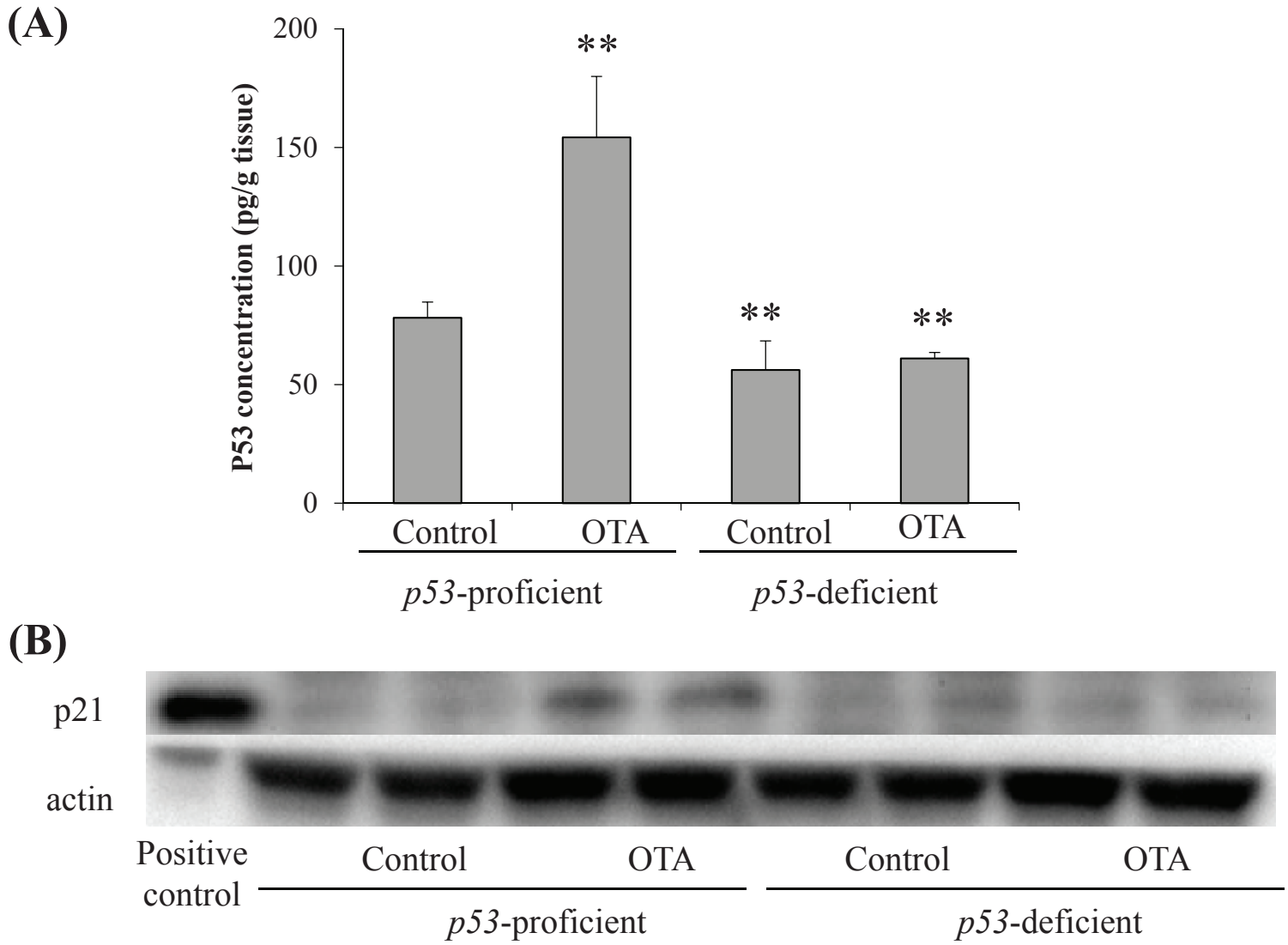

Figure 2-4 (A) Protein contents of p53 in the kidney of *p53*-pfoficient and -deficient mice treated with vehicle control or OTA at 5 mg/kg for 4 weeks.

Values are mean ± SD of data for 5 mice. **: Significantly different from the control group of *p53*-proficient mice.

(B) Western blotting results of p21 in the kidney of *p53*-proficient and -deficient mice treated with vehicle control or OTA at 5 mg/kg for 4 weeks.

Positive control: lysates of p21-transfected 293 cells.

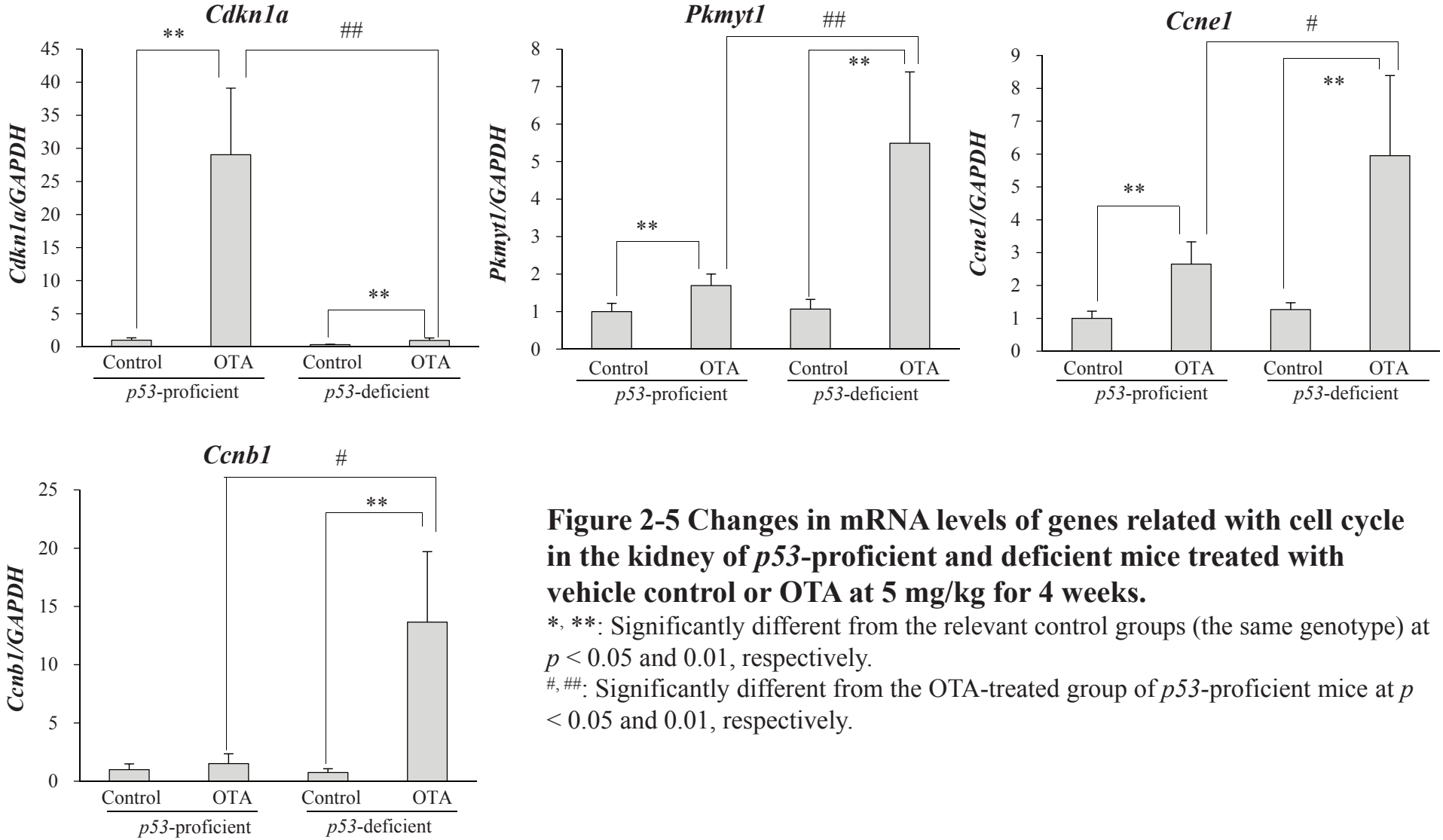

Figure 2-5 Changes in mRNA levels of genes related with cell cycle in the kidney of *p53*-proficient and deficient mice treated with vehicle control or OTA at 5 mg/kg for 4 weeks.

*, **: Significantly different from the relevant control groups (the same genotype) at $p < 0.05$ and 0.01, respectively.

#, ##: Significantly different from the OTA-treated group of *p53*-proficient mice at $p < 0.05$ and 0.01, respectively.

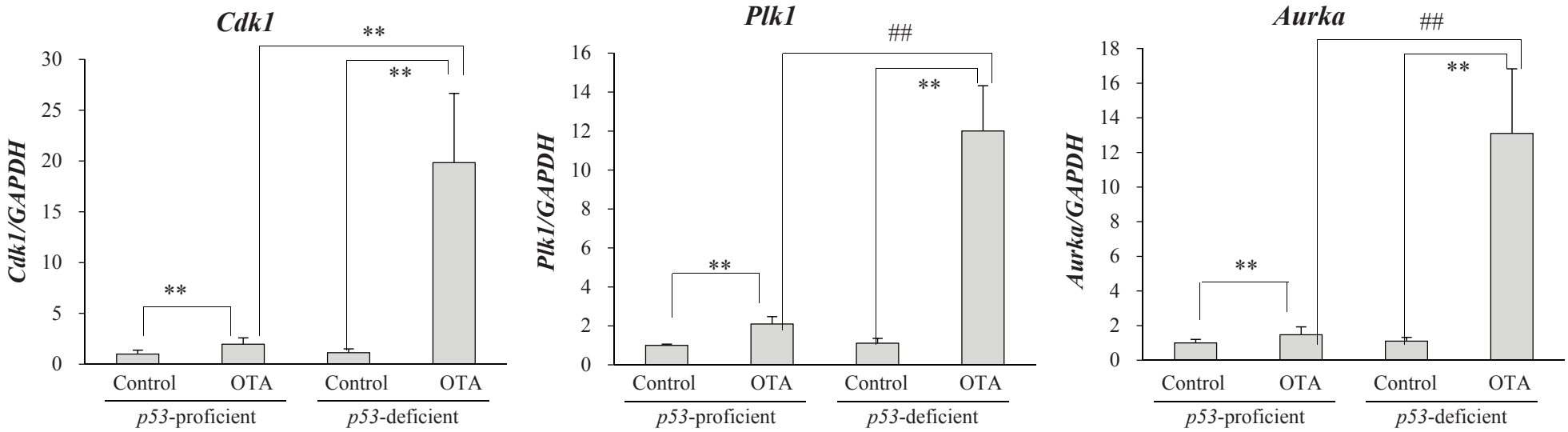

Figure 2-6 Changes in mRNA levels of genes related with cell cycle in the kidney of *p53*-proficient and deficient mice treated with vehicle control or OTA at 5 mg/kg for 4 weeks.

*, **: Significantly different from the relevant control groups (the same genotype) at $p < 0.05$ and 0.01, respectively.

#, ##: Significantly different from the OTA-treated group of *p53*-proficient mice at $p < 0.05$ and 0.01, respectively.

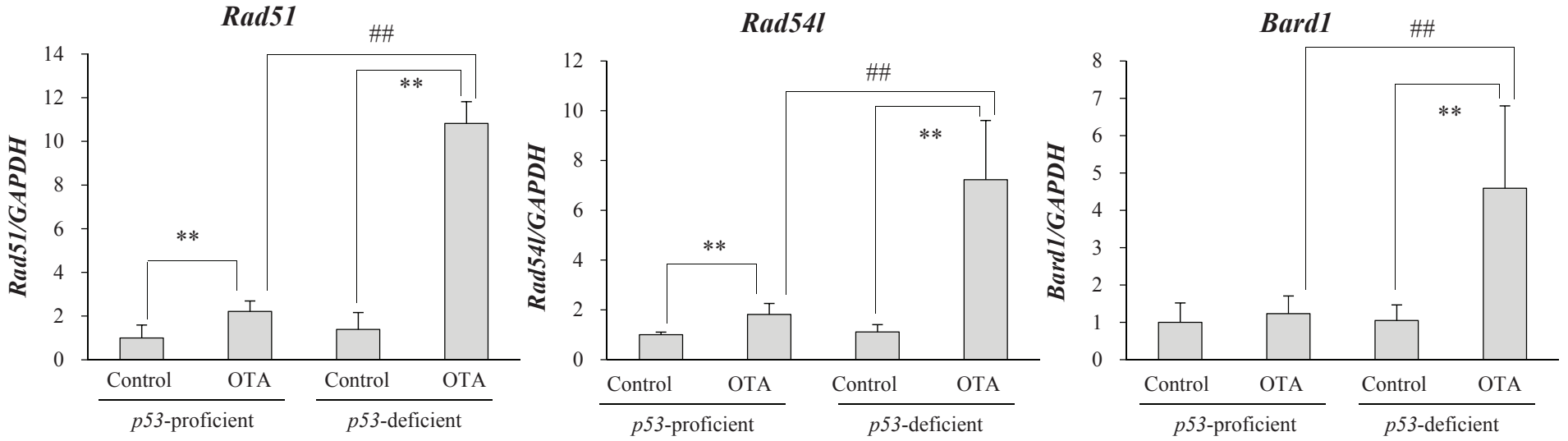

Figure 2-7 Changes in mRNA levels of genes related with DNA damager/repair in the kidney of *p53*-proficient and deficient mice treated with vehicle control or OTA at 5 mg/kg for 4 weeks.

*, **: Significantly different from the relevant control groups (the same genotype) at $p < 0.05$ and 0.01, respectively.

#, ##: Significantly different from the OTA-treated group of *p53*-proficient mice at $p < 0.05$ and 0.01, respectively.

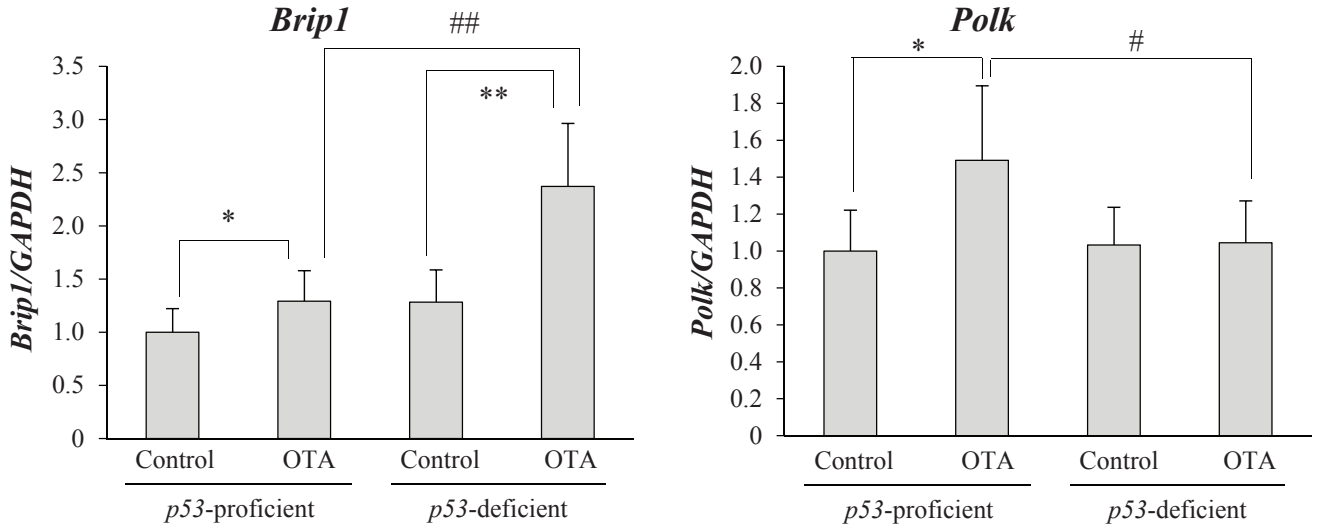

Figure 2-8 Changes in mRNA levels of genes related with DNA damager/repair in the kidney of *p53*-proficient and deficient mice treated with vehicle control or OTA at 5 mg/kg for 4 weeks.

*, **: Significantly different from the relevant control groups (the same genotype) at $p < 0.05$ and 0.01, respectively.

#, ##: Significantly different from the OTA-treated group of *p53*-proficient mice at $p < 0.05$ and 0.01, respectively.

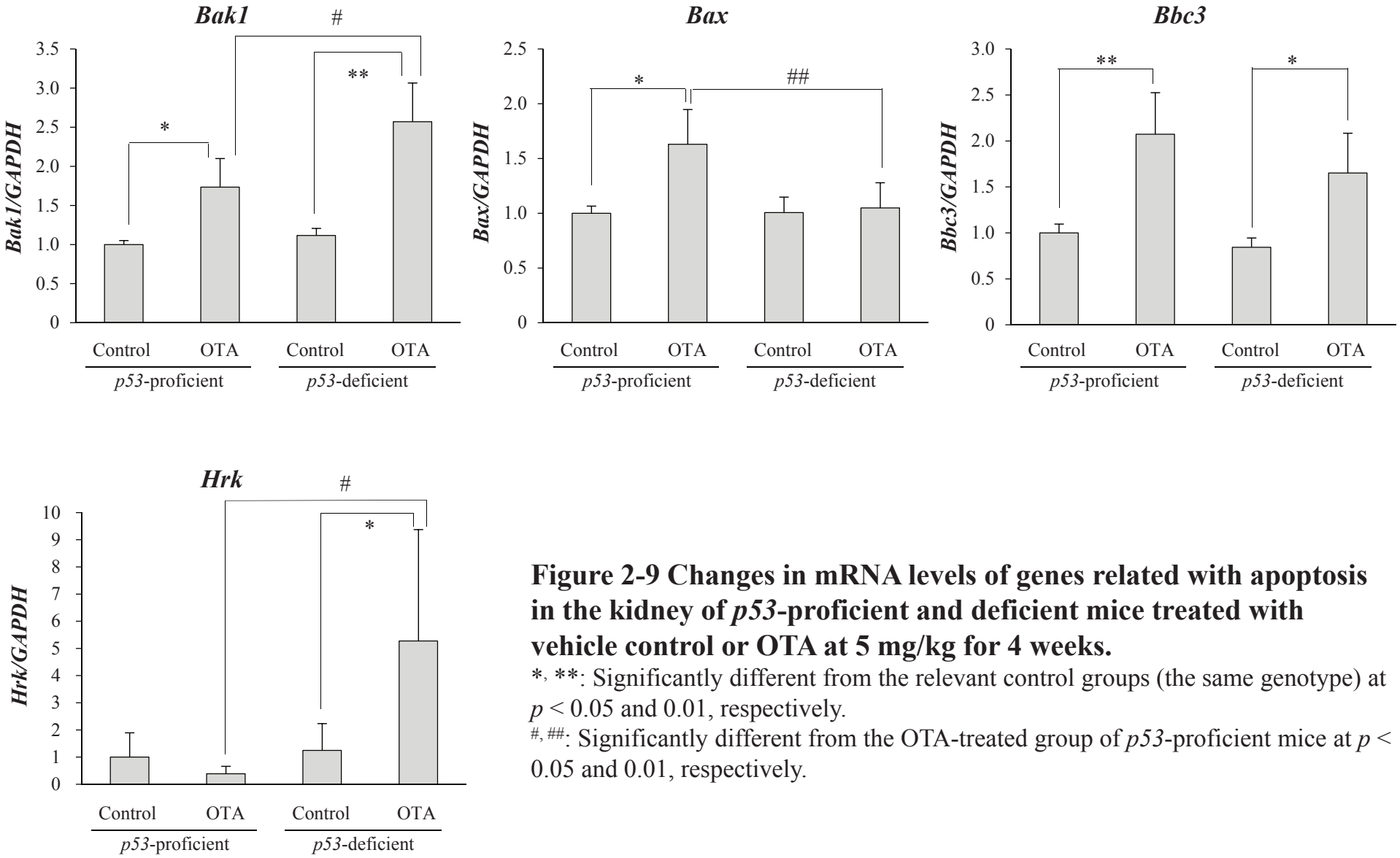

Figure 2-9 Changes in mRNA levels of genes related with apoptosis in the kidney of *p53*-proficient and deficient mice treated with vehicle control or OTA at 5 mg/kg for 4 weeks.

*, **: Significantly different from the relevant control groups (the same genotype) at $p < 0.05$ and 0.01, respectively.

#, ##: Significantly different from the OTA-treated group of *p53*-proficient mice at $p < 0.05$ and 0.01, respectively.

Table 2-1 Comet assays in the kidneys of *p53*-proficient and -deficient mice treated with OTA for 3 days.

Genotype	Treatment	Head intensity (%)	% Tail DNA	Tail length (μm)	Tail moment
p53-proficient	Control	32.7 ± 0.7[a]	0.8 ± 0.3	17.3 ± 1.4	0.1 ± 0.1
	OTA 5 mg/kg	33.9 ± 0.6	3.1 ± 1.2**	20.0 ± 1.7*	0.7 ± 0.4*
	MMS 50 mg/kg	32.7 ± 0.9	18.0 ± 5.2**	34.0 ± 6.3*	3.1 ± 1.1*
p53-deficient	Control	32.4 ± 0.9	0.5 ± 0.2	15.8 ± 0.5	0.1 ± 0.1
	OTA 5 mg/kg	33.6 ± 1.0	3.5 ± 1.4**	19.6 ± 2.3**	0.8 ± 0.4**
	MMS 50 mg/kg	33.2 ± 0.9	27.6 ± 5.8**, #	43.1 ± 2.3**, #	5.8 ± 1.2**, ##

[a]: Mean ± SD

*, ** Significantly different from the relevant control group in the same genotype at $p < 0.05$ and $p < 0.01$, respectively.

#, ## Significantly different from the MMS-treated groups in *p53*-proficient mice at $p < 0.05$ and $p < 0.01$, respectively.

Head intensity: the amount of DNA in the comet head, used for standarlization of each cells.

% Tail DNA: the amount of DNA in the comet head, used to evaluate the extent of DNA damages.

Tail length: the distance of DNA migration from the body of the nuclear and it is used to evaluate the extent of DNA damages.

Tail moment: tail intensity x tail length, used to detect small size of DNA damages.

Table 2-2 Final body and kidney weights and percentages of karyomegalic and apoptotic cells in the outer stripe of outer medulla (OSOM) of *p53*-proficient and -deficient mice treated with OTA for 4 weeks.

Genotype	Treatment	Final body weight (g)	Kidney weight		Karyomegaly (% cells) in the OSOM	Apoptosis (% cells) in the OSOM
			Absolute (g)	Relative (g%)		
p53-deficient	Control	27.4 ± 2.9	0.34 ± 0.05	1.25 ± 0.14	0.06 ± 0.09	0.04 ± 0.05
	OTA 5 mg/kg	24.7 ± 1.4**	0.23 ± 0.03**	0.96 ± 0.07**	2.70 ± 2.07*	0.11 ± 0.12
p53-proficient	Control	27.4 ± 2.6	0.31 ± 0.03	1.14 ± 0.09	0.07 ± 0.10	0.03 ± 0.05
	OTA 5 mg/kg	25.6 ± 2.8*	0.28 ± 0.04*,##	1.10 ± 0.10##	10.13 ± 1.77**,##	0.90 ± 0.12**,##

*, ** Significantly different from the relevant control group in the same genotype at $p < 0.05$ and $p < 0.01$, respectively.

Significantly different from the OTA-treated groups in *p53*-proficient mice at $p < 0.01$.

Table 2-3 Genes extracted from cDNA microarray analysis that were up- or down-regulated by OTA treatment in the kidneys of *p53*-proficient and -deficient mice.

Category	Gene name	Gene symbol	Fold change	
			p53-proficient Control vs OTA	*p53*-deficient Control vs OTA
Cell cycle				
G1/S arrest	cyclin-dependent kinase inhibitor 1A (p21, Cip1)	*Cdkn1a*	38.1	2.8
	cyclin-dependent kinase inhibitor 2A	*Cdkn2a*	-	2
G2/M arrest	protein kinase, membrane associated tyrosine/threonine 1	*Pkmyt1*	1.9	4.9
	checkpoint kinase 2	*Chek2*	-	2.2
G1/S prgression	cyclin E1	*Ccne1*	2.1	3.6
	E2F transcription factor 1	*E2f1*	1.6	3.7
G2/M progression	cyclin B1	*Ccnb1*	1.8	22.2
	cyclin-dependent kinase 1	*Cdk1*	2.2	28.7
	cell division cycle 25 homolog B (S. pombe)	*Cdc25b*	-	1.6
	cell division cycle 25 homolog C (S. pombe)	*Cdc25c*	-	15.9
	polo-like kinase 1	*Plk1*	2.2	15.9
Chromosome segregation	topoisomerase 2	*Top2a*	1.9	25.6
	aurora kinase A	*Aurka*	-	16.5

Listed genes were extracted under the cutoff condition of $p < 0.05$ and exhibited at least 1.5-fold change in expression when comparing the *p53*-proficient and -deficient mice of OTA-treated groups.

Table 2-4 Genes extracted from cDNA microarray analysis that were up- or down-regulated by OTA treatment in the kidneys of *p53*-proficient and -deficient mice.

Category	Gene name	Gene symbol	Fold change	
			p53-proficient Control vs OTA	*p53*-deficient Control vs OTA
DNA damage/repair				
Homologous recombination repiar	RAD51 homolog (S. cerevisiae)	*Rad51*	1.7	7.9
	RAD51-like 1 (S. cerevisiae)	*Rad51l1*	1.7	5.2
	RAD54 homolog B (S. cerevisiae)	*Rad54b*	2.2	7.8
	RAD54-like (S. cerevisiae)	*Rad54l*	1.7	5.4
	BRCA1 associated RING domain 1	*Bard1*	1.3	3.4
	BRCA1 interacting protein C-terminal helicase 1	*Brip1*	-4.4	-
	exonuclease 1	*Exo1*	-	9.9
	Gen endonuclease homolog 1 (Drosophila)	*Gen1*	-	3.1
DNA double strand break	H2A histone family, member X	*H2afx*	1.2	3.1
direct DNA repair of damaged bases	O-6-methylguanine-DNA methyltransferase	*Mgmt*	2.3	-
translesion synthesis	polymerase (DNA directed), kappa	*Polk*	1.6	-
	RAD18 homolog (S. cerevisiae)	*Rad18*	-	1.9
Apoptosis				
proapoptotic factor	BCL2-associated X protein	*Bax*	1.5	-
	BCL2 binding component 3	*Bbc3*	2	1.8
	harakiri, BCL2 interacting protein (contains only BH3 domain)	*Hrk*	-	2
p53 signaling	tumor necrosis factor receptor superfamily, member 10b	*Tnfrsf10b*	2.6	-
	tumor protein p53 inducible nuclear protein 1	*Trp53inp1*	2.1	-
	cyclin G1	*Ccng1*	2.4	-
negative regulator of p53	Mdm2, p53 E3 ubiquitin protein ligase homolog (mouse)	*Mdm2*	1.7	-

Listed genes were extracted under the cutoff condition of $p < 0.05$ and exhibited at least 1.5-fold change in expression when comparing the *p53*-proficient and -deficient mice of OTA-treated groups.

Table 2-5 Spi$^-$ mutant frequencies (MFs) in the kidney of *p53*-proficient and deficient *gpt* delta mice treated with OTA for 4 weeks.

Genotype	Treatment	Animal No.	Plaques within XL-1 Blue MRA ($\times 10^5$)	Plaques within WL95 (P2)	MFs ($\times 10^{-6}$)	Mean ± SD
p53-proficient	Control	6	72.8	28	3.85	3.30 ± 0.63
		7	75.0	17	2.27	
		8	90.6	33	3.64	
		9	61.5	22	3.58	
		10	101.5	32	3.15	
	OTA 5 mg/kg	26	77.2	15	1.94	2.57 ± 0.52
		27	75.8	22	2.9	
		28	85.6	28	3.27	
		29	70.6	16	2.27	
		30	85.1	21	2.47	
p53-deficient	Control	35	45.3	4	0.88	2.48 ± 1.28
		36	55.4	20	3.61	
		37	51.2	13	2.54	
		38	65.5	25	3.82	
		39	58.8	9	1.53	
	OTA 5 mg/kg	56	64.2	21	3.27	4.04 ± 0.78*
		57	47.3	26	5.07	
		58	67.7	25	3.55	
		59	45.2	21	4.65	
		60	35.6	13	3.66	

*: Significantly different from the relevant control group in the same genotype at $p < 0.05$.

Table 2-6 Mutation spectra of Spi$^-$ mutants in the kidney of *p53*-proficient and deficient *gpt* delta mice treated with OTA for 4 weeks.

Genotype	*p53*-proficient						*p53*-deficient					
Treatment	Control			OTA 5 mg/kg			Control			OTA 5 mg/kg		
	No.	%	Specific mutation frequencies ($\times 10^{-6}$)	No.	%	Specific mutation frequencies ($\times 10^{-6}$)	No.	%	Specific mutation frequencies ($\times 10^{-6}$)	No.	%	Specific mutation frequencies ($\times 10^{-6}$)
1bp deletion	106	80	2.67 ± 0.62	84	82	2.12 ± 0.31	47	66	1.64 ± 0.71	62	60	2.43 ± 0.51
Simple G/C	14	11	0.34 ± 0.29	11	11	0.27 ± 0.18	7	10	0.27 ± 0.25	7	7	0.29 ± 0.22
A/T	1	1	0	2	2	0.05 ± 0.07	0	0	0	1	1	0.03 ± 0.07
In run G/C	38	29	0.94 ± 0.39	33	32	0.83 ± 0.20	12	17	0.41 ± 0.32	27	26	1.09 ± 0.39*
A/T	53	40	1.37 ± 0.42	38	37	0.97 ± 0.22	28	39	0.96 ± 0.55	27	26	1.03 ± 0.35
4 bp	0	0	0	1	1	0.03 ± 0.06	0	0	0	0	0	0
100 to 500 bp	1	1	0.03 ± 0.07	0	0	0	0	0	0	2	2	0.09 ± 0.13
>1 kb + Complex	9	7	0.22 ± 0.12	10	10	0.24 ± 0.33	20	28	0.70 ± 0.71	15	15	0.61 ± 0.25
Insertion	5	4	0	2	2	0.05 ± 0.07	1	1	0.04 ± 0.09	8	8	0.35 ± 0.26*
Base substitution	11	8	0.27 ± 0.10	5	5	0.13 ± 0.13	3	4	0.10 ± 0.14	16	16	0.56 ± 0.33*

*: Significantly different from the relevant control group in the same genotype at $p < 0.05$.

Chapter 3

Cell cycle progression, but not genotoxic activity, mainly contributes to citrinin-induced renal carcinogenesis

Abstract

Citrinin (CTN) is a food-contaminating mycotoxin that efficiently induces renal tumors in rats. However, the modes of carcinogenic action are still unknown, preventing assessment of the risks of CTN in humans. In the present study, the proliferative effects of CTN and its causal factors were investigated in the kidneys of *gpt* delta rats. In addition, three *in vivo* genotoxicity assays (reporter gene mutation using *gpt* delta rats and comet and micronucleus assays using F344 rats) were performed to clarify whether CTN was genotoxic *in vivo*. CTN was administrated at 20 and 40 mg/kg/day, the higher dose being the maximal tolerated dose and a nearly carcinogenic dose. In the kidney cortex of *gpt* delta rats, significant increases in the labeling indices of proliferating cell nuclear antigen (PCNA)-positive cells were observed at all doses of CTN. Increases in the mRNA expression levels of *Ccna2*, *Ccnb1*, *Ccne1*, and its transcription factor *E2f1* were also detected, suggesting induction of cell cycle progression at all tested doses of CTN. However, histopathological changes were

found only in rats treated with the higher dose of CTN, which was consistent with increases in the mRNA expression levels of mitogenic factors associated with tissue damage/regeneration, such as *Hgf* and *Lcn2*, at the same dose. Thus, the proliferative effects of CTN may result not only from compensatory reactions, but also from direct mitogenic action. Western blot analysis showed that ERK phosphorylation was increased at all doses, implying that cell cycle progression may be mediated by activation of the ERK pathway. On the other hand, *in vivo* genotoxicity analyses were negative, implying that CTN did not have the potential for inducing DNA damage, gene mutations, or chromosomal aberrations. The overall data clearly demonstrated the molecular events underlying CTN-induced cell cycle progression, which could be helpful to understand CTN-induced renal carcinogenesis.

Introduction

Citrinin (CTN), a mycotoxin produced by several fungal species, including genera *Aspergillus*, *Penicillium*, and *Monascus*, occurs mainly in stored grains, but can also be found in beans, fruits, and dairy products (10, 115). Human exposure to CTN has not been determined because of insufficient information on the actual residual level of CTN in foods (10). However, a recent report found that CTN could be detected in the blood and urine of human, revealing the reality of human exposure to CTN (8, 116). Additionally, CTN is suspected to be one of the etiological agents of Balkan endemic nephropathy (BEN) and urinary tract tumors in humans (8, 117, 118). In fact, CTN-specific DNA adducts were detected in the renal tumors of patients with BEN (67).

In a long-term bioassay, 80-week exposure of F344 rats to CTN at a concentration of 0.1% in the diet induced renal cell adenomas at a high frequency (14). The two-stage carcinogenicity model using SD rats demonstrated the potential tumor

promotion activity of CTN (119). Tumor promoters are thought to induce the expansion of initiated cells, and this process is mediated by various biological events including increases of cell proliferations, and decreases of apoptotic cell death (5, 120). Although cell proliferation is known to be induced following exposure to CTN in the kidneys of mice (121), CTN is not carcinogenic in the mouse kidney (122). In the kidney of rats, there have been no reports of cell proliferation, and the underlying molecular pathogenesis remains unknown.

In addition to clarifying the mechanisms of the tumor-promoting activity of CTN, to know whether CTN has genotoxic potential is also critical to understanding CTN-induced renal carcinogenesis. In fact, CTN has yielded both negative or positive scores in Ames tests and in *in vitro* comet assays (22, 23, 24, 25) and positive scores in *in vitro* and *in vivo* chromosomal aberration tests (23, 26, 27, 28). These inconsistent outcomes make it especially difficult to judge whether CTN-induced renal carcinogenesis involves genotoxic mechanisms.

In the present study, to investigate the proliferative effects of CTN and its causal factors, mRNA and protein levels of various molecules related to cell proliferation and histopathological examination were measured using the kidneys of F344 *gpt* delta rats. Additionally, I performed three *in vivo* genotoxicity assays to detect genotoxicity by different endpoints: an *in vivo* reporter gene mutation assay using the kidneys of F344 *gp*t delta rats, an *in vivo* comet assay, and an *in vivo* micronucleus assay using the kidneys and bone marrow of F344 rats, respectively.

Materials and Methods

Experimental Animals and Housing Conditions

The protocol for this study was approved by the Animal Care and Utilization Committee of the National Institute of Health Sciences. Specific pathogen-free, five-week-old male F344/NSlc-Tg (*gpt* delta) rats carrying about five tandem copies of the transgene lambda EG10 per haploid genome and five-week-old male F344 rats were obtained from Japan SLC (Shizuoka, Japan) and acclimated for one week prior to the commencement of testing. Animals were housed in a room with a barrier system and maintained under constant temperature (23 ± 2°C) and relative humidity (55 ± 5%). The air was changed 12 times/h and lighting was on a 12 h light-dark cycle with free access to an Oriental CRF-1-basal diet (Oriental Yeast Co., Ltd, Tokyo, Japan) and tap water.

Test Compound

Citrinin (CTN) was extracted from cultures of *Penicillium citrinum* (TSY0222).

A 500 mL Fernbach flask containing 200 mL of Czapek yeast extract broth {3.5% Czapek dox broth (Difco Laboratories Inc., Franklin Lakes, NJ, USA), 0.5% yeast extract and 3% sucrose} was inoculated with fungal spores, and incubated at 30°C for two weeks. After removal of the fungal mats from the culture, the culture fluids from the flasks were acidified to pH 2.0 to 4.0 with HCl, and extracted with an equal volume of ethyl acetate. The extract was evaporated to dryness. The residue was dissolved in a small amount of xylene. The lysate was filtered to remove brown insoluble material, and then gently chilled in an Erlenmeyer flask for crystallization of CTN. The crystals were dissolved in acetonitrile:water (50:50). The measured purity of CTN was > 95% from the area percentage of the chromatogram (data not shown). CTN was stored in a refrigerator and dissolved in the vehicle (5% w/v sodium bicarbonate in water) just before use. Ethylnitrosourea (ENU), methylmethanesulfonate (MMS) and cyclophosphamide (CP) were purchased from Sigma-Aldrich Co. LLC (St. Louis, MO, USA). ENU was dissolved in saline, and MMS and CP were dissolved in distilled

water.

Experiment 1: 28-day repeated administration using F344 gpt delta rats

Animal treatment

Groups of five male F344 *gpt* delta rats were orally administered CTN by gavage using 40 and 20 mg/ten mL/kg/day for 28 days (day zero to day 27). Animals in the control group received vehicle only. A dose level of 40 mg/kg was selected as the maximal dose which can be repeatedly administered based on a preliminary four-day study in F344 rats (data not shown). The maximal dose of 40 mg/kg was decreased to 30 mg/kg on day four because of severe weight loss. Animals were necropsied three days after the last dosing, and the kidneys were extirpated. In the control and CTN-treated groups, the kidneys were cut along the long axis and 1/2 of unilateral kidney was fixed in 10% neutral buffered formalin and routinely processed for hematoxylin and eosin (HE) staining and immunohistochemical staining. The residual

cortex of the kidney was macroscopically separated with curving scissors using the arcuate arteries at the boundary of the cortex and medulla as landmarks, as described in a previous report (34). For the positive control group for *in vivo* mutation assay, ENU at a dose of 50 mg/ten mL/kg/day were intraperitoneally administrated to five male rats from day zero to day four (five days), and thereafter the whole kidneys extirpated on day 30 were used. The cortices and whole kidneys were stored at -80°C, and used for quantitative PCR, SDS-PAGE and Western blotting, 8-OHdG and thiobarbituric acid reactive substances (TBARS) measurement, and *in vivo* reporter gene mutation assay.

Immunohistochemical staining for proliferating cell nuclear antigen (PCNA)

Immunohistochemical staining was performed using monoclonal anti-mouse PCNA antibodies (1:100; Dako Denmark A/S, Glostrup, Denmark) followed by incubation with a high polymer stain (HISTOFINE Simple Stain, Nichirei Bioscience Inc., Tokyo, Japan). At least 2000 intact tubular cells in the cortex per animal were

counted and labeling indices (LIs) was calculated as the percentages of cells positive for PCNA staining.

RNA isolation and quantitative real-time PCR for mRNA expression

The kidney cortices from all animals were soaked overnight in RNAlater-ICE (Life Technologies) at -20°C, and total RNA was extracted using an RNeasy Mini kit (QIAGEN K.K., Tokyo, Japan) according to the manufacturer's instruction. cDNA copies of total RNA were obtained using a High Capacity cDNA Reverse Transcription kit (Life Technologies). All PCR reactions were performed with primers for rat *Ccnd1*, *Ccne1*, *Ccna2*, *ccnb1*, *E2f1*, *Hgf*, *Lcn2* and TaqMan® Rodent GAPDH Control Reagents as an endogenous reference in the Applied Biosystems 7900HT FAST Real-Time PCR Systems using TaqMan® Fast Universal PCR Master Mix and TaqMan® Gene Expression Assays (Life Technologies). The expression levels of the target gene were calculated by the relative standard curve method and were determined

as ratios to *GAPDH* levels. Data are presented as fold-change values of treated samples relative to controls.

SDS-PAGE and Western blotting

The kidney cortices from all animals were used for SDS-PAGE and Western blotting. The procedure for sample preparation was described in Chapter 1. For detection of target proteins, membranes were incubated with anti-phospho ERK1/2 monoclonal antibody, anti-ERK1/2 monoclonal antibody (Cell Signaling Technology, Inc., Danvers, MA, USA) and anti-actin monoclonal antibody (pan Ab-5; Thermo Fisher Scientific, Fremont, CA, USA) at 4 °C overnight. Secondary antibody incubation was performed using horseradish peroxidase-conjugated secondary anti-rabbit or mouse antibodies (Cell Signaling Technology) at room temperature. Protein detection was facilitated by chemiluminescence using ECL Plus (GE Healthcare Japan Ltd., Tokyo, Japan), and protein levels were quantified using Image Lab software

(BioRad laboratories, Hercules, CA, USA). Cell extracts for positive and negative control were purchased from Cell Signaling Technology.

Measurement of nuclear 8-OHdG

The kidney cortices from all animals were used. In order to prevent 8-OHdG formation as a by-product during DNA isolation (123), kidney DNA was extracted using a slight modification of the method by Nakae et al. (124). Briefly, nuclear DNA was extracted with a DNA Extractor WB Kit (Wako). For further prevention of artifactual oxidation in the cell lysis step, deferoxamine mesylate (Sigma-Aldrich) was added to the lysis buffer. The DNA was digested to deoxynucleotides by treatment with nuclease P1 and alkaline phosphatase, using the 8-OHdG Assay Preparation Reagent Set (Wako). The levels of 8-OHdG (8-OHdG/10^5 dG) were measured by high-performance liquid chromatography with an electrochemical detection system (Coulochem II; ESA, Bedford, MA, USA).

Measurement of thiobarbituric acid reactive substances (TBARS)

The kidneys were homogenized with a nine volumes of ice-cold KCl solution (1.15%) to form 10% homogenates and were centrifuged at 3,000 rpm for ten min. Fifty μL aliquots of supernatant were incubated with a reaction mixture consisting of 0.2 mL of 8.1% sodium lauryl sulfate, three mL of 0.4% thiobarbituric acid (pH 3.5), and 0.75 mL of distilled water at 95°C for 60 minutes. A standard malondialdehyde (MDA) series was prepared by hydrolysis of 1,1,3,3, -tetramethoxypropane (Wako). The reaction products were extracted with a mixture of n-butanol and pyridine (15:1, v/v) and separated by centrifugation. The butanol phase was collected, and its absorbance was measured at 553 nm. TBARS results are expressed as the amount of free MDA equivalents through the calibration curve generated from 1,1,3,3 -tetramethoxypropane. Protein assays were performed with the Advanced Protein Assay (Cytoskeleton) to allow expression of renal TBARS content as nmol MDA

equivalents/mg protein.

In vivo reporter gene mutation assay

The protocol for the *in vivo* reporter gene mutation assay was followed the OECD guideline for Transgenic Rodent Somatic and Germ Cell Gene Mutation Assays (OECD, 2011). 6-Thioguanine (6-TG) and Spi^- selections were performed using the method of Nohmi et al. (32). Briefly, genomic DNA was extracted from the kidneys of animals in each group using Recover Ease DNA isolation kits (Agilent Technologies, Santa Clara, CA, USA), and lambda EG10 DNA (48 kb) was rescued as phages by *in vitro* packaging using Transpack Packaging Extract (Agilent technologies). For 6-TG selection, packaged phages were incubated with *Escherichia coli* YG6020, which expresses Cre recombinase, and converted to plasmids carrying genes encoding *gpt* and chloramphenicol acetyltransferase. Infected cells were mixed with molten soft agar and poured onto agar plates containing chloramphenicol and 6-TG. In order to

determine the total number of rescued plasmids, infected cells were also poured on plates containing chloramphenicol without 6-TG. The plates were then incubated at 37°C for selection of 6-TG-resistant colonies, and *gpt* mutant frequencies (MFs) was calculated by dividing the number of *gpt* mutants after clonal correction by the number of rescued phages. For Spi$^-$ selection, detail procedure was described in Chapter 1.

Experiment 2: In vivo comet assay

The *in vivo* comet assay was run according to the standard protocol. Groups of five male F344 rats were orally administered 40 and 20 mg CTN /ten mL/kg/day by gavage for two days. Animals in the control groups received vehicle only. Animals were necropsied three h after the last dosing, and the kidneys were extirpated. The positive control group animals received MMS at 220 mg/kg once, and were sacrificed 24 h later. The cortices of the kidneys (the control and CTN-treated group) and whole kidney (the positive control group) were used for comet assay. The procedure was

described in Chapter 1.

Experiment 3: In vivo micronucleus assay

The protocol of for the *in vivo* micronucleus assay followed standard methods. Groups of four to five male F344 rats were orally administered 40 and 20 mg CTN /ten mL/kg/day by gavage for two days. Animals in the control group received vehicle only. Animals were necropsied 24 hours after the last dosing, and the bone marrow was extirpated. The positive control group animals received 120 CP mg/kg once and were sacrificed 24 h later. The cells were collected from the bone marrow using fetal bovine serum (Sigma-Aldrich) and were smeared on the slide glass. After drying, the cells were fixed in methanol, and the slides were stored at room temperature. The cells were stained with acridine orange solution and immediately observed by fluorescence microscope. Micronucleated polychromatic erythrocytes (MNPCEs) were recorded based on the observation of 2000 polychromatic erythrocytes (PCEs), and the

MNPCE/PCE ratio was calculated. In addition, 1000 total erythrocytes (PCEs + normochromatic erythrocytes (NCEs)) were scored for PCE frequency (PCN/NCE ratio) for each treatment and animal.

Statistical analysis

The data for body and kidney weights, mRNA expression levels, 8-OHdG and TBARS measurements, *gpt* and Spi^- MFs, parameters in comet assay, PCE/NCE ratio, were analyzed with ANOVA, followed by the Dunnett's multiple comparison test. The significance of difference for positive control data was analyzed with the Student-Welch test. The data for MNPCE/NCE ratio was analyzed with a conditional binomial test using Kastenbaum & Bowman's table (125). A P value less than 0.05 was considered statistically significant.

Results

Experiment 1

General signs, body weight and kidney weight

Two of the five animals in the 40 mg CTN/kg group showed severe body weight loss at day three, so the maximum dose of 40 mg/kg was decreased to 30 mg/kg from day four. Although one animal did not recover and died on day seven, the other animals in the highest CTN dose group increased in body weight. Body weight gain was reduced in 40/30 mg/kg group by days 27 and 30 (Fig. 3-7). Data for final body and kidney weights are summarized in Table 3-1. Compared with the control group, final body weight was significantly decreased and relative kidney weight was significantly increased in the 40/30 mg/kg group.

Histopathological examination and PCNA analysis of the kidney

Histopathological examination showed regeneration of tubules in the kidney cortex

of the 40/30 mg/kg group. In two animals of the 40/30 mg/kg group, one of which showed decrease in body weight at day three, the histopathological findings were relatively severe. No remarkable changes were observed in the 20 mg/kg group (Fig. 3-1). The number of PCNA-positive tubular cells in the cortex was significantly increased in the 20 and 40/30 mg/kg groups compared with the control group (Fig. 3-2). Kidney cells in the histopathological lesions such as regeneration of tubules were exclude for PCNA counting.

Quantitative real time RT-PCR and Western blotting

Expression of levels of *Ccne1*, *Ccna2* and *Ccnb1* mRNA were significantly increased in the 20 and 40/30 mg/kg groups. *E2f1*, a transcription factor of *Ccne1*, was also increased in the 20 and 40/30 mg/kg groups. *Ccnd1* mRNA did not change in any of the groups (Fig. 3-3). On the other hand, expression levels of *Hgf* and *Lcn2* mRNA were significantly increased only in the 40/30 mg/kg group (Fig. 3-4).

Increases of *Hgf* and *Lcn2* levels were consistent with the severity of histopathological findings. Western blot analysis using the anti-phospho ERK1/2 monoclonal antibody demonstrated increases in kidney cortex protein levels treated with CTN 20 and 40/30 mg/kg, in contrast to a lack of changes in total ERK1/2 level (Fig. 3-5A). In addition, there were significant increases in the density of phospho-ERK1/2 relative to actin at CTN doses of 20 and 40/30 mg/kg (Fig. 3-5B).

Measurement of 8-OHdG and TBARS

The levels of 8-OHdG and TBARS are shown in Fig. 3-6. There were no significant differences in 8-OHdG and TBARS level in any of the treated groups.

In vivo mutation assays

Data for *gpt* MFs analyzed by 6-TG selection are summarized in Table 3-2. There were no significant increases of *gpt* MFs in the kidney cortex DNA of the CTN-treated

gpt delta rats compared to the control values. Data for Spi$^-$ selection assessing deletion mutations are summarized in Table 3-3. Again, there was no significant variation in Spi$^-$ MFs values between CTN-treated and control rats. Spi$^-$ MF of animal No.13 showed extremely high value compared with those of the same group, and the value was excluded for the calculation based on the result of Smirnov's outlier test.

Experiment 2: In vivo comet assay

The DNA damage parameters determined by *in vivo* comet assays are summarized in Table 3-4. There were no significant differences in tail intensity and tail length in any of the CTN-treated groups. Although the tail moment at a CTN dose of 40 mg/kg was significantly increased as compared with the control group, this result was considered insufficient to indicate DNA damage because the change was very slight and there was lack of changes in other major parameters.

Experiment 3: In vivo micronucleus assay

Data for *in vivo* micronucleus assays are summarized in Table 3-5. There was no statistical significant change in the MNPCE/PCE ratio in any of the CTN-treated groups.

Discussion

In the present study, 28-day administration of CTN at the higher dose caused regenerative tubules mainly in the kidney cortex of *gpt* delta rats, in line with previous reports (126, 127). The site-specific toxicity of CTN on the segment I proximal tubule likely resulted from high concentration of CTN by uptake through specific organic anion transporters present in the region (126, 128). Based on the fact that CTN-induced renal adenoma was also observed in the kidney cortex (14), the present experimental data using the kidney cortex appeared to be useful in the elucidation of the molecular mechanisms underlying CTN-induced carcinogenesis. In the kidney cortex of *gpt* delta rats treated with CTN, the labeling index of PCNA-positive cells was significantly increased at all doses compared with that of the control group. Moreover, mRNA expression analysis revealed that increases in *Ccna2*, *Ccnb1*, *Ccne1*, and its transcription factor *E2f1* were present following treatment with both doses of CTN, suggesting that either dose promoted cell cycle progression. In contrast, regenerative

tubules were observed only in the 40/30 mg/kg group and not in the 20 mg/kg group. In fact, increases in the expression of *Hgf* and *Lcn2* mRNAs were observed only in the high-dose group, both of which are known to be highly expressed in tubular epithelial cells during regeneration after tissue damage and exert mitogenic effects on kidney cells (129, 130). Therefore, there is no doubt that the cell proliferation observed in the high-dose group involved cell injury-associated compensatory mechanisms. Moreover, the cell proliferation observed in the low-dose group, which was not accompanied by any histopathological alterations or signal transduction activity related to compensatory regeneration, may result from the direct mitogenic activity of CTN. Renal tumor formation in F344 rats due to treatment with CTN at a concentration of 0.1% in the diet (approximately 50 mg/kg/day) was accompanied by histopathological injury, such as interstitial fibrosis and nephritis (14). Another study using SD rats demonstrated that CTN at 0.02 and 0.05% in the diet (approximately 10 and 25 mg/kg) did not have any carcinogenicity in the kidney by 48-week treatment (119). Thus, it is likely that the

proliferative effects of CTN at carcinogenic doses may involve compensatory mechanisms. Although there were less atypical types of cells in the regeneration of tubules observed in the present 4-week study, it is likely that these lesions may alter histopathological changes related to carcinogenesis. The present data strongly suggested that the direct mitogenic activity of CTN may exert additional effects on cell cycle progression, thereby contributing to renal carcinogenesis.

Cell cycle progression is regulated by various mitogenic signal transduction pathways, including the MEK/ERK and PI3K/AKT cascades (131, 132). In particular, ERK, which is constitutively activated via phosphorylation in many human cancer cells, is activated by CTN treatment in HEK293 and HeLa cells (133, 134). For the first time, the present study demonstrated that CTN treatment led to the phosphorylation of ERK *in vivo*, especially in the kidney cortex as a carcinogenic target site. CTN showed phosphor-ERK2-specific increase in the present study, which is consistent with previous *in vitro* results (133). It was reported that ERK2 mediates proliferative

effects while ERK1 does not (135), which is possibly related with the present results. Phosphorylated ERK activates the cyclin D-CDK4/6 complex, leading to subsequent Rb phosphorylation. The resulting activation of the *E2F* family of genes results in the expression of target genes, including cyclin E (131, 136). The present analysis of mRNA expression levels showed phosphorylation of ERK and overexpression of cell cycle-related genes, except *Ccnd1*. This exception may be due to the instability of *Ccnd1* mRNA (137). As upstream factors responsible for ERK activation, various events have been proposed, such as oxidative stress, the PKC signaling pathway, crosstalk with cAMP signaling, and the HGF/c-Met signaling pathway (138, 139, 140, 141). Accordingly, it seems likely that the activity of the HGF/c-Met pathway following renal epithelial cell injury is responsible for ERK activation in the high-dose group. Then, to clarify the factors resulting in ERK activation in the low-dose group, I assessed 8-OHdG levels as a measure of oxidized DNA damage and TBARS levels as a marker of lipid peroxidation, based on the fact that CTN generates oxidative stress in

cultured cells and mouse skin (142, 143). However, no changes in either parameter were detected in the CTN-treated group relative to the control group. Alternatively, because CTN increases intracellular calcium concentrations (144), activation of PKC signaling may contribute to CTN-induced cell cycle progression.

In vivo genotoxic assays, such as reporter gene and comet assays, are fairly sensitive to genomic damage, and both of which can be applied to a variety of organs (32, 145). Furthermore, when agents are found at specific locations, the ability to extract DNA from these sites makes such genotoxic assays even more sensitive. In fact, I have already demonstrated that reporter gene mutations could be detected following exposure to ochratoxin A using DNA extracted from the outer medulla of the kidney, but not from the whole kidney (34). In the present *in vivo* reporter gene mutation assays, no remarkable increases in *gpt* or Spi^- MFs were observed in DNA extracted from the kidney cortices of *gpt* delta rats following treatment with CTN, suggesting that genomic mutations were not induced. Also, in the comet assay using kidney cortices, no

changes in main parameters were seen, indicating a lack of DNA damage. Several studies have reported either negative or positive results in Ames tests and *in vitro* comet assays (22, 23, 24). Although CTN-specific DNA adducts were detected by ^{32}P postlabeling method in human kidney tumor (67), the chemical structure and mutagenic potential of these adducts are unclear. Additionally, there is no report of the presence of CTN-specific adducts in the rat kidney. Thus, in light of the fact that the present data assessed *in vivo* reporter gene mutation and *in vivo* comet assays in the kidneys of rats, it is likely that CTN does not induce DNA damage or gene mutations at the carcinogenic target site. In the micronucleus assay using bone marrow cells, there was no significant increase in the MNPCE/PCE ratio at any dose of CTN. CTN has been shown to induce numerical chromosomal abnormalities *in vitro*, resulting from inhibitory effects on microtubule organization (26, 28, 146). In addition, structural chromosomal abnormalities suggestive of direct DNA damage were observed in the bone marrow cells of mice treated with CTN by single i.p. administration at 0.9 mg/kg

and repeated oral administration at 0.1 mg/kg/day twice a week for 8 weeks (23, 27). However, a 70-week feeding of 200 ppm CTN in mice, equating to approximately 30 mg/kg/day, did not induce any tumors in the kidneys of these mice (122). Overall, the negative results obtained in *in vivo* micronucleus assays using a carcinogenic target species allowed us to conclude that chromosomal abnormalities were not significantly involved in CTN-induced renal carcinogenesis in rats. Consequently, I propose that genotoxic mechanisms are not the primary mechanism involved in CTN-induced renal carcinogenesis.

In conclusion, the present data strongly suggested that exposure to CTN led to cell proliferation. Such progression was triggered by both direct mitogenic and compensatory activities that contributed to renal carcinogenesis, without significant contributions from genotoxic mechanisms.

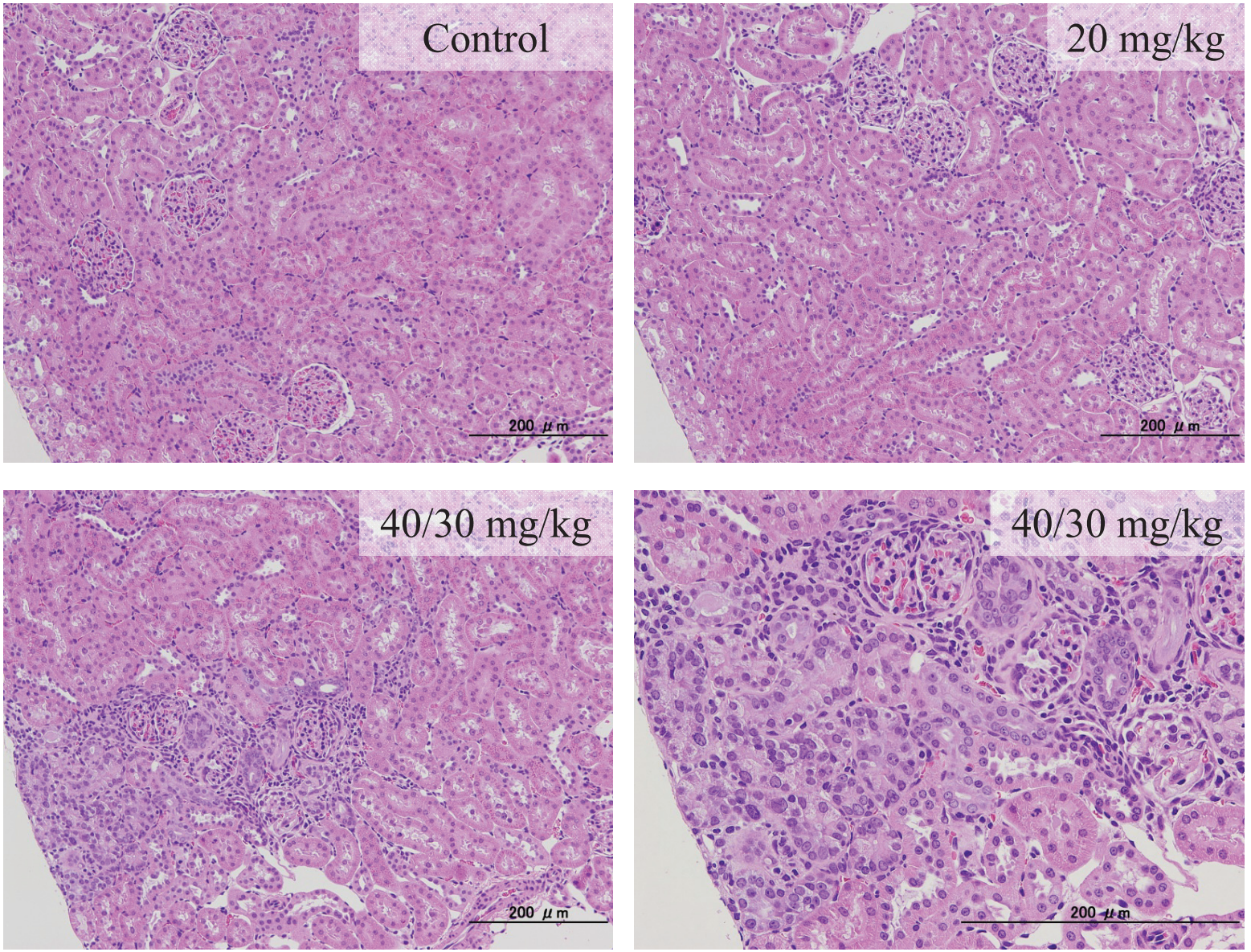

Figure 3-1 Histopathological features in the kidney of *gpt* delta rats treated with CTN for 28 days.
Note that there were no obvious alterations in the control and 20 mg/kg groups, whereas regenerations of tubules were observed mainly in the cortex of the 40/30 mg/kg group. HE staining was used.

(A)

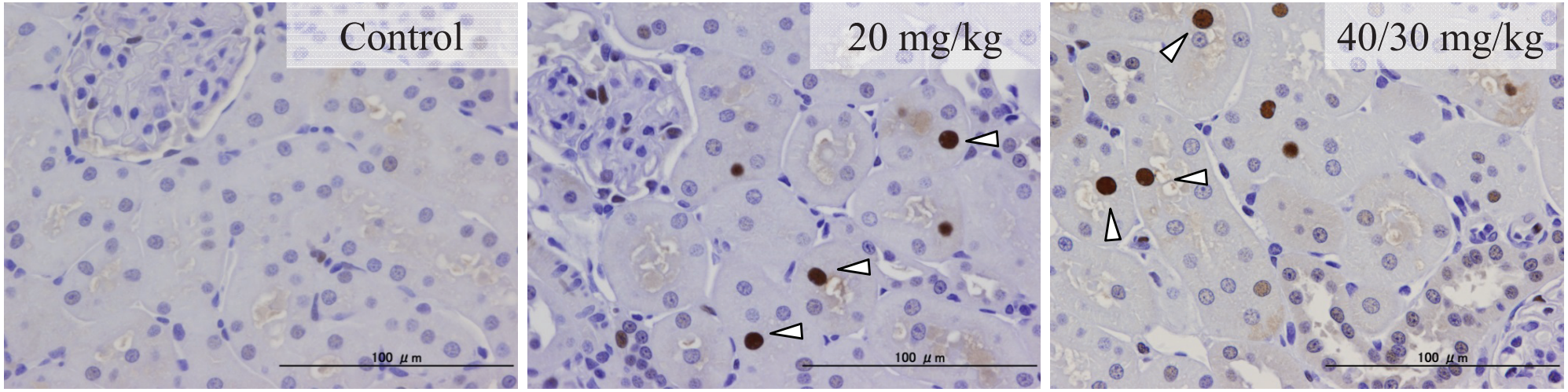

(B)

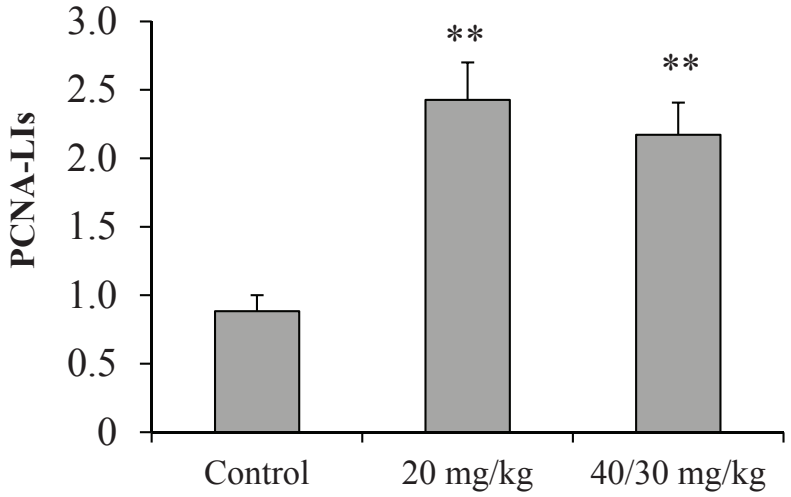

Figure 3-2 (A) Immunohistochemical staining of proliferating cell nuclear antigen (PCNA) in the kidney of *gpt* delta rats treated with CTN for 28 days.

Arrow heads show PCNA-positive nuclei.

(B) PCNA-labeling indices (LIs) for tubular epithelial cells in the kidney cortices.

Values are means ± SD of data for five rats. **: Significantly different from the control at $p < 0.01$.

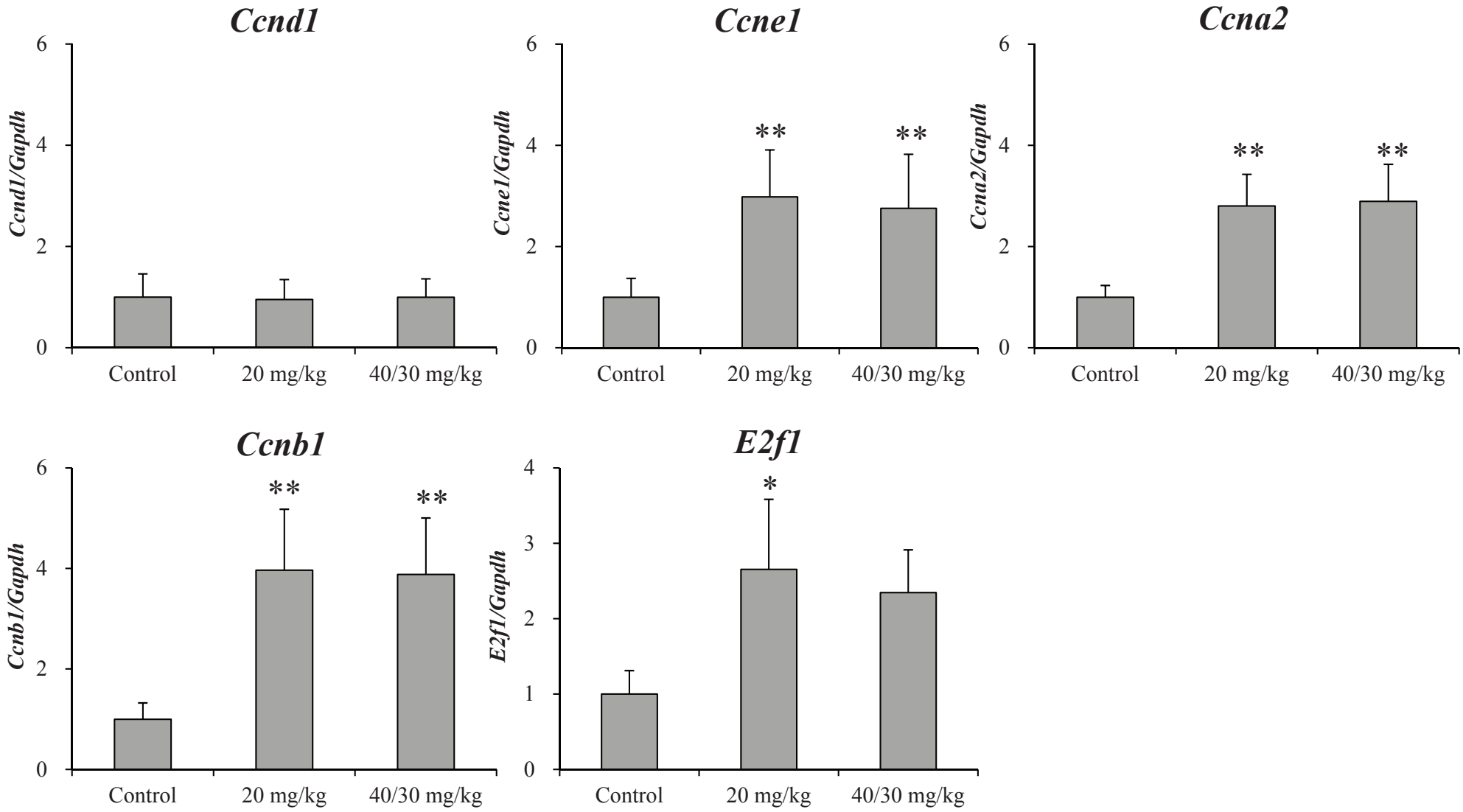

Figure 3-3 Changes in mRNA levels of cell-cycle related factors (*Ccna2*, *Ccnb1*, *Ccnd1*, *Ccne1, E2f1*) in the kidney cortices of *gpt* delta rats treated with CTN for 28 days.

Values are means ± SD of data for five rats. Normalization is to *Gapdh* mRNA levels. *, **: Significantly different from the control group at $p < 0.05$ and 0.01, respectively.

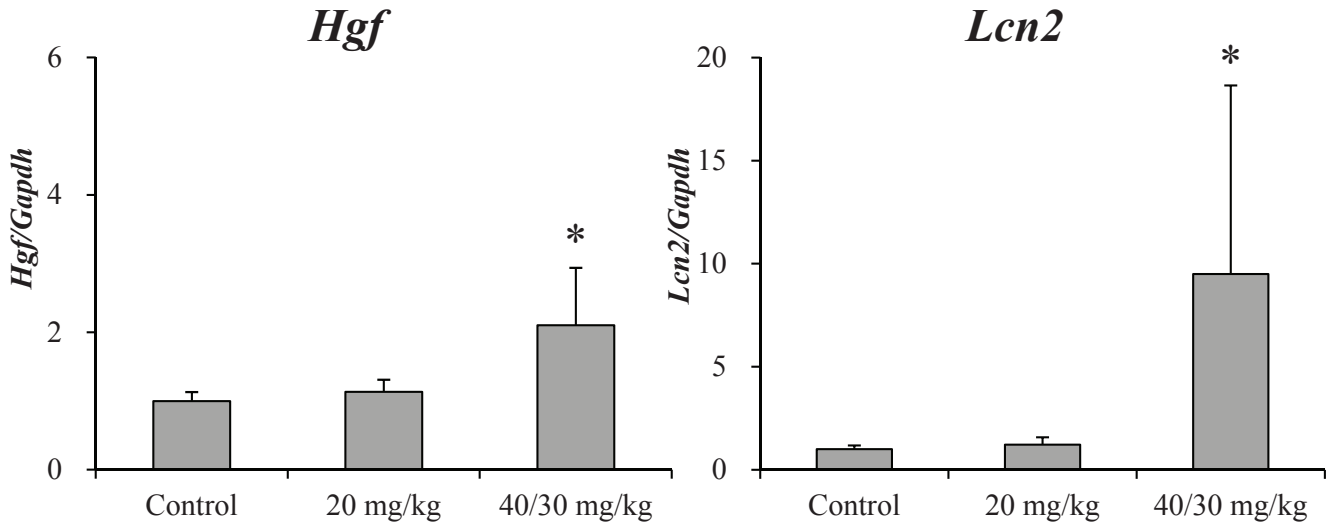

Figure 3-4 Changes in mRNA levels of mitogenic factors associated with tissue damage/regeneration (*Hgf*, *Lcn2*) in the kidney cortices of *gpt* delta rats treated with CTN for 28 days.

Values are means ± SD of data for five rats. Normalization is to *Gapdh* mRNA levels. *, **: Significantly different from the control group at $p < 0.05$ and 0.01, respectively.

(A)

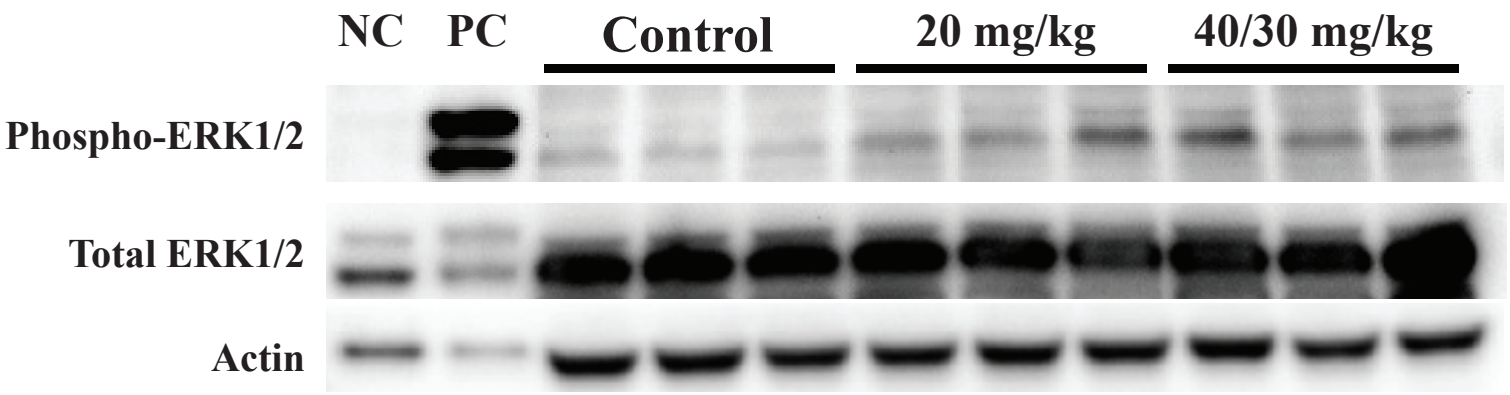

(B)

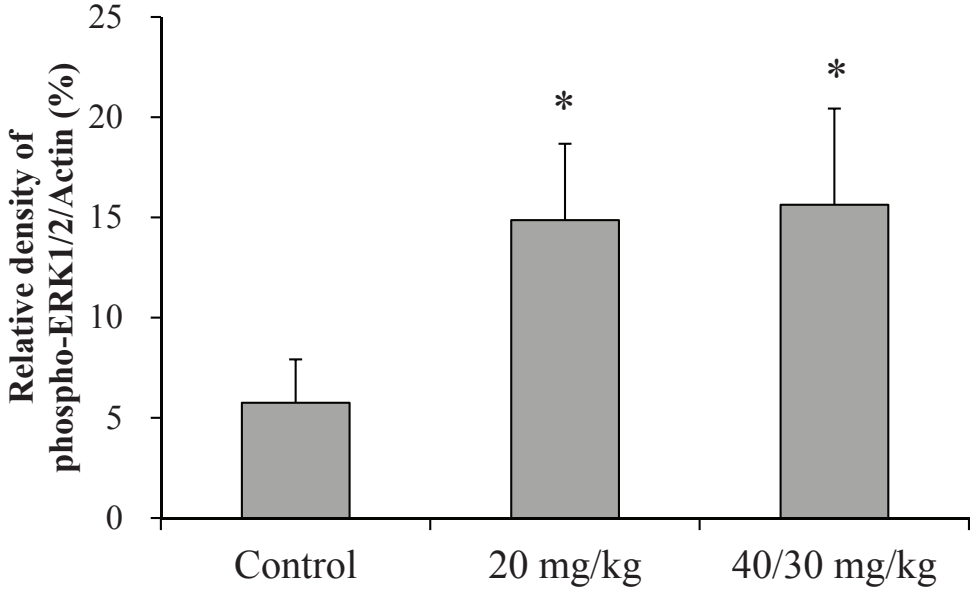

Figure 3-5 (A) Western blot analysis of phospho-ERK1/2 and ERK1/2 from the kidney cortices of *gpt* delta rats treated with CTN for 28 days.
(B) Densitometric analysis of Western blot results normalized to actin levels in the same tissue sample.
The values are means ± SD for three rats. *: Significantly different from the control at $p < 0.05$. NC (negative control): ERK1/2 cell extracts treated with U0126 (MEK inhibitor). PC (Positive control): ERK1/2 cell extract treated with 12-*O*-tetradecanoylphorbol-13-acetate (TPA).

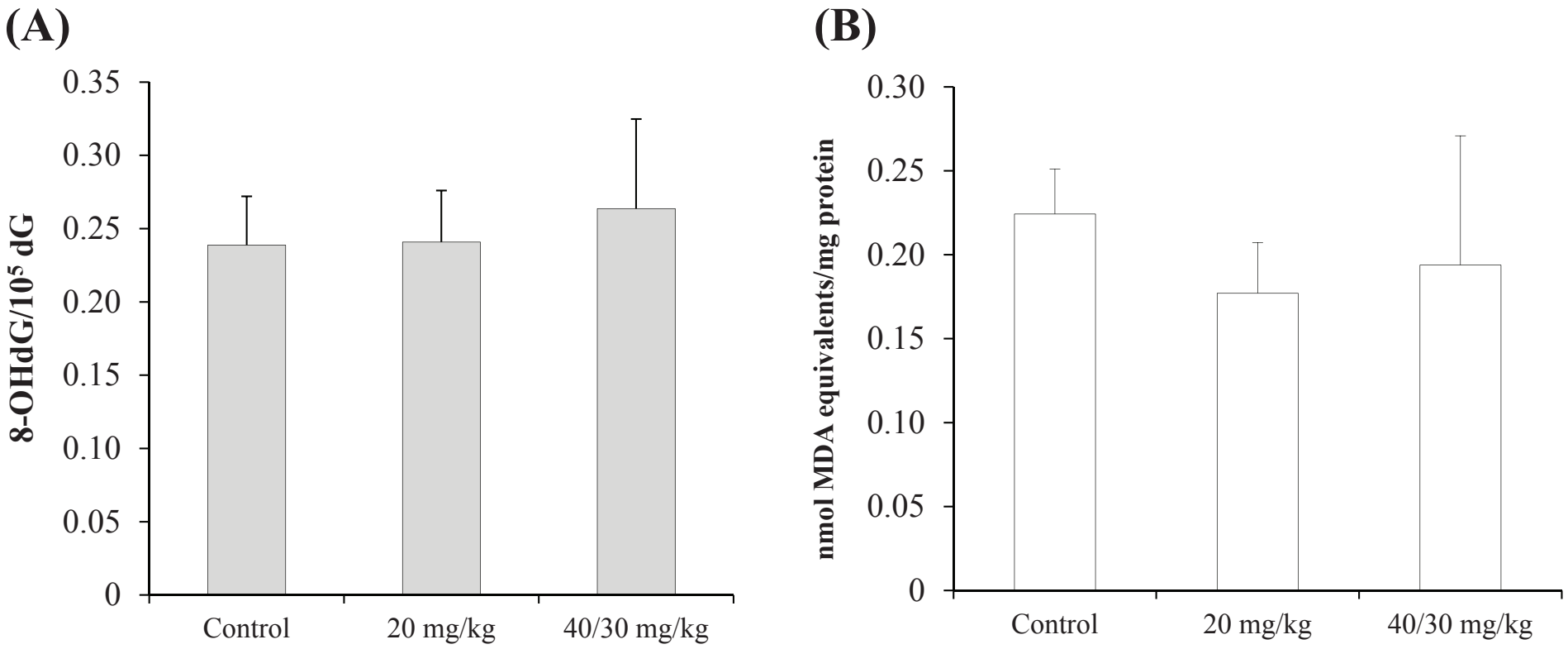

Figure 3-6 Changes in 8-OHdG levels (A) and TBARS (B) in the kidney cortices of *gpt* delta rats treated with CTN for 28 days.

Values are means ± SD of data for five rats.

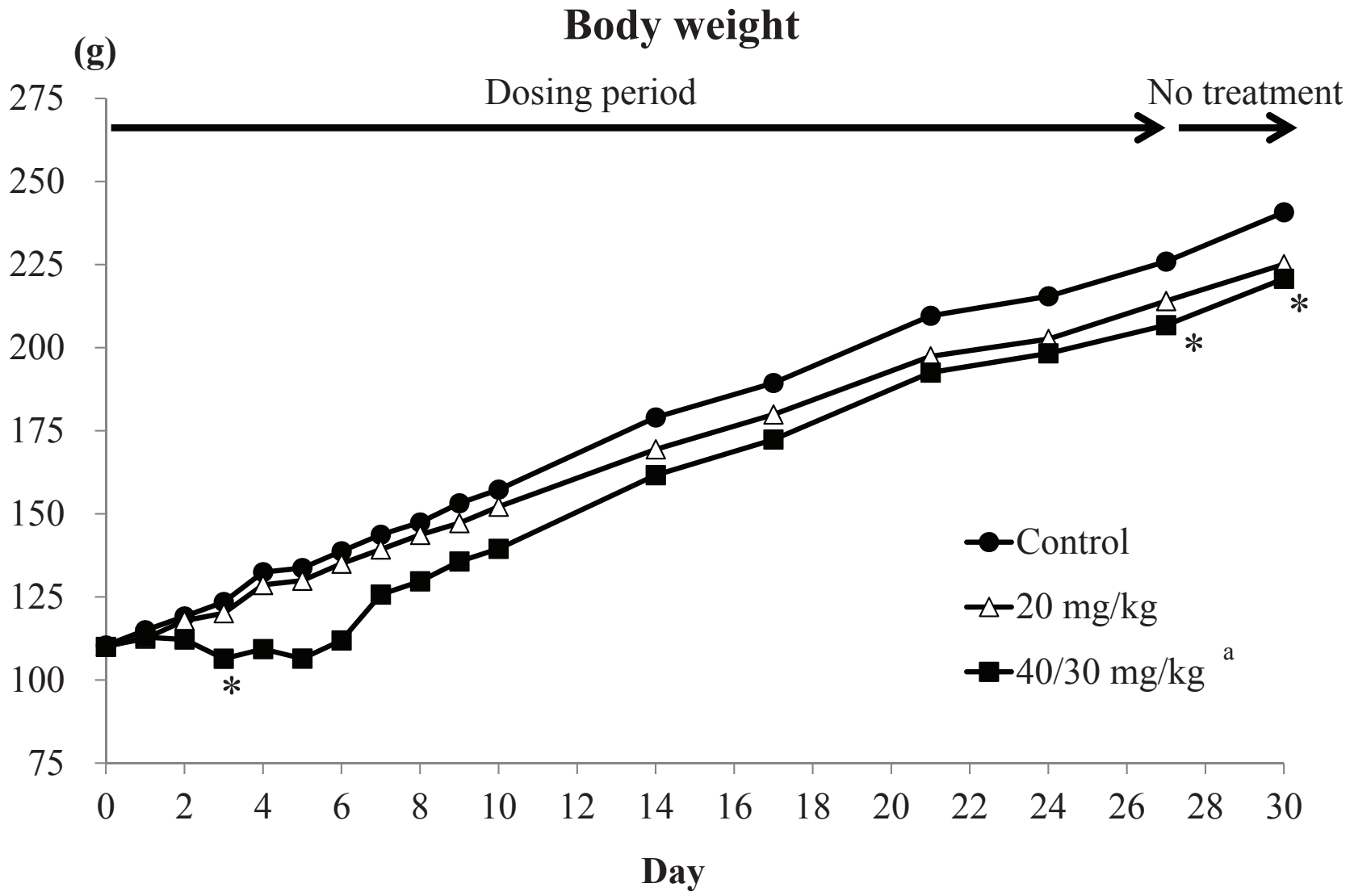

Figure 3-7 Body weight changes of *gpt* delta rats treated with CTN for 28 days.

[a]: The dose of 40 mg/kg was decreased to 30 mg/kg at Day 4 because of severe weight loss. *: $p < 0.05$ vs. Control.

Table 3-1 Final body and kidney weights in F344 *gpt* delta rats treated with CTN for 28 days.

Group	n	Final body weight (g)	Kidney weight	
			Absolute (g)	Relative (g/100g BW)
Control	5	240.8±13.2[a]	1.66 ± 0.15	0.69 ± 0.03
CTN 20 mg/kg	5	225.1±8.6	1.66 ± 0.08	0.74 ± 0.02
CTN 40/30 mg/kg[b]	4	220.8±7.7*	2.18 ± 0.43	0.99 ± 0.23*

[a]: Mean±SD

[b]: The dose of 40 mg/kg was decreased to 30 mg/kg on day four because of severe weight loss of the animals.

* : Significantly different from the control group at $p < 0.05$.

Table 3-2 *gpt* mutant frequencies (MFs) in the kidney cortex of F344 *gpt* delta rats treated with CTN for 28 days.

Group	Animal No.	Cm^R colonies ($\times 10^5$)	6-TG^R and Cm^R colonies	MFs ($\times 10^{-5}$)	Mean ± SD
Control	1	24.7	4	0.16	0.12 ± 0.11
	2	27.9	0	0.00	
	3	23.5	2	0.09	
	4	19.8	1	0.05	
	5	17.0	5	0.29	
CTN 20 mg/kg	6	18.0	2	0.11	0.14 ± 0.06
	7	23.6	2	0.08	
	8	17.2	2	0.12	
	9	20.4	5	0.25	
	10	16.0	2	0.12	
CTN 40/30 mg/kg	11	25.2	0	0.00	0.12 ± 0.04
	13	25.0	3	0.12	
	14	19.6	4	0.20	
	15	14.1	2	0.14	
ENU 50 mg/kg (positive control)	16	21.3	73	3.42	3.51 ± 0.67**
	17	16.8	60	3.57	
	18	21.2	52	2.45	
	19	21.6	85	3.93	
	20	14.3	60	4.19	

**: Significantly different from the control group at $p < 0.01$.

Table 3-3 Spi$^-$ mutant frequencies (MFs) in the kidney cortex of F344 *gpt* delta rats treated with CTN for 28 days

Group	Animal No.	Plaques within XL-1 Blue MRA (× 10^5)	Plaques within WL95 (P2)	MFs (× 10^{-5})	Mean ± SD
Control	1	45.1	4	0.09	0.28 ± 0.15
	2	42.6	18	0.42	
	3	48.9	7	0.14	
	4	27.2	15	0.55	
	5	39.3	8	0.20	
CTN 20 mg/kg	6	33.4	7	0.21	0.31 ± 0.17
	7	41.4	5	0.12	
	8	23.3	12	0.51	
	9	37.9	14	0.37	
	10	21.8	7	0.32	
CTN 40/30 mg/kg	11	41.9	6	0.14	0.26 ± 0.16
	13	30.6	100	3.27[a]	
	14	48.0	9	0.19	
	15	22.9	10	0.44	
ENU 50 mg/kg (positive control)	16	38.6	51	1.32	1.34 ± 0.11**
	17	26.8	38	1.42	
	18	26.8	39	1.45	
	19	36.2	48	1.33	
	20	23.3	27	1.16	

[a]: Data of animal No.13 was excluded for the caclulation based on the result of Smirnov's outlier test.

**: Significantly different from the control group at $p < 0.01$.

Table 3-4 Comet assay in the kidney of F344 rats treated with CTN for 2 days.

Group	n	Head intensity (%)	% Tail DNA	Tail length (μm)	Tail moment
Control	5	34.9 ± 2.6[a]	3.9 ± 0.9	22.7 ± 2.1	0.7 ± 0.2
CTN 20 mg/kg	5	34.9 ± 2.8	3.2 ± 0.4	22.1 ± 2.3	0.5 ± 0.1
CTN 40 mg/kg	5	34.9 ± 2.4	4.7 ±0.7	24.5 ± 2.2	0.9 ± 0.1*
MMS 220 mg/kg (positive control)	5	36.2 ± 1.7	32.4 ± 6.4**	48.8 ± 5.1**	7.2 ± 1.9**

[a]: Mean±SD

*, ** : Significantly different from the control group at $p < 0.05$ and 0.01, respectively.

Table 3-5 Micronucleus test in the bone marrow of F344 rats treated with CTN for 2 days.

Group	n	MNPCE/PCE	PCE/NCE
Control	5	0.08 ± 0.03[a]	0.54 ± 0.24
CTN 20 mg/kg	5	0.09 ± 0.05	0.49 ± 0.11
CTN 40 mg/kg	5	0.17 ± 0.07	0.71 ± 0.31
CP 120 mg/kg (positive control)	5	0.88 ± 0.25*	0.25 ± 0.08*

[a]: Mean±SD

* : Significantly different from the control group at $p < 0.05$.

MNPCEs: micronucleated polychromatic erythrocytes

PCEs: polychromatic erythrocytes

NCEs: normochromatic erythrocytes

General discussion

Mutagenesis of OTA in the rats and mice kidneys

Four-week exposure to OTA at a carcinogenic dose increased Spi^- MFs in the renal outer medullas (ROMs), the carcinogenic target site of *gpt* delta rats, and the mutation spectrum analysis of Spi^- mutants demonstrated that OTA caused large deletion (over 1,000 base pairs) mutations in the *red/gam* genes. It has been known that large deletion mutations in the *red/gam* genes are induced by exposures of *gpt* delta mice to DNA double strand break (DSB)-inducing agents such as ionizing radiation (IR), ultraviolet B (UVB), and mytomycin C (MMC) (37), suggesting the occurrence of DSBs is thought to be a trigger for large deletion mutations (37, 55, 56). As a matter of fact, western blot analysis using protein extracts from ROMs of *gpt* delta rats treated with OTA demonstrated obvious increases in γ-H2AX expression, a well-established DSB marker, in an OTA dose-dependent manner. In addition, immunohistochemical analysis clearly demonstrated the site-specific localization of γ-H2AX-positive cells in

the tubular epithelium of the outer stripe of the ROM. Together with the positive results in the comet assays, obtained results suggest OTA induces DSBs in the ROMs of *gpt* delta rats.

Gene mutations derived from DSBs arise during the repair process, and there are 2 major pathways mediating DSBs repair, non-homologous end-joining (NHEJ) and homologous recombination repair (HR) (47, 48, 75). The results of quantitative PCR analysis and western blotting using ROMs of *gpt* delta rats has shown that OTA increased the expression levels of HR-related factors (*Rad51*, *Rad 18* and *Brip1*), but not NHEJ-related factors (*Xrcc5*, *Xrcc6*, and *Lig4*). As is known that HR is more active in S/G_2 phase, the results appeared to be related with OTA-specific cell cycle control, in which OTA induces G_2/M arrest and increases cell proliferation through another functional mechanism, thereby increasing the ratio of cells in S/G_2 phase (80, 81, 82). Although HR is believed to be an error-free repair system, there have been several evidences that HR can induce large deletion mutations (37, 87). Overall data

suggested that OTA-induced DSBs appeared to be predominantly repaired by HR, consequently leading to large deletion mutations.

In the mice kidney, OTA increased DNA damage parameters in comet assay, and also increased the numbers of γ-H2AX-positive cells at ROMs. However, experiments using *p53*-deficient mice demonstrated that the absence of p53 effects only on the numbers of γ-H2AX-positive cells, but not on the degree of DNA damage parameters in comet assay. Given that comet assay can detect strand breaks and alkali-labile sites derived from DNA base modification such as alkylated bases and bulky base adducts (96), it is speculated that p53 prevents formation of DSBs, but not DNA modification itself. Although p53 has several functions in DNA repair, global gene expression analysis demonstrated that cell cycle control, one of conventional function of p53/p21 axis, is responsible for preventive effects on DSBs formation. On the other hand, mutation frequency of *red/gam* genes were increased only in *p53*-defidicent mice, but not in wild type mice. However, because histopathological changes indicated that the

site-specific localization of OTA in the kidneys of mice were similar to that of rats, this site specificity, but not p53 function, might be responsible for the negative outcome of *in vivo* mutagenicity. Consistent with rats study, increases of several mRNAs related with HR were detected in *p53*-deficient *gpt* delta mice, and these changes are considered to reflect repairs of DSB induced by OTA. However, the mutation pattern of rats and mice were quite different, and predominant mutation pattern in *p53*-deficient *gpt* delta mice was single base mutations. Such species difference between rats and mice in mutation spectrum induced by mutagen are observed other chemicals (unpublished data). It remains unclear whether these differences come from p53 status or species difference in DNA repair system, and its biological significance is unknown.

There still remains unclear the mechanism of DSBs formation by OTA exposure. The formation of OTA-specific DNA adducts were observed in human tissues by ^{32}P postlabeling methods and mass spectrum analysis in animal tissues (17, 66, 67 68). The appearance of apurinic/apyrimidinic (AP) sites in the rat kidney, as well as

inhibition of topoisomerase II (TOPOII) activity in cultured cells, have also been reported (69, 70). It has been accepted that DSBs occur through various causes, such as inhibition of the replication fork due to the formation of bulky adducts, cleavage of AP sites during base excision repair, and suppression of TOPOII activity (71, 72, 73). Further studies should be needed for understanding the DSBs induction mechanism of OTA.

OTA experiments using rats and mice demonstrated that OTA clearly induced DSBs in the kidneys of both species. Additionally, p53 prevents DSBs formation and following gene mutations via p53/p21-mediated cell cycle control. It has been suggested that the key events of OTA-induced carcinogenesis include disruption of mitosis, cell proliferation, and genetic instability (62, 81). These events appeared to be related with formation of oxidative stress, inhibition of histone acetyltransferase, cellular injury, and so on (62, 146, 148). Although increases of mutation frequencies induced by OTA in the present study were mild, it is highly probable that OTA exerts its

carcinogenicity via complicated pathway, and the present results suggest that genotoxic event represented by formation of DSBs and following gene mutations are involved in certain steps of OTA-induced carcinogenesis. In this aspect, further analysis focused on whether OTA reacts directly DNA or not should be investigated to conclude the contribution of genotoxic events on OTA-induced carcinogenesis.

Major mechanism underlying CTN-induced carcinogenesis

In contrast to genotoxic potential of OTA, CTN did not alter any parameters in *in vivo* reporter gene mutation assays, comet assays and micronucleus assays. There has been only one report demonstrating CTN-specific DNA adducts detected by ^{32}P postlabeling method in human kidney tumor (67). However, the chemical structure and mutagenic potential of these adducts are unclear, and the presence of CTN-specific adducts in rats kidney has not been reported. Therefore, in the rat kidneys, the carcinogenic target site, it is likely that CTN does not induce DNA damage or gene mutations.

CTN has been demonstrated as tumor promoter in the 2-stage carcinogenicity assay using rats (119), and as generally accepted, tumor promoter agents increase cell proliferation in the target organs. In fact, in the kidney cortex of *gpt* delta rats treated with CTN, the labeling index of PCNA-positive cells was significantly increased compared with that of the control group. Quantitative PCR analysis and western

blotting demonstrated CTN increased mRNA expression of cell cycler-related genes (*Ccna2*, *Ccnb1*, *Ccne1*, and its transcription factor *E2f1*), which is followed by increase of ERK1/2 protein. It has been proposed that non-genotoxic carcinogens are classified as cytotoxic compounds which cause cell death and compensatory hyperplasia, or as mitogenic compounds which induce cell proliferation through interatction with specific cellular receptor (149). In the present study, consistent with the histopathological injury observed in the higher dose (40/30 mg/kg) of CTN-treated kidney, the expression of *Hgf* and *Lcn2* were also detected, both of which are known to be highly expressed in tubular epithelial cells during regeneration after tissue damage and exert mitogenic effects on kidney cells (129, 130). On the other hand, in the low-dose (20 mg/kg) group, there was not any histopathological alterations or signal transduction activity related to compensatory regeneration, suggesting direct mitogenic activity of CTN. In a long time bioassay, CTN at a concentration of 0.1% in the diet (approximately 50 mg/kg/day) induced renal tumor in F344 rats, which accompanied by histopathological

injury such as interstitial fibrosis and nephritis (14). Another study demonstrated that CTN at 0.02 and 0.05% in the diet (approximately 10 and 25 mg/kg) did not have any carcinogenicity in the kidney by 48-week treatment (119). Thus, it is likely that the proliferative effects of CTN at carcinogenic doses may involve compensatory mechanisms. However, the present data strongly suggested that the direct mitogenic activity of CTN may exert additional effects on cell cycle progression, thereby contributing to renal carcinogenesis.

OTA and CTN

This study focused on modes of action of two mycotoxins which have clear renal carcinogenicity in rodents. *In vivo* mutation assay using *gpt* delta rats and mice treated with OTA clearly demonstrated that OTA induces DSBs at the carcinogenic target site, which followed by gene mutations in the reporter genes. On the other hand, *in vivo* genotoxicity assays of CTN showed negative results, but progression of cell cycle were detected. Obtained results suggest that these two mycotoxins exert its carcinogenicity via different mechanisms. Some of the OTA producing fungi are also able to produce the CTN, so that simultaneous contamination of OTA and CTN has been identified in cereals and cereal-based products (150, 151). Considering that cell proliferating agents have enhancing effect on *in vivo* mutagenicity of genotoxic agents (152), further studies focused on the combination effect of OTA and CTN should be investigated.

Conclusion

This study focused on the carcinogenic mechanism of two mycotoxins which have clear renal carcinogenicity in rodents. *In vivo* mutation assay and protein/mRNA expression analysis using *gpt* delta rats and mice treated with OTA demonstrated that OTA induces DSBs at the carcinogenic target site, and DSBs may lead gene mutation in the reporter genes in both species. Additionally, experiments using *p53*-deficient mice demonstrated that p53 inhibits DSBs and following gene mutations in the kidney of *gpt* delta mice, and global gene expression analysis revealed that p53/p21-mediated cell cycle control plays key role in its preventive effects. Based on these data, it is suggested that genotoxic events may part a role in OTA-induced renal carcinogenesis. On the other hand, all of three *in vivo* genotoxicity assays (reporter gene mutation, comet and micronucleus assays) of CTN showed negative results, alternatively clear progression of cell cycle were detected, which appeared to be main mechanism involved in CTN-induced renal carcinogenesis. Obtained results showed different mechanism

mainly contributes OTA and CTN-induced renal carcinogenesis, and these results provide useful information to evaluate risk of these mycotoxins in human life.

Acknowledgements

I extends my deepest gratitude to following persons of the United Graduate school of Veterinary Sciences, Gifu University, for their help in the completion of this thesis: Professor Dr. T. Yanai, Associate Professor Dr. H. Sakai, Professor Dr. M. Goryo for their excellent guidance and supervision, and Professor Dr. T. Unno, Professor Dr. M. Shibutani, Professor Dr. Y. Kobayashi for excellent advices.

I also appreciate Dr. T. Umemura, Dr. K. Ogawa, Dr. Y. Ishii, Dr. S. Takasu, Mr. K. Matsushita, Dr. Y. Yokoo and Ms. A. Kijima of Division of Pathology, National Institute of Health Sciences, for their important advice and assistance throughout the experiments and paper works.

Finally, I thank my family for gentle support of my life.

References

1) Doll, R. and Peto, R. (1981). The causes of cancer: quantitative estimates of avoidable risks of cancer in the Unites States today. J. Natl Cancer Inst., 66, 1191-1308.

2) O'Brien, J., Renwick, A.G., Constable, A., Dybing, E., Müller, D.J., Schlatter, J., Slob, W., Tueting, W., van Benthem, J., Williams, G.M., Wolfreys, A. (2006). Approaches to the risk assessment of genotoxic carcinogens in food: a critical appraisal. Food Chem Toxicol. 44, 1613-35.

3) Sugimura, T. (2000). Nutrition and dietary carcinogens. Carcinogenesis 21, 387-395.

4) Barrett, J.C. (1993). Mechanisms of multistep carcinogenesis and carcinogen risk assessment. Environ Health Perspect. 100, 9-20.

5) Oliveira, P.A., Colaço, A., Chaves, R., Guedes-Pinto, H., De-La-Cruz, P. L.F., Lopes, C. (2007). Chemical carcinogenesis. An Acad Bras Cienc. 79, 593-616.

6) Peraica, M., Radić, B., Lucić, A., Pavlović, M. (1999). Toxic effects of mycotoxins in humans. Bull World Health Organ. 77, 754-766.

7) Cicoňová, P., Laciaková, A., and Máté, D. (2010). Prevention of ochratoxin A contamination of food and ochratoxin A detoxification by microorganisms - a review. Czech J Food Sci. 2010 28, 465-474.

8) Flajs, D., Peraica, M. (2009). Toxicological properties of citrinin. Arh. Hig. Rada Toksikol.60, 457-464.

9) European Food Safety Authority (EFSA). (2006). Opinion of the Scientific Panel on Contaminants in the Food Chain on a Request from the Commission Related to Ochratoxin A in Food. EFSA J. 365, 1-56.

10) European Food Safety Authority (EFSA). (2012). Scientific Opinion on the risks for public and animal health related to the presence of citrinin in food and feed. EFSA J. 10, 2605.

11) Boorman, G. A., McDonald, M. R., Imoto, S., and Persing, R. (1992). Renal lesions

induced by ochratoxin A exposure in the F344 rat. Toxicol. Pathol. 20, 236-245.

12) Bendele, A. M., Carlton, W. W., Krogh, P., and Lillehoj, E. B. (1985). Ochratoxin A carcinogenesis in the (C57BL/6J X C3H) F1 mouse. J. Natl. Cancer Inst. 75, 733-742.

13) National Toxicology Program (NTP). (1989). Toxicology and Carcinogenesis Studies of Ochratoxin A (CAS No. 303-47-9) in F344/N Rats (Gavage Studies). Natl. Toxicol. Program Tech. Rep. Ser. 358, 1-142.

14) Arai, M., Hibino, T. (1983). Tumorigenicity of citrinin in male F344 rats. Cancer Lett. 17, 281–287.

15) Pfohl-Leszkowicz, A., Petkova-Bocharova, T., Chernozemsky, I. N., and Castegnaro, M. (2002). Balkan endemic nephropathy and associated urinary tract tumours: a review on aetiological causes and the potential role of mycotoxins. Food Addit Contam. 19, 282-302.

16) International Agency for Research on Cancer (IARC). (1993). Monographs on the

Evaluation of Carcinogenic Risks to Humans. Volume 56, 489-521.

17) Mantle P. G., Faucet-Marquis V., Manderville R. A., Squillaci B., and Pfohl-Leszkowicz A. (2010). Structures of covalent adducts between DNA and ochratoxin A: a new factor in debate about genotoxicity and human risk assessment. Chem. Res. Toxicol. 23, 89-98.

18) Delatour, T., Mally, A., Richoz, J., Ozden, S., Dekant, W., Ihmels, H., Otto, D., Gasparutto, D., Marin-Kuan, M., Schilter, B., and Cavin, C. (2008). Absence of 2'-deoxyguanosine-carbon 8-bound ochratoxin A adduct in rat kidney DNA monitored by isotope dilution LC-MS/MS. Mol. Nutr. Food Res. 52, 472-482.

19) Joint FAO/WHO Expert Committee on Food Additives (JECFA). (2001). Ochratoxin A JECFA Food Addit. Ser. 47

20) Obrecht-Pflumio, S., Chassat, T., Dirheimer, G., and Marzin, D. (1999). Genotoxicity of ochratoxin A by Salmonella mutagenicity test after bioactivation by mouse kidney microsomes. Mutat. Res. 446, 95-102.

21) Hennig, A., Fink-Gremmels, J. and Leistner, L. (1991). Mutagenicity and effects of ochratoxin A on the frequency of sister chromatid exchange after metabolic activation. IARC Sci. Publ. 115, 255-260.

22) Sabater-Vilar, M., Maas, R.F., Fink-Gremmels, J. (1999). Mutagenicity of commercial Monascus fermentation products and the role of citrinin contamination. Mutat. Res. 444, 7-16.

23) Bouslimi, A., Bouaziz, C., Ayed-Boussema, I., Hassen, W., Bacha, H. (2008). Individual and combined effects of ochratoxin A and citrinin on viability and DNA fragmentation in cultured Vero cells and on chromosome aberrations in mice bone marrow cells. Toxicology 251, 1-7.

24) Knasmüller, S., Cavin, C., Chakraborty, A., Darroudi, F., Majer, B.J., Huber, W.W., Ehrlich, V.A. (2004). Structurally related mycotoxins ochratoxin A, ochratoxin B, and citrinin differ in their genotoxic activities and in their mode of action in human-derived liver (HepG2) cells: implications for risk assessment. Nutr. Cancer

50, 190-197.

25) Liu, B.H., Yu, F.Y., Wu, T.S., Li, S.Y., Su, M.C., Wang, M.C., Shih, S.M. (2003). Evaluation of genotoxic risk and oxidative DNA damage in mammalian cells exposed to mycotoxins, patulin and citrinin. Toxicol. Appl. Pharmacol. 191, 255-263.

26) Chang, C.H., Yu, F.Y., Wu, T.S., Wang, L.T., Liu, B.H. (2011). Mycotoxin citrinin induced cell cycle G2/M arrest and numerical chromosomal aberration associated with disruption of microtubule formation in human cells. Toxicol. Sci. 119, 84-92.

27) Jeswal, P. (1996). Citrinin-induced chromosomal abnormalities in the bone marrow cells of Mus musculus. Cytobios 86, 29-33.

28) Pfeiffer, E., Gross, K., Metzler, M. (1998). Aneuploidogenic and clastogenic potential of the mycotoxins citrinin and patulin. Carcinogenesis 19, 1313-1318.

29) World Health Organization (WHO). (2006). TRANSGENIC ANIMAL MUTAGENICITY ASSAYS. Environmental Health Criteria 233.

30) Tasaki, M., Umemura, T., Suzuki, Y., Hibi, D., Inoue, T., Okamura, T., Ishii, Y., Maruyama, S., Nohmi, T., and Nishikawa, A. (2010). Oxidative DNA damage and reporter gene mutation in the livers of gpt delta rats given non-genotoxic hepatocarcinogens with cytochrome P450-inducible potency. Cancer Sci. 101, 2525-2530.

31) Umemura, T., Kanki, K., Kuroiwa, Y., Ishii, Y., Okano, K., Nohmi, T., Nishikawa, A., and Hirose, M. (2006). In vivo mutagenicity and initiation following oxidative DNA lesion in the kidneys of rats given potassium bromate. Cancer Sci. 97, 829-835.

32) Nohmi, T., Suzuki, T., and Masumura, K. (2000). Recent advances in the protocols of transgenic mouse mutation assays. Mutat Res. 455, 191-215.

33) Masumura, K. (2009). Spontaneous and induced *gpt* and Spi$^-$ mutant frequencies in gpt transgenic rodents. Genes and Environment 31, 105-118.

34) Hibi D., Suzuki Y., Ishii Y., Jin M., Watanabe M., Sugita-Konishi Y., Yanai T.,

Nohmi T., Nishikawa A., Umemura T. (2011). Site-specific in vivo mutagenicity in the kidney of gpt delta rats given a carcinogenic dose of ochratoxin A. Toxicol Sci. 122, 406-414.

35) Hibi D., Kijima A., Suzuki Y., Ishii Y., Jin M., Sugita-Konishi Y., Yanai T., Nishikawa A., Umemura T. (2013). Effects of p53 knockout on ochratoxin A-induced genotoxicity in p53-deficient gpt delta mice. Toxicology 304: 92-99.

36) Joint FAO/WHO Expert Committee on Food Additives (JECFA). (2008). Safety Evaluation of Certain Food Additives and Contaminants. WHO Food Additives Series, 59, 357-429.

37) Nohmi, T. and Masumura, K. (2005). Molecular nature of intrachromosomal deletions and base substitutions induced by environmental mutagens. Environ Mol Mutagen., 45, 150-161.

38) Masumura, K., Matsui, K., Yamada, M., Horiguchi M, Ishida K, Watanabe M, Wakabayashi K, Nohmi T. (2000). Characterization of mutations induced by

2-amino-1-methyl-6-phenylimidazo[4,5-b]pyridine in the colon of *gpt* delta transgenic mouse: novel G:C deletions beside runs of identical bases. Carcinogenesis, 21, 2049-2056.

39) Masumura. K., Totsuka, Y., Wakabayashi, K., Nohmi, T. (2003). Potent genotoxicity of aminophenylnorharman, formed from non-mutagenic norharman and aniline, in the liver of *gpt* delta transgenic mouse. Carcinogenesis, 24, 1985-1993.

40) Nohmi, T., Suzuki, M., Masumura, K., Yamada, M., Matsui, K., Ueda, O., Suzuki, H., Katoh, M., Ikeda, H., Sofuni, T. (1999). Spi$^-$ selection: An efficient method to detect gamma-ray-induced deletions in transgenic mice. Environ Mol Mutagen. 34, 9-15.

41) Horiguchi, M., Masumura, K., Ikehata, H., Ono, T., Kanke, Y., Nohmi, T.. Molecular nature of ultraviolet B light-induced deletions in the murine epidermis. (2001). Cancer Res. 61, 3913-3918.

42) Takeiri, A., Mishima, M., Tanaka, K., Shioda, A., Ueda, O., Suzuki, H., Inoue, M., Masumura, K., Nohmi, T. (2003). Molecular characterization of mitomycin C-induced large deletions and tandem-base substitutions in the bone marrow of *gpt* delta transgenic mice. Chem Res Toxicol. 16, 171-179.

43) Hibi, D., Kijima, A., Kuroda, K., Suzuki, Y., Ishii, Y., Jin, M., Nakajima, M., Sugita-Konishi, Y., Yanai, T., Nohmi, T., Nishikawa, A., Umemura, T. (2013). Molecular mechanisms underlying ochratoxin A-induced genotoxicity: global gene expression analysis suggests induction of DNA double-strand breaks and cell cycle progression. J Toxicol Sci. 38: 57-69.

44) Rogakou, E.P., Pilch, D.R., Orr, A.H., Ivanova, V.S., Bonner, W.M. (1998). DNA double-stranded breaks induce histone H2AX phosphorylation on serine 139. J Biol Chem. 273, 5858-5868.

45) Fernandez-Capetillo, O., Celeste, A., Nussenzweig, A. (2004). Focusing on foci: H2AX and the recruitment of DNA-damage response factors. Cell Cycle, 2,

426-427.

46) Scully, R. and Xie, A. (2013). Double strand break repair functions of histone H2AX. Mutat Res. 750: 5-14.

47) Puget N., Torchard D., Serova-Sinilnikova O.M., Lynch H.T., Feunteun J., Lenoir G.M., Mazoyer S. (1997). A 1-kb Alu-mediated germ-line deletion removing BRCA1 exon 17. Cancer Res. 57, 828-831.

48) Khanna K.K., Jackson S.P. (2001). DNA double-strand breaks: signaling, repair and the cancer connection. Nat Genet. 27, 247-254.

49) Kumata K., Amano R., Ichinoe M., Uchiyama S. (1980). Culture conditions and purification method for large-scale production of ochratoxins by *Aspergillus ochraceus*. Shokuhin Eiseigaku Zasshi 21, 171-176.

50) Sugita-Konishi Y., Tanaka T., Nakajima M., Fujita K., Norizuki H., Mochizuki N., Takatori, K. (2006). The comparison of two clean-up procedures, multifunctional column and immunoaffinity colomn, for HPLC determination of ochratoxin A in

cereals, raisins and green coffee beans. Talanta, 69, 650-655.

51) Mantle P., Kulinskaya E., Nestler S. (2005). Renal tumourigenesis in male rats in response to chronic dietary ochratoxin A. Food Addit Contam. 22 (Suppl. 1), 58-64.

52) Masumura K., Sakamoto Y., Ikeda M., Asami Y., Tsukamoto T., Ikehata H., Kuroiwa Y., Umemura T., Nishikawa A., Tatematsu M., Ono T., Nohmi T. (2011). Antigenotoxic effects of p53 on spontaneous and ultraviolet light B-induced deletions in the epidermis of *gpt* delta transgenic mice. Environ Mol Mutagen. 52, 244-252.

53) de Groene EM, Jahn A, Horbach GJ, Fink-Gremmels J. (1996). Mutagenicity and genotoxicity of the mycotoxin ochratoxin A. Environ Toxicol Pharmacol. 15: 21-26

54) Masumura K., Kuniya K., Kurobe T., Fukuoka M., Yatagai F., Nohmi T. (2002). Heavy-ion-induced mutations in the *gpt* delta transgenic mouse: comparison of mutation spectra induced by heavy-ion, X-ray, and gamma-ray radiation. Environ Mol Mutagen. 40, 207-215.

55) Varga T., Aplan P.D. (2005). Chromosomal aberrations induced by double strand DNA breaks. *DNA Repair (Amst)*, 4, 1038-1046.

56) Pollard L.M., Bourn R.L., Bidichandani S.I. (2008). Repair of DNA double-strand breaks within the (GAA*TTC)n sequence results in frequent deletion of the triplet-repeat sequence. Nucleic Acids Res. 36, 489-500.

57) Kastan M.B. (2008). DNA damage responses: mechanisms and roles in human disease: (2007). G.H.A. Clowes Memorial Award Lecture. Mol Cancer Res., 6, 517-524.

58) Summers K.C., Shen F., Sierra Potchanant E.A., Phipps E.A., Hickey R.J., Malkas LH. (2011). Phosphorylation: the molecular switch of double-strand break repair. Int J Proteomics, 2011, 373816.

59) Sonoda E., Zhao G.Y., Kohzaki M., Dhar P.K., Kikuchi K., Redon C., Pilch D.R., Bonner W.M., Nakano A., Watanabe M., Nakayama T., Takeda S., Takami Y. (2007). Collaborative roles of γH2AX and the Rad51 paralog Xrcc3 in homologous

recombinational repair. DNA Repair (Amst) 6, 280-292.

60) Koike M., Mashino M., Sugasawa J., Koike A. (2008). Histone H2AX phosphorylation independent of ATM after X-irradiation in mouse liver and kidney in situ. J Radiat Res. 49, 445-449.

61) Redon C.E., Nakamura A.J., Martin O.A., Parekh P.R., Weyemi US, Bonner WM. (2011). Recent developments in the use of γ-H2AX as a quantitative DNA double-strand break biomarker. Aging (Albany NY), 3, 168-174.

62) Mally A. (2012). Ochratoxin A and mitotic disruption: mode of action analysis of renal tumor formation by ochratoxin A. Toxicol Sci. 127, 315-330.

63) Zeljezić D., Domijan A.M., Peraica M. (2006). DNA damage by ochratoxin A in rat kidney assessed by the alkaline comet assay. Braz J Med Biol Res. 39, 1563-1568.

64) Kane A., Creppy E.E., Roth A, Röschenthaler R., Dirheimer G. (1986). Distribution of the [3H]-label from low doses of radioactive ochratoxin A ingested by rats, and evidence for DNA single-strand breaks caused in liver and kidneys. Arch Toxicol.

58, 219-224.

65) Creppy E.E., Kane A., Dirheimer G., Lafarge-Frayssinet C., Mousset S., Frayssinet C. (1985). Genotoxicity of ochratoxin A in mice: DNA single-strand break evaluation in spleen, liver and kidney. Toxicol Lett. 28, 29-35.

66) Pfohl-Leszkowicz A., Manderville R.A. (2012). An update on direct genotoxicity as a molecular mechanism of ochratoxin a carcinogenicity. Chem Res Toxicol. 25, 252-262.

67) Pfohl-Leszkowicz A., Tozlovanu M., Manderville R., Peraica M., Castegnaro M., Stefanovic V. (2007). New molecular and field evidences for the implication of mycotoxins but not aristolochic acid in human nephropathy and urinary tract tumor. Mol Nutr Food Res. 51, 1131-1146.

68) Faucet V., Pfohl-Leszkowicz A., Dai J., Castegnaro M., Manderville R.A. (2004). Evidence for covalent DNA adduction by ochratoxin A following chronic exposure to rat and subacute exposure to pig. Chem Res Toxicol. 17, 1289-1296.

69) Cavin C., Delatour T., Marin-Kuan M., Holzhäuser D., Higgins L., Bezençon C., Guignard G., Junod S., Richoz-Payot J., Gremaud E., Hayes J.D., Nestler S., Mantle P., Schilter B. (2007). Reduction in antioxidant defenses may contribute to ochratoxin A toxicity and carcinogenicity. Toxicol Sci. 96, 30-39.

70) Cosimi S., Orta L., Mateos S., Cortés F. (2009). The mycotoxin ochratoxin A inhibits DNA topoisomerase II and induces polyploidy in cultured CHO cells. Toxicol In Vitro. 23, 1110-1115.

71) Bi X., Slater D.M., Ohmori H., Vaziri C. (2005). DNA polymerase kappa is specifically required for recovery from the benzo[a]pyrene-dihydrodiol epoxide (BPDE)-induced S-phase checkpoint. J Biol Chem. 280, 22343-22355.

72) Boiteux S., Guillet M. (2004). Abasic sites in DNA: repair and biological consequences in Saccharomyces cerevisiae. DNA Repair (Amst) 3, 1-12.

73) Smart D.J., Halicka H.D., Schmuck G., Traganos F., Darzynkiewicz Z., Williams G.M. (2008). Assessment of DNA double-strand breaks and γH2AX induced by the

topoisomerase II poisons etoposide and mitoxantrone. Mutat Res. 641**,** 43-47.

74) Pfohl-Leszkowicz A., Bartsch H., Azémar B., Mohr U., Estève J., Castegnaro M. (2002). MESNA protects rats against nephrotoxicity but not carcinogenicity induced by ochratoxin A, implicating two separate pathway. Facta Universitatis, Series: Medicine and Biology 9, 57- 63.

75) Chapman J.R., Taylor M.R., Boulton S.J. (2012). Playing the end game: DNA double-strand break repair pathway choice. Mol Cell, 47, 497-510.

76) Escribano-Díaz C., Orthwein A., Fradet-Turcotte A., Xing M., Young J.T., Tkáč J., Cook M.A., Rosebrock A.P., Munro M., Canny M.D., Xu D., Durocher D. (2013). A cell cycle-dependent regulatory circuit composed of 53BP1-RIF1 and BRCA1-CtIP controls DNA repair pathway choice. Mol Cell, 49, 872-883.

77) Burma S., Chen B.P., Chen D.J. (2006). Role of non-homologous end joining (NHEJ) in maintaining genomic integrity. DNA Repair (Amst), 5, 1042-1048.

78) Krejci L., Altmannova V., Spirek M., Zhao X. (2012). Homologous recombination

and its regulation. Nucleic Acids Res. 40, 5795-5818.

79) Brandsma I., Gent D.C. (2012). Pathway choice in DNA double strand break repair: observations of a balancing act. Genome Integr. 3, 9.

80) Palma N., Cinelli S., Sapora O., Wilson S.H., Dogliotti E. (2007). Ochratoxin A-induced mutagenesis in mammalian cells is consistent with the production of oxidative stress. Chem Res Toxicol. 20, 1031-1037.

81) Adler M., Müller K., Rached E., Dekant W., Mally A. (2009). Modulation of key regulators of mitosis linked to chromosomal instability is an early event in ochratoxin A carcinogenicity. Carcinogenesis, 30, 711-719.

82) Mally A., Pepe G., Ravoori S., Fiore M., Gupta R.C., Dekant W., Mosesso P. (2005). Ochratoxin a causes DNA damage and cytogenetic effects but no DNA adducts in rats. Chem Res Toxicol. 18, 1253-1261.

83) Ting L., Jun H., Junjie C. (2010). RAD18 lives a double life: Its implication in DNA double-strand break repair. DNA Repair (Amst), 9, 1241-1248.

84) Dohrn L., Salles D., Siehler S.Y., Kaufmann J., Wiesmüller L. (2012). BRCA1-mediated repression of mutagenic end-joining of DNA double-strand breaks requires complex formation with BACH1. Biochem J., 441, 919-926.

85) Yatagai F., Kurobe T., Nohmi T., Masumura K., Tsukada T., Yamaguchi H., Kasai-Eguchi K., Fukunishi N. (2002). Heavy-ion-induced mutations in the *gpt* delta transgenic mouse: effect of p53 gene knockout. Environ Mol Mutagen. 40, 216-225.

86) Kulkarni R., Thomas R.A., Tucker J.D. (2011). Expression of DNA repair and apoptosis genes in mitochondrial mutant and normal cells following exposure to ionizing radiation. Environ Mol Mutagen. 52, 229-237.

87) Bertrand P., Rouillard D., Boulet A., Levalois C., Soussi T., Lopez B.S. (1997). Increase of spontaneous intrachromosomal homologous recombination in mammalian cells expressing a mutant p53 protein. Oncogene 14: 1117-1122.

88) Pfohl-Leszkowicz A. (2008). Formation, persistence and significance of DNA

adduct formation in relation to some pollutants from a board perspective. Adv Toxicol. 2, 183-240.

89) Kuroda, K., Hibi, D., Ishii, Y., Takasu, S., Kijima, A., Matsushita, K., Masumura, K., Watanabe, M., Sugita-Konishi, Y., Sakai, H., Yanai, T., Nohmi, T., Ogawa, K., Umemura, T. (2014). Ochratoxin A induces DNA double-strand breaks and large deletion mutations in the carcinogenic target site of gpt delta rats. Mutagenesis 29, 27-36.

90) Gatz, S.A., Wiesmüller, L. (2006). p53 in recombination and repair. Cell Death Differ. 13, 1003-1016

91) Velasco-Miguel, S., Richardson, JA., Gerlach, V.L., Lai, W.C., Gao, T., Russell, L.D., Hladik, C.L., White, C.L., Friedberg, EC. (2003). Constitutive and regulated expression of the mouse Dinb (Polkappa) gene encoding DNA polymerase kappa. DNA Repair (Amst). 2, 91-106.

92) Batchelor, E., Loewer, A., Lahav, G. (2009). The ups and downs of p53:

understanding protein dynamics in single cells. Nat Rev Cancer. 9, 371-377.

93) Tsukada, T., Tomooka, Y., Takai, S., Ueda, Y., Nishikawa, S., Yagi, T., Tokunaga, T., Suda Y, Abe S, et al. (1993). Enhanced proliferative potential in culture of cells from p53-deficient mice. Oncogene 8: 3313-3322.

94) Nohmi, T., Katoh, M., Suzuki, H., Matsui, M., Yamada, M., Watanabe, M., Suzuki, Horiya N., Ueda O., Shibuya T., Ikeda H, Sofuni T. (1996). A new transgenic mouse mutagenesis test system using Spi- and 6-thioguanine selections. Environ Mol Mutagen. 28: 465-470.

95) Nohmi, T. and Masumura, K. (2005). Molecular nature of intrachromosomal deletions and base substitutions induced by environmental mutagens. Environ Mol Mutagen., 45, 150-161.

96) Tendler, Y., Weisinger, G., Coleman, R., Diamond, E., Lischinsky, S., Kerner, H., Rotter, V., Zinder, O. (1999). Tissue-specific p53 expression in the nervous system. *Brain Res Mol Brain Res.* **72**: 40-46.

97) Lodygin, D., Menssen, A., Hermeking, H. (2002). Induction of the Cdk inhibitor p21 by LY83583 inhibits tumor cell proliferation in a p53-independent manner. *J Clin Invest*. 110: 1717-1127.

98) Sasaki, YF., Sekihashi, K., Izumiyama, F., Nishidate, E., Saga, A., Ishida, K., Tsuda, S. (2000). The comet assay with multiple mouse organs: comparison of comet assay results and carcinogenicity with 208 chemicals selected from the IARC monographs and U.S. NTP Carcinogenicity Database. Crit Rev Toxicol. 30, 629-799.

99) Lian, H., Cui, J., Wang, Y., Liu, J., Wang, J., Shen, H., Xing, L., Wang, J., Yan, X., Zhang, X. (2014). Downregulation of Rad51 participates in OTA-induced DNA double-strand breaks in GES-1 cells in vitro. Toxicol Lett. 226, 214-221.

100) Seo, YR., Fishel, ML., Amundson, S., Kelley, MR., Smith, ML. (2002). Implication of p53 in base excision DNA repair: in vivo evidence. Oncogene 21, 731-737.

101) Smith, ML., Seo YR. (2002). p53 regulation of DNA excision repair pathways. Mutagenesis 17, 149-156.

102) Kondo N., Takahashi A., Ono K., Ohnishi T. (2010). DNA damage induced by alkylating agents and repair pathways. J Nucleic Acids. 2010:543531.

103) Harper, JW., Elledge, SJ., Keyomarsi, K., Dynlacht, B., Tsai, LH., Zhang, P., Dobrowolski, S., Bai, C., Connell-Crowley, L., Swindell, E., et al. (1995). Inhibition of cyclin-dependent kinases by p21. Mol Biol Cell. 6, 387-400.

104) Inturi, S., Tewari-Singh, N., Agarwal, C., White, CW., Agarwal, R. (2014). Activation of DNA damage repair pathways in response to nitrogen mustard-induced DNA damage and toxicity in skin keratinocytes. Mutat Res (Fundam Mol Mech Mutagen). 13, 53-63.

105) Quiros, S., Roos, W.P., Kaina, B. (2010). Processing of O6-methylguanine into DNA double-strand breaks requires two rounds of replication whereas apoptosis is also induced in subsequent cell cycles. Cell Cycle 9, 168-178.

106) Roos, W.P., Kaina, B. (2013). DNA damage-induced cell death: from specific DNA lesions to the DNA damage response and apoptosis. Cancer Lett. 332, 237-248.

107) Chipuk, J.E.., Kuwana, T., Bouchier-Hayes, L., Droin, NM., Newmeyer, DD., Schuler, M., Green, DR. (2004). Direct activation of Bax by p53 mediates mitochondrial membrane permeabilization and apoptosis. Science 303, 1010-1014.

108) Inohara, N., Ding, L., Chen, S., Núñez, G. (1997). harakiri, a novel regulator of cell death, encodes a protein that activates apoptosis and interacts selectively with survival-promoting proteins Bcl-2 and Bcl-X(L). EMBO J. 16, 1686-1694.

109) Lomonosova, E., Chinnadurai, G. (2008). BH3-only proteins in apoptosis and beyond: an overview. Oncogene 27 Suppl 1, S2-19.

110) Kaina, B. (2003). DNA damage-triggered apoptosis: critical role of DNA repair, double-strand breaks, cell proliferation and signaling. Biochem Pharmacol. 66, 1547-1554.

111) Deem, A., Keszthelyi, A., Blackgrove, T., Vayl, A., Coffey, B., Mathur, R., Chabes, A., Malkova, A. (2011). Break-induced replication is highly inaccurate. PLoS Biol. 9, e1000594

112) Llorente, B., Smith, CE., Symington, LS. (2008). Break-induced replication: what is it and what is it for? Cell Cycle 7, 859-864.

113) Akman SA, Adams M, Case D, Park G, Manderville RA. (2012). Mutagenicity of ochratoxin A and its hydroquinone metabolite in the SupF gene of the mutation reporter plasmid Ps189. Toxins (Basel). 4, 267-280.

114) Ali R, Guo X, Lin H, Khan QM, Ismail M, Waheed U, Ali T, Bhalli JA. (2014). Mutant frequency in comparison to oxidative DNA damage induced by ochratoxin A in L5178Y tk+/- (3.7.2C) mouse lymphoma cells. Drug Chem Toxicol. 37, 227-232.

115) Bennett, J.W. and Klich M. (2003). Mycotoxins. Clin Microbiol Rev. 16, 497-516.

116) Blaszkewicz, M., Muñoz, K., Degen G.H., 201. Methods for analysis of citrinin in human blood and urine. Arch Toxicol. 87, 1087-1094.

117) Peraica, M., Domijan, A. M., Miletić-Medved, M., Fuchs, R. (2008). The involvement of mycotoxins in the development of endemic nephropathy. Wien Klin Wochenschr. 120, 402-407.

118) Vrabcheva, T., Usleber, E., Dietrich, R., Märtlbauer, E. (2000). Co-occurrence of ochratoxin A and citrinin in cereals from Bulgarian villages with a history of Balkan endemic nephropathy. J. Agric. Food. Chem. 48, 2483-2488.

119) Shinohara, Y., Arai, M., Hirao, K., Sugihara, S., Nakanishi K. (1976). Combination effect of citrinin and other chemicals on rat kidney tumorigenesis. Gann 67, 147-155.

120) Klaunig, JE., Kamendulis L.M. (2004). The role of oxidative stress in carcinogenesis. Annu. Rev. Pharmacol. Toxicol. 44. 239-267.

121) Hayashi, H., Itahashi, M., Taniai, E., Yafune, A., Sugita-Konishi, Y., Mitsumori,

K., Shibutani M. (2012). Induction of ovarian toxicity in a subchronic oral toxicity study of citrinin in female BALB/c mice. J. Toxicol. Sci. 37, 1177-1190.

122) Kanisawa, M. (1984). Synergistic effect of citrinin on hepatorenal carcinogenesis of ochratoxin A in mice. Developments in food science 7, 245-254

123) Kasai, H. (2002). Chemistry-based studies on oxidative DNA damage: formation, repair, and mutagenesis. Free Radic. Biol. Med. 33, 450-456.

124) Nakae, D., Mizumoto, Y., Kobayashi, E., Noguchi, O., Konishi, Y. (1995). Improved genomic/nuclear DNA extraction for 8-hydroxydeoxyguanosine analysis of small amounts of rat liver tissue. Cancer Lett. 87, 233-230.

125) Kastenbaum, M. A., Bowman, K.O. (1970). Tables for determining the statistical significance of mutation frequencies. Mutat. Res. 9, 527-549.

126) Lockard, V.G., Phillips, R.D., Hayes, A.W., Berndt, W.O., O'Neal, R.M. (1980). Citrinin nephrotoxicity in rats: a light and electron microscopic study. Exp. Mol. Pathol. 32, 226-240.

127) Phillips, R.D., Hayes, A.W., Berndt, W.O., Williams, W.L. (1980). Effects of citrinin on renal function and structure. Toxicology 16, 123-137.

128) Berndt, W.O. (1983). Transport of citrinin by rat renal cortex. Arch. Toxicol. 54, 35-40.

129) Vargas, G. A., Hoeflich, A., Jehle, P. M. (2000). Hepatocyte growth factor in renal failure: promise and reality. Kidney Int. 57, 1426-1436.

130) Vinuesa, E., Sola, A., Jung, M., Alfaro, V., Hotter, G. (2008). Lipocalin-2-induced renal regeneration depends on cytokines. Am. J. Physiol. Renal Physiol. 295, F1554-1562.

131) Chambard, J.C., Lefloch, R., Pouysségur, J., Lenormand, P. (2007). ERK implication in cell cycle regulation. Biochim. Biophys. Acta. 1773, 1299-1310.

132) Naihan, Xu, Yuanzhi, Lao, Yaou, Zhang, David, A. Gillespie. (2012). Akt: A Double-Edged Sword in Cell Proliferation and Genome Stability. J. Oncol. 2012, 951724.

133) Chang, C.H., Yu, F.Y., Wang, L.T., Lin, Y. S., Liu, B.H. (2009). Activation of ERK and JNK signaling pathways by mycotoxin citrinin in human cells. Toxicol. Appl. Pharmacol. 237, 281-287

134) Hoshino, R., Chatani, Y., Yamori, T., Tsuruo, T., Oka, H., Yoshida, O., Shimada, Y., Ari-i, S., Wada, H., Fujimoto, J., Kohno, M. (1999). Constitutive activation of the 41-/43-kDa mitogen-activated protein kinase signaling pathway in human tumors. Oncogene 18, 813-822.

135) McCubrey, J.A., Steelman, L.S., Abrams, S.L., Lee, J.T., Chang, F., Bertrand, F.E., Navolanic, P.M., Terrian, D.M., Franklin, R.A., D'Assoro, A.B., Salisbury, J.L., Mazzarino, M.C., Stivala, F. and Libra, M. (2006). Roles of the RAF/MEK/ERK and PI3K/PTEN/AKT pathways in malignant transformation and drug resistance. Adv Enzyme Regul. 46, 249-279.

136) Ohtani, K., DeGregori, J., Nevins, J. R. (1995). Regulation of the cyclin E gene by transcription factor E2F1. Proc. Natl. Acad. Sci. U. S. A. 92, 12146-12150.

137) Alao, J.P. (2007). The regulation of cyclin D1 degradation: roles in cancer development and the potential for therapeutic invention. Mol. Cancer. 6, 24.

138) Borowiak, M., Garratt, A.N., Wüstefeld, T, Strehle M., Trautwein, C., Birchmeier, C. (2004). Met provides essential signals for liver regeneration. Proc. Natl. Acad. Sci. U S A. 101, 10608-10613.

139) Chowdhury, R., Chatterjee, R., Giri, A.K., Mandal, C., Chaudhuri, K. (2010). Arsenic-induced cell proliferation is associated with enhanced ROS generation, Erk signaling and Cyclin A expression. Toxicol. Lett. 198, 263-271.

140) Cobb, M.H., Goldsmith, E.J. (1995). How MAP kinases are regulated. J. Biol. Chem. 270, 14843-14846.

141) Gerits, N., Kostenko, S., Shiryaev, A., Johannessen, M., Moens, U. (2008). Relations between the mitogen-activated protein kinase and the cAMP-dependent protein kinase pathways: comradeship and hostility. Cell. Signal. 20, 1592-1607.

142) Chen, C.C., Chan, W.H. (2009). Inhibition of citrinin-induced apoptotic

biochemical signaling in human hepatoma G2 cells by resveratrol. Int. J. Mol. Sci. 10, 3338-3357.

143) Kumar, R., Dwivedi, P. D., Dhawan, A., Das, M., Ansari, K. M. (2011). Citrinin-generated reactive oxygen species cause cell cycle arrest leading to apoptosis via the intrinsic mitochondrial pathway in mouse skin. Toxicol. Sci. 122, 557-566.

144) Klarić, M. S., Zelježić, D., Rumora, L., Peraica, M., Pepeljnjak, S., Domijan, A. M. (2012). A potential role of calcium in apoptosis and aberrant chromatin forms in porcine kidney PK15 cells induced by individual and combined ochratoxin A and citrinin. Arch. Toxicol. 86, 97-107.

145) Brendler-Schwaab, S., Hartmann, A., Pfuhler, S., Speit, G. (2005). The *in vivo* comet assay: use and status in genotoxicity testing. Mutagenesis 20, 245-254.

146) Dönmez-Altuntas, H., Dumlupinar, G., Imamoglu, N., Hamurcu, Z., Liman, B.C. (2007). Effects of the mycotoxin citrinin on micronucleus formation in a

cytokinesis-block genotoxicity assay in cultured human lymphocytes. J. Appl. Toxicol. 27, 337-341.

147) Sorrenti V., Di Giacomo C., Acquaviva R., Barbagallo I., Bognanno M., Galvano F. (2013). Toxicity of ochratoxin A and its modulation by antioxidants: a review. Toxins (Basel). 5, 1742-1766.

148) Czakai K., Müller K., Mosesso P., Pepe G., Schulze M., Gohla A., Patnaik D., Dekant W., Higgins J.M., Mally A. (2011). Perturbation of mitosis through inhibition of histone acetyltransferases: the key to ochratoxin a toxicity and carcinogenicity? Toxicol Sci. 122, 317-329.

149) Cohen, S. M., Garland, E. M. and Ellwein, L. B. (1992). Cancer enhancement by cell proliferation. Prog Clin Biol Res 374, 213–229.

150) Klarić M.S., Rašić D., Peraica M. (2013). Deleterious effects of mycotoxin combinations involving ochratoxin A. Toxins (Basel). 5, 1965-1987.

151) Polisenska I., Pfohl-Leszkowicz A., Hadjeba K., Dohnal V., Jirsa O., Denesova

O., Jezkova A., Macharackova P. (2010). Occurrence of ochratoxin A and citrinin in Czech cereals and comparison of two HPLC methods for ochratoxin A detection. Food Addit Contam Part A Chem Anal Control Expo Risk Assess. 27, 1545-1557.

152) Kuroda K., Kijima A., Ishii Y., Takasu S., Jin M., Matsushita K., Kodama Y., Umemura T. (2013). Flumequine enhances the in vivo mutagenicity of MeIQx in the mouse liver. Arch Toxicol. 87, 1609-1619.